On the Dynamic Response of Nonlinear Uncertain Systems

Thesis by

Ching-Tung Huang

In Partial Fulfillment of the Requirements
for the Degree of
Doctor of Philosophy

California Institute of Technology
Pasadena, California

1996
(Submitted May 21, 1996)

Acknowledgements

I would like to express my greatest appreciation to my advisor, Professor W. D. Iwan, for his continuous patience, encouragement and guidance throughout my graduate study. Without him, the completion of this thesis work would never be possible.

I would also like to thank the entire faculty of Thomas Lab. for their excellent teaching. The financial support from California Institute of Technology is also fully appreciated.

Special thanks are due to Dr. L. Paparizos, my former advisor in Carnegie Mellon University, for encouraging and assisting me in pursuing doctoral study at California Institute of Technology.

Thanks are also due to Dr. C. Papadimitriou for valuable discussions on this research subject, and to E. Chan for technical assistance in setting up my computing environment.

Finally, this thesis work is dedicated to my family for their unconditional love and support.

Abstract

This thesis presents an approach for performing second moment analyses of nonlinear dynamic systems with parameter uncertainty. The uncertain parameters are modeled as time-independent random variables. The set of orthogonal polynomials associated with the probability density function is used as the solution basis. When a deterministic excitation source is considered, the response variables are expanded in terms of a finite sum of these polynomials with time-dependent coefficients. The weighted residual method is employed to derive a set of deterministic nonlinear differential equations that can be solved numerically for evaluations of response statistics.

This solution approach is further extended to nonlinear continuous systems involving inhomogeneous random media. A discrete representation is obtained via a spatial discretization procedure for the continuous response variables as well as the random continuum. Thus, the continuous random system can then be treated as in the case of the discrete random systems. The solution approach is applied to a study of a nonlinear random shear-beam model subjected to a near-field earthquake ground motion.

The response uncertainty for nonlinear uncertain systems subjected to external stochastic excitation is also investigated. A general solution procedure based on equivalent linearization is presented. In this solution methodology, the instantaneous equivalent stiffness and damping matrices are approximated as quadratic random functions. The resulting Liapunov system with explicit random coefficients can then be solved using the newly developed solution approach. Applications to single-degree-of-freedom uncertain systems are given and the accuracy of the results is validated.

Contents

List of Figures

Chapter 1

Introduction

The treatment of systems with parameter uncertainties has become an increasingly important problem in many areas of dynamic analysis. Mathematical models for dynamical systems, as well as solution techniques, have become increasingly refined and more precise. Therefore, the most important factor controlling the uncertainty of the solution is usually the uncertainty of the system and excitation parameters. For example, it is now possible to perform very detailed analyses of the response of buildings to earthquakes including modeling of the fault rupture process, wave propagation path effects, and local site effects, as well as a full nonlinear structural analysis including soil-structure interaction. However, the precision with which these analyses can be performed masks the fact that the results are only as meaningful as the model parameters assumed. Often, the model parameters are only poorly known, and the uncertainty in these parameters may have a large effect on the reliability of any conclusions based on deterministic analyses.

There is a need for more efficient and accurate analysis techniques that allow the effects of parameter uncertainty to be included in the analysis of both linear and nonlinear dynamical systems. Previous studies have focused primarily on linear systems. However, many dynamical systems of importance are inherently nonlinear. The development of solution techniques that are applicable to nonlinear systems has proven to be a formidable challenge.

The studies of uncertain linear systems with deterministic dynamic loads may be classified into statistical frequency-domain analyses [1, 2] and statistical transient

time-domain analyses [3, 4, 5, 6, 7, 8, 9]. The property that a harmonic time function is preserved under linear transformations makes the response amplitude statistics a well-defined measure of the response variability of linear systems. However, the amplitude statistics may not be appropriate in the presence of nonlinearity, since multiple steady-state solutions may exist. Therefore, the analysis of nonlinear systems is generally not practical using frequency-domain analysis techniques.

Existing solution methods for statistical nonlinear transient time-domain analyses are mostly based on simulation [10, 11] and the perturbation approach [3, 4, 5]. The simulation method is applicable to both linear and nonlinear problems. A major disadvantage of this approach is that it requires considerable computational efforts for accurate results. Liu, Belytschko and Mani [3] have formulated a perturbation approach for calculating the first and the second-order response sensitivity vectors. This method is used to study short duration transient excitation of yielding multi-degree-of-freedom structures with random stiffnesses. This technique has also been implemented for nonlinear continuous systems involving inhomogeneous random media [4]. However, in [5], it is concluded that the accuracy of the perturbation-based solutions deteriorates for large time due to secular terms, and therefore removal of the secularity is required for consistent results.

As previously mentioned, the excitation uncertainty represents another major source of uncertainty, particularly for systems under random dynamical loadings. The analyses of stochastically excited uncertain systems are primarily performed on the basis of the random vibration theory with an additional consideration of parameter uncertainty. In the past decades, exact linear solutions for most stationary and non-stationary problems were obtained in closed forms [12]. The effect of parameter uncertainty can then be assessed directly, and the task is technically straightforward. Although exact analyses are currently possible for a few nonlinear problems [13, 14, 15], great difficulties generally exist, especially when the nonstationarity is considered or

multi-degree-of-freedom systems are attempted. Consequently, appropriate approximation techniques become particularly useful when time-costly Monte-Carlo simulation is to be avoided.

The method of equivalent linearization has become a standard technique for obtaining approximated solutions of nonlinear random vibration problems. This method originated from the work by Caughey [16], generalized by Iwan [17, 18], Iwan and Yang [19], Spanos [20] and Atalik [21] for multi-degree-of-freedom systems, and by Mason and Iwan [22] for nonstationary problems. This technique has also been implemented by Wen [23], and Iwan and Asano [24] for solving nonlinear systems exhibiting hysteretic behavior.

Previous research studies of uncertain nonlinear systems subjected to stochastic excitation are mostly based on the equivalent linearization method combined with other techniques for treating the additional randomness due to uncertain parameters. Cherng and Wen [25] apply a second-order perturbation technique for analyzing uncertain nonlinear hysteretic structures. A similar perturbation technique is adopted by Chang and Yang [26] for treating uncertain flexible beams with geometric nonlinearity. Klosner, Haber and Voltz [27] apply a numerical integration technique combined with a linearized Fokker-Plank equation to investigate uncertain two-degree-of-freedom systems. Despite the fact that the nonlinear physical models differ in the above mentioned studies, equivalent linearization was reported as a suitable analysis means for nonlinear analyses of uncertain systems. Unfortunately, the implementation of equivalent linearization is confined within the scope of stationary response, and nonstationary applications have not been fully explored.

It is the objective of this thesis to develop an alternative solution method for analyzing nonlinear uncertain dynamical systems subjected to deterministic as well as stochastic excitation sources. Emphasis is given to the second-moment analysis of transient response when a deterministic excitation source is considered, and of

nonstationary response when a stochastic excitation source is considered. The organization of this thesis is briefly described below.

In Chapter 2, a solution method is proposed for analyzing discrete nonlinear dynamical systems with parameter uncertainty. The uncertain parameters are idealized as time-independent random variables. The response variables are expanded in terms of a set of orthogonal polynomials and then the method of weighted residues is used to derived a coupled deterministic nonlinear equation set. Applications of the proposed solution method are also given.

Chapter 3 considers continuous dynamical problems exhibiting uncertain material properties idealized as a Gaussian random field. The random field is represented in terms of a finite sum of independent random variables via a discretization of the covariance function. The solution method developed in Chapter 2 can then be applied to an equation of motion resulting from a generalized spatial discretization of the random continuum. A concrete application is given in Chapter 4 where a nonlinear shear-beam model subjected to a near-field base earthquake is studied.

Chapter 5 presents a solution framework for nonlinear random vibration problems with parameter uncertainty. The method of equivalent linearization is adopted in this solution framework for obtaining an equivalent random linear system. To allow an efficient treatment, the random equivalent stiffness and damping are approximated as quadratic random functions. The resulting random Liapunov system can then be converted into a deterministic Liapunov system to be evaluated numerically. In Chapter 6, the proposed solution framework is used to obtain nonstationary response for several uncertain single-degree-of-freedom systems. Other solution techniques are also provided for comparative studies.

A summary and conclusions together with recommendations for future research are given in Chapter 7.

Chapter 2

Nonlinear Discrete Systems with Uncertain Parameters

2.1 Introduction

This chapter is aimed at providing a solution method to evaluate the response variability of discrete nonlinear systems subjected to deterministic dynamic loadings. The proposed method is based on an orthogonal polynomial expansion in conjunction with a variational method in the sense of Galerkin. Comparative studies of different solution methods are also presented in order to investigate their transient behavior under the effect of parameter uncertainties.

2.2 Formulation

The transient analysis of nonlinear structural systems with parameter uncertainty requires the solution to an equation of motion of the form

$$\mathbf{M}\ddot{\mathbf{x}}(t) + \mathbf{C}\dot{\mathbf{x}}(t) + \mathbf{K}\mathbf{x}(t) + \mathbf{g}(\dot{\mathbf{x}}(t), \mathbf{x}(t), \boldsymbol{\gamma}) = \mathbf{f}(t) \tag{2.1}$$

where $\mathbf{x}(t)$ is the generalized displacement vector, and the matrices $\mathbf{M}$, $\mathbf{C}$ and $\mathbf{K}$ represent the deterministic components of the mass, damping and stiffness, respectively. The vector $\boldsymbol{\gamma} = \{\gamma_1, \gamma_2, \cdots, \gamma_N\}^T$ represents N time-independent uncertain paramet-

ers, $\mathbf{g}(\cdot,\cdot,\cdot)$ is a vector of linear and/or nonlinear functions of their arguments, and $\mathbf{f}(t)$ is a vector of external forcing functions that are assumed to be deterministic.

For a mathematically concise representation, the uncertain parameters are idealized as random variables with a prescribed probabilistic distribution. Consider the case where the set of uncertain parameters $\boldsymbol{\gamma}$ are modeled as correlated random variables and their second moment representations are given by $E[\boldsymbol{\gamma}] = \bar{\boldsymbol{\gamma}}$ and $Cov[\boldsymbol{\gamma}, \boldsymbol{\gamma}] = \boldsymbol{\Gamma}$. Then, these correlated random variables can be transformed into uncorrelated variables using a matrix decomposition of the covariance matrix $\boldsymbol{\Gamma}$. Let

$$\boldsymbol{\Gamma} = \boldsymbol{\Phi}\boldsymbol{\Lambda}\boldsymbol{\Phi}^T \tag{2.2}$$

where $\boldsymbol{\Lambda}$ is a diagonal matrix containing the eigenvalues of the covariance matrix, and $\boldsymbol{\Phi}$ is the eigenvector matrix. Let the eigenvectors be normalized such that

$$\boldsymbol{\Phi}\boldsymbol{\Phi}^T = \mathbf{I} \tag{2.3}$$

where $\mathbf{I}$ is the identity matrix.

Define a new set of random variables, $\mathbf{b} = \{b_1, b_2, \cdots, b_N\}^T$, through the transformation

$$\mathbf{b} = \boldsymbol{\Lambda}^{-1/2}\boldsymbol{\Phi}^T(\boldsymbol{\gamma} - \bar{\boldsymbol{\gamma}}) \tag{2.4}$$

Then, the transformed random variables satisfy $E[\mathbf{b}] = \mathbf{0}$ and $Cov[\mathbf{b}, \mathbf{b}] = \mathbf{I}$. These newly defined random variables are related to the correlated variables by the relationship

$$\boldsymbol{\gamma} = \bar{\boldsymbol{\gamma}} + \boldsymbol{\Phi}\boldsymbol{\Lambda}^{1/2}\mathbf{b} \tag{2.5}$$

Substituting Eqn. (2.5) into Eqn. (2.1) and suppressing the deterministic argu-

ments for simplicity yields

$$\mathbf{M}\ddot{\mathbf{x}}(t,\mathbf{b}) + \mathbf{C}\dot{\mathbf{x}}(t,\mathbf{b}) + \mathbf{K}\mathbf{x}(t,\mathbf{b}) + \tilde{\mathbf{g}}(\dot{\mathbf{x}}(t,\mathbf{b}),\mathbf{x}(t,\mathbf{b}),\mathbf{b}) = \mathbf{f}(t) \tag{2.6}$$

The solution of random differential equation of type of Eqn. (2.6) poses many mathematical challenges. Various techniques developed for uncertain *linear* analysis are not applicable in this case since the inverse of a nonlinear random differential operator is not defined. This inherent difficulty limits the available solution methods to a very small number. One method that can be used is the perturbation method which is discussed in the next section.

2.3 Perturbation Method

The perturbation method is based on the assumption that the parameter uncertainties are small. Since the solution variables depend continuously on the random parameters, the solutions can be perturbed about the mean values of the uncertain parameters using the Taylor series expansion [3, 4, 28]. For notational simplicity, let $\mathbf{s}(t,\mathbf{b})$ be a vector of time-varying random functions and denote the nth-order Taylor coefficient of $\mathbf{s}(t,\mathbf{b})$ by $\mathbf{s}^{[n]}_{i\cdots j}(t)$. Then, $\mathbf{s}^{[n]}_{i\cdots j}(t)$ is given by

$$\mathbf{s}^{[n]}_{\underbrace{i\cdots j}_{n}}(t) = \left.\frac{\partial^n \mathbf{s}(t,\mathbf{b})}{\underbrace{\partial b_i \cdots \partial b_j}_{n}}\right|_{\mathbf{b}=\mathbf{0}} \tag{2.7}$$

The perturbation for the displacement variable $\mathbf{x}(t,\mathbf{b})$ becomes

$$\begin{aligned}\mathbf{x}(t,\mathbf{b}) \;=\; & \mathbf{x}^{[0]}(t) + \sum_{i=1}^{N} \mathbf{x}^{[I]}_i(t) b_i + \frac{1}{2!}\sum_{i=1}^{N}\sum_{j=1}^{N} \mathbf{x}^{[II]}_{ij}(t) b_i b_j + \\ & \frac{1}{3!}\sum_{i=1}^{N}\sum_{j=1}^{N}\sum_{k=1}^{N} \mathbf{x}^{[III]}_{ijk}(t) b_i b_j b_k + \cdots\end{aligned} \tag{2.8}$$

Similarly, the nonlinear random function $\tilde{\mathbf{g}}(\dot{\mathbf{x}}, \mathbf{x}, \mathbf{b})$ can also be expanded as

$$\begin{aligned}\tilde{\mathbf{g}}(\dot{\mathbf{x}}, \mathbf{x}, \mathbf{b}) &= \tilde{\mathbf{g}}^{[0]}(t) + \sum_{i=1}^{N} \tilde{\mathbf{g}}_i^{[I]}(t) b_i + \frac{1}{2!} \sum_{i=1}^{N} \sum_{j=1}^{N} \tilde{\mathbf{g}}_{ij}^{[II]}(t) b_i b_j + \\ &\quad \frac{1}{3!} \sum_{i=1}^{N} \sum_{j=1}^{N} \sum_{k=1}^{N} \tilde{\mathbf{g}}_{ijk}^{[III]}(t) b_i b_j b_k + \cdots \end{aligned} \tag{2.9}$$

where $\tilde{\mathbf{g}}_{i\cdots j}^{[n]}(t)$ are obtained through the chain rule of partial differentiation with respect to the dependent variables $\dot{\mathbf{x}}(t, \mathbf{b})$ and $\mathbf{x}(t, \mathbf{b})$.

Substituting Eqn. (2.8) and Eqn. (2.9) into Eqn. (2.6) and collecting terms of the same order in b_i will yield an infinite set of deterministic equations. These deterministic equations can be arranged in a hierarchical order. Truncating the equations at different hierarchical levels will correspond to different orders of approximation. Given an order of approximation, the resulting equation set contains only the Taylor coefficients less than or equal to the given order. Hence, it can be solved directly without recourse to particular closure techniques.

For a *linear* problem, this equation set has identical homogeneous parts subjected to different forcing terms. Great efficiency can be achieved by solving this set sequentially. In the nonlinear case, this advantage is generally lost due to the resulting coupling of nonlinear terms. Therefore, this set of equations must be solved simultaneously.

The response statistics can be evaluated using the numerical results of the time-domain solution of the resulting deterministic equations. When a second-order scheme is adopted, the mean response is given by

$$E[\mathbf{x}(t, \mathbf{b})] = \mathbf{x}^{[0]}(t) + \frac{1}{2} \sum_{i=1}^{N} \mathbf{x}_{ii}^{[II]}(t) \tag{2.10}$$

The covariance matrix is given by

$$Cov[\mathbf{x}(t,\mathbf{b}),\mathbf{x}(t,\mathbf{b})] = \sum_{i=1}^{N}\mathbf{x}_i^{[I]}(t)\mathbf{x}_i^{[I]^T}(t) - \frac{1}{4}\sum_{i=1}^{N}\mathbf{x}_{ii}^{[II]}(t)\sum_{j=1}^{N}\mathbf{x}_{jj}^{[II]^T}(t) + \frac{1}{4}\sum_{i=1}^{N}\sum_{j=1}^{N}\sum_{k=1}^{N}\sum_{l=1}^{N}E[b_ib_jb_kb_l]\mathbf{x}_{ij}^{[II]}(t)\mathbf{x}_{kl}^{[II]^T}(t) \tag{2.11}$$

When a third-order scheme is used, the mean response is also given by Eqn. (2.10). However, the expression for the covariance matrix involves higher order terms, and is given by

$$Cov[\mathbf{x}(t,\mathbf{b}),\mathbf{x}(t,\mathbf{b})] = \sum_{i=1}^{N}\mathbf{x}_i^{[I]}(t)\mathbf{x}_i^{[I]^T}(t) - \frac{1}{4}\sum_{i=1}^{N}\mathbf{x}_{ii}^{[II]}(t)\sum_{j=1}^{N}\mathbf{x}_{jj}^{[II]^T}(t)$$

$$+\sum_{i=1}^{N}\sum_{j=1}^{N}\sum_{k=1}^{N}\sum_{l=1}^{N}E[b_ib_jb_kb_l]\left(\frac{1}{4}\mathbf{x}_{ij}^{[II]}(t)\mathbf{x}_{kl}^{[II]^T}(t) + \frac{1}{6}\mathbf{x}_i^{[I]}(t)\mathbf{x}_{jkl}^{[III]^T}(t) + \frac{1}{6}\mathbf{x}_{jkl}^{[III]}(t)\mathbf{x}_i^{[I]^T}(t)\right)$$

$$+\frac{1}{36}\sum_{i=1}^{N}\sum_{j=1}^{N}\sum_{k=1}^{N}\sum_{l=1}^{N}\sum_{m=1}^{N}\sum_{n=1}^{N}E[b_ib_jb_kb_lb_mb_n]\mathbf{x}_{ijk}^{[III]}(t)\mathbf{x}_{lmn}^{[III]^T}(t) \tag{2.12}$$

Certain problems exist when performing an analysis of uncertain systems based on the perturbation method. For both the second-order and third-order schemes, the expression for the mean response makes no distinction as to the type of probability distribution associated with the uncertain parameters. Accordingly, this method is insensitive to the dependence of response statistics on the probability distribution of the uncertain parameters. In addition, the accuracy of the results depends highly on the order of approximation within the effective range of the uncertain parameters. However, the degree of response fluctuation within this range is generally not known in advance, especially when external force, system nonlinearity and time factors take effect. Thus, conclusions based on the perturbation approach may be misleading.

2.4 Proposed Method

In viewing the problems related to the use of the perturbation method, an alternative approach is proposed. This approach may be considered as an extension of the method suggested by Jensen and Iwan [29]. In the proposed method, a set of multi-dimensional orthogonal polynomials is used as a solution basis. The response variables are expanded in terms of a finite sum of the orthogonal polynomials with time-dependent coefficients. A set of deterministic nonlinear differential equation is derived using the weighted residual method. The formulation of the proposed method may be cast in a general format as indicated in the following sections.

2.4.1 Solution Basis

The solution basis adopted in the proposed method is the set of orthogonal polynomials with respect to the probability density function. Consider a zero mean, unit variance random variable b, with probability density function $P(b)$, and the range of probability Ω_b. The set of orthogonal polynomials that will be employed is the set of polynomials $\{H_l(b)\}_{l=0}^{\infty}$ satisfying the orthogonality relationship,

$$E[H_l(b)H_s(b)] = \int_{\Omega_{b'}} P(b')H_l(b')H_s(b')db' = \delta_{ls} \tag{2.13}$$

where δ_{ls} is the Kronecker delta. This orthogonal polynomial set can be generalized to a multi-dimensional setting as follows.

Consider the set of N random variables $\mathbf{b}$ given previously. An N-dimensional orthogonal polynomial is constructed as

$$H_{l_1 l_2 \cdots l_N}(\mathbf{b}) = \prod_{n=1}^{N} H_{l_n}(b_n) \tag{2.14}$$

The set of N-dimensional orthogonal polynomials is denoted as $\{H_{l_1 l_2 \cdots l_N}(\mathbf{b})\}_{|\mathbf{l}|=0}^{\infty}$,

where $|\mathbf{l}|$ represents the associated norm. The norm of the a multi-dimensional polynomial provides a measure of the order of the polynomial. It can be taken as

$$|\mathbf{l}| = \sum_{n=1}^{N} l_n \tag{2.15}$$

The orthogonality condition for this case is given by

$$E[H_{l_1 l_2 \cdots l_N}(\mathbf{b}) H_{s_1 s_2 \cdots s_N}(\mathbf{b})] = \prod_{n=1}^{N} \delta_{l_n s_n} \tag{2.16}$$

To satisfy this orthogonality condition, the selection of the orthogonal polynomial sets must be according to the type of the probability distribution. For example, Hermite polynomials are used for the case of normally distributed random variables. Similarly, Legendre polynomials correspond to a uniform distribution [30]. In addition to these two widely used distributions, a family of distribution, namely the Ultraspherical distribution with index M, is considered herein in modeling the uncertain parameters. When $M = 1$, this corresponds to the Tchebycheff polynomial of the second kind. This family set is capable of generating bounded probability distributions with various degrees of "tightness". The nature of the Ultraspherical distribution is shown in Figs. 2.1 and 2.2 where the uniform and normal distributions are also plotted for comparison. In the case of Hermite polynomials, this polynomial set is identical to that developed by Ghanem and Spanos [31, 32, 33] except for the normalizing constants.

2.4.2 Deterministic Equations

As a means of obtaining an approximate solution of Eqn. (2.6), the solution variable $\mathbf{x}(t, \mathbf{b})$ is first expanded as a finite sum of deterministic time variables multiplied by

the orthogonal polynomials. The expansion to order NP is given by

$$\mathbf{x}(t,\mathbf{b}) = \sum_{|\mathbf{l}|=0}^{NP} \hat{\mathbf{x}}_{l_1 l_2 \cdots l_N}(t) H_{l_1 l_2 \cdots l_N}(\mathbf{b}) \tag{2.17}$$

The method of weighted residuals is used to minimize the equation residual resulting from this approximation. The weighting function chosen is based on the Galerkin approach in a statistical sense.

Substituting Eqn. (2.17) into Eqn. (2.6), multiplying by the members of the series of orthogonal polynomials, performing the expectation operation, and using orthogonality leads to

$$\mathbf{M}\ddot{\hat{\mathbf{x}}}_{l_1 l_2 \cdots l_N}(t) + \mathbf{C}\dot{\hat{\mathbf{x}}}_{l_1 l_2 \cdots l_N}(t) + \mathbf{K}\hat{\mathbf{x}}_{l_1 l_2 \cdots l_N}(t) +$$

$$E[\hat{\mathbf{g}}(\dot{\hat{\mathbf{x}}}, \hat{\mathbf{x}}, \mathbf{b}) H_{l_1 l_2 \cdots l_N}(\mathbf{b})] = \mathbf{f}(t) \prod_{n=1}^{N} \delta_{0 l_n}, \qquad |\mathbf{l}| = 0, \cdots, NP \tag{2.18}$$

Eqn. (2.18) is a set of deterministic equations with uncoupled linear parts and fully coupled nonlinear parts. A similar expansion method has been implemented by Ghanem and Spanos [34] in studying the nonlinear random vibration of deterministic systems subjected to non-white random excitation. This technique is also implemented by Dham and Ghanem [35] and Ghanem et al. [36] in solving transient random linear/nonlinear systems in engineering applications other than structural dynamics.

To evaluate Eqn. (2.18) numerically requires an explicit deterministic expression for the nonlinear terms under the expectation operator. These terms correspond to multi-dimensional probabilistic integrals which are difficult to solve in general. However, explicit expressions exist for those cases where the nonlinear terms are expressible as polynomials and the uncertain parameters appear as coefficients. Hence, the proposed solution method is particularly suitable for a problem of this type. The coupling effect may lead to computational difficulties, particularly when higher order

solutions are sought or a large number of random variables are present. Fortunately, the nonlinearities encountered in many engineering problems can be modeled as a power series in the state variables and the response uncertainty is usually dominated by only a few uncertain parameters. Hence, the proposed method is potentially applicable to a fairly wide class of nonlinear problems.

For those cases where the expressions of the probabilistic integrals are not directly available, approximation techniques such as series expansion methods can be employed to obtain approximate numerical values. However, this process may lead to mathematical complication, especially when a higher-order approximation is to be used. Hence, this technique can only reliably be applied to the problems where a low-order approximation scheme is appropriate. Applications for problems of this type are given in Chapter 5 and Chapter 6, where a low-order series expansion is used to approximate moment equations resulting from the analysis of nonlinear random vibration problems with parameter uncertainties.

The discrete time solution of Eqn. (2.18) can be evaluated numerically in time using a step-by-step solution procedure. The response statistics are then calculated using

$$\begin{aligned} E[\mathbf{x}(t,\mathbf{b})] &= \sum_{|\mathbf{l}|=0}^{NP} \hat{\mathbf{x}}_{l_1 l_2 \cdots l_N}(t) E[H_{l_1 l_2 \cdots l_N}(\mathbf{b})] \\ &= \hat{\mathbf{x}}_{00\cdots 0}(t) \end{aligned} \tag{2.19}$$

and

$$\begin{aligned} Cov[\mathbf{x}(t,\mathbf{b}),\mathbf{x}(t,\mathbf{b})] &= \sum_{|\mathbf{l}|=1}^{NP} \sum_{|\mathbf{m}|=1}^{NP} \hat{\mathbf{x}}_{l_1 l_2 \cdots l_N}(t) \hat{\mathbf{x}}^T_{m_1 m_2 \cdots m_N}(t) E[H_{l_1 l_2 \cdots l_N}(\mathbf{b}) H_{m_1 m_2 \cdots m_N}(\mathbf{b})] \\ &= \sum_{|\mathbf{l}|=1}^{NP} \hat{\mathbf{x}}_{l_1 l_2 \cdots l_N}(t) \hat{\mathbf{x}}^T_{l_1 l_2 \cdots l_N}(t) \end{aligned} \tag{2.20}$$

The application of the proposed method is demonstrated through the analysis of

structural systems possessing hardening or softening uncertain stiffness. These are two important cases of nonlinearity in the context of structural dynamics. Individual formulations and numerical results are given in Section 2.5 and Section 2.6.

2.5 Application to Uncertain Hardening Systems

Consider a single-degree-of-freedom hardening system modeled as a Duffing oscillator. The response process $x(t)$ is governed by the differential equation

$$\ddot{x}(t) + 2\zeta\omega_n\dot{x}(t) + \omega_n^2[x(t) + \epsilon x^3(t)] = a(t) \tag{2.21}$$

where ζ and ω_n denote the damping ratio and the undamped natural frequency of the associated linear system, respectively, $a(t)$ is the external excitation and ϵ is a positive parameter representing a measure of the degree of nonlinearity. The degree of nonlinearity depends on both the amplitude of the response and the magnitude of the parameter ϵ. Let the peak response of the linear system be denoted by x_m. Also let $u(t) = x(t)/x_m$ and $h(t) = a(t)/x_m$. Then, the differential equation can be written as

$$\ddot{u}(t) + 2\zeta\omega_n\dot{u}(t) + \omega_n^2[u(t) + \gamma u^3(t)] = h(t) \tag{2.22}$$

where the dimensionless nonlinear parameter, γ, is defined as $\gamma = \epsilon x_m^2$. The normalized restoring force versus normalized displacement for the hardening system is shown in Fig. 2.3 for various values of γ. The source of uncertainty is assumed to arise from the restoring force due to variations of the nonlinear parameter. This results in nearly deterministic stiffness for small amplitudes of response with increasing degree of uncertainty as the amplitude of response increases.

Let the uncertain parameter be modeled as

$$\gamma = \bar{\gamma} + \lambda b \tag{2.23}$$

where the overbar denotes the mean value, λ is the standard deviation, and b is a random variable with zero mean and unit variance. Since only one random variable is present in this analysis, the solution variable is expanded as

$$u(t,b) = \sum_{i=0}^{NP} \xi_i(t) H_i(b) \tag{2.24}$$

Following the procedure of the previous section, the final deterministic equation set for the ξ_i is

$$\ddot{\xi}_i(t) + 2\zeta\omega_n\dot{\xi}_i(t) + \omega_n^2\xi_i(t) +$$

$$\omega_n^2 \sum_{j=0}^{NP}\sum_{k=0}^{NP}\sum_{l=0}^{NP}(\bar{\gamma}R_{ijkl} + \lambda S_{ijkl})\xi_j(t)\xi_k(t)\xi_l(t) = h(t)\delta_{0i}, \quad i = 0, \cdots, NP \tag{2.25}$$

where R_{ijkl} and S_{ijkl} are constants given by

$$R_{ijkl} = E[H_i(b)H_j(b)H_k(b)H_l(b)] \tag{2.26}$$

and

$$S_{ijkl} = E[bH_i(b)H_j(b)H_k(b)H_l(b)] \tag{2.27}$$

The constants R_{ijkl} and S_{ijkl} can be evaluated efficiently using the power relations for the orthogonal polynomials. The major computational demand in obtaining the time-domain solution of Eqn. (2.25) lies in the evaluation of the triple-summed coupled nonlinear terms. Since the number of operations increases dramatically as higher order approximations are considered, it is necessary to avoid redundant computations by making use of the symmetry property of the constant coefficients and the cubic-product of the solution variables. Eqn. (2.25) can be rearranged accordingly to

facilitate numerical computation.

2.5.1 Numerical Examples

A hardening structural system subjected to earthquake base excitation is considered herein as a numerical illustration of the method. The input excitation chosen is the N00E component of 1940 El Centro earthquake record. The acceleration time history of the input excitation is shown in Fig. 2.4.

The response statistics are evaluated using three different methods: the proposed method, perturbation method (PM) and simulation method (SM). Both the proposed method and the PM use a fourth-order Runge-Kutta explicit time-integration scheme. In the SM, 100 equally-spaced samples over the random space are generated. In each sample, the displacement solution is evaluated through Newmark's average acceleration method. The mean and standard deviation of the displacement are calculated using Simpson's rule of integration. By varying the sample size, it has been verified that the combination of the integration rule and the sample size selected for the examples is capable of providing accurate results. Hence, these SM solutions are considered as "exact solutions" and are used to verify the accuracy of solutions obtained by the proposed method and PM. The comparison of the response statistics is presented for two special cases.

case (I)

The first case considered is a 5% damped structure with linearized natural frequency $f_n = \omega_n/2\pi = 1$ Hz. The nonlinear parameter γ is uniformly distributed with $\bar{\gamma} = 0.5$ and $\lambda = 0.25$. The proposed method and the PM are first executed using a second-order scheme. The mean and standard deviation of the normalized displacement response given by the proposed method and SM are plotted in Fig. 2.5. Likewise, a comparison of solutions given by the PM and SM is given in Fig. 2.6. In the standard

deviation response plot of Fig. 2.6, the solution obtained by the PM deviates significantly from that of the SM after a time of approximately 5 seconds and yields about 70% peak overshoot thereafter. On the other hand, the proposed method provides a good estimate of both response statistics.

Both approximation methods are further examined using a third-order scheme. A comparison of the response statistics is given in Fig. 2.7 and Fig. 2.8. In Fig. 2.7, the mean response given by the proposed third-order scheme almost coincides with the SM solution for all time. Excellent performance of the standard deviation response result is also demonstrated. By contrast, the third-order perturbation scheme still yields unsatisfactory results, although the response prediction is slightly improved as the order of approximation increases.

To better understand the differences in the response predictions of the three methods, the displacement solutions are plotted as a function of $\gamma/\bar{\gamma}$ for a fixed time in Fig. 2.9. The comparison of second-order solutions is given for $t = 6.66$ sec. in Fig. 2.9(a). It is seen that the PM provides an exact curvature at $\gamma = \bar{\gamma}$, but results in a large overall error away from this point. The proposed method seeks a best quadratic curve fit equally weighted over the range of $\gamma/\bar{\gamma}$, which is a direct consequence of the uniform distribution assumed for the uncertain parameter γ. Similarly, the third-order solutions are plotted for $t = 8.80$ sec. in Fig. 2.9(b) and distinct solution characteristics for these two approximation methods are also observed. The solution of the proposed method and PM respectively represent a cubic curve best-fitted in a global and local sense. These examples reveal the very different nature of the two approximation methods.

case (II)

The second case considered is a lightly damped system with the same properties as the first example, except that $\zeta = 1\%$ and $\lambda = 0.05$. The numerical results are presented

in Figs. 2.10 and 2.11. Note that the standard deviation of the nonlinear parameter is substantially smaller in this case than in case (I). However, the maximum standard deviation of the solution increases from about 0.4 to 0.7. This example demonstrates that small parameter uncertainty can result in very pronounced response uncertainty. Recall that larger response implies larger degree of randomness in the assumed model of uncertainty. The factors involved in large responses include the small damping coefficient and the interaction between the instantaneous effective stiffness and the external excitation. It follows that, the response uncertainty is greatly influenced by the response history in addition to the time-independent uncertain parameters.

For the case of Fig. 2.10, both response statistics of the second-order PM go off scale for large time. A comparison with the results in case (I) shows that the large time behavior of the perturbation approach is sensitive to the amount of damping in the system and gives unreliable results for the lightly damped case. The results of Fig. 2.11 demonstrate that much better performance is again achieved by the proposed method.

The convergence of the proposed method is demonstrated through the response statistics plot given in Fig. 2.12 where the results of a third-order and fourth-order approximation are given. The trend in approaching the SM solutions as the order of approximation increases is clearly demonstrated for both the response mean and standard deviation.

2.6 Application to Uncertain Softening Systems

The applicability of the proposed method to softening system is also examined. A direct implementation is possible by changing the sign of the cubic coefficient in the Duffing system. However, despite the simplicity of this approach, negative stiffness could occur for large displacements and therefore a better representation of the soften-

ing nonlinearity is needed.

Consider the system

$$\ddot{u}(t) + 2\zeta\omega_n\dot{u}(t) + \omega_n^2 z(t) = h(t) \tag{2.28}$$

where $u(t)$ and $h(t)$ are both normalized variables as defined previously, and $z(t)$ is given by

$$\dot{z}(t) = \dot{u}(t)\left(1 - (\frac{z(t)}{\beta})^n\right) \tag{2.29}$$

A similar form was proposed by Jennings [37] to model the skeleton curves of hysteretic systems. This formulation provides a smooth restoring force with an asymptotic value approaching a "yield" level β. The parameter n must be an even integer in order to maintain the symmetry of the restoring force. When $n = 2$, the restoring force curve is identical to the hyperbolic tangent function. This case will be employed in the present formulation.

The stiffness characteristics of this model are shown in Fig. 2.3 where the nonlinear parameter γ is defined as $\gamma \equiv -1/\beta^2$. As in the case of hardening example, the uncertainty will be associated with the variation of the parameter γ. In addition, uncertain damping is incorporated into the analysis. It is assumed that the damping coefficient and the nonlinear parameter are independent random variables given by

$$\zeta = \bar{\zeta} + \lambda_1 b_1 \tag{2.30}$$

and

$$\gamma = \bar{\gamma} + \lambda_2 b_2 \tag{2.31}$$

Then, the equation of motion is written as

$$\ddot{u}(t, b_1, b_2) + 2(\bar{\zeta} + \lambda_1 b_1)\omega_n\dot{u}(t, b_1, b_2) + \omega_n^2 z(t, b_1, b_2) = h(t)$$

$$\dot{z}(t,b_1,b_2) - \dot{u}(t,b_1,b_2)\left[1 + (\bar{\gamma} + \lambda_2 b_2) z^2(t,b_1,b_2)\right] = 0 \tag{2.32}$$

The solution of Eqn. (2.32) is expanded in terms of two-dimensional orthogonal polynomials as

$$u(t,b_1,b_2) = \sum_{|\mathbf{i}|=0}^{NP} \xi_{i_1 i_2}(t) H_{i_1 i_2}(b_1,b_2) \tag{2.33}$$

$$z(t,b_1,b_2) = \sum_{|\mathbf{i}|=0}^{NP} \eta_{i_1 i_2}(t) H_{i_1 i_2}(b_1,b_2) \tag{2.34}$$

The final deterministic equation set to be evaluated numerically then becomes

$$\ddot{\xi}_{i_1 i_2}(t) + 2\bar{\zeta}\omega_n \dot{\xi}_{i_1 i_2}(t) + 2\lambda_1 \omega_n \sum_{|\mathbf{j}|=0}^{NP} T_{i_1 j_1} \dot{\xi}_{j_1 j_2}(t)\delta_{i_2 j_2} + \omega_n^2 z_{i_1 i_2}(t) = h(t)\delta_{0 i_1}\delta_{0 i_2}$$

$$\dot{\eta}_{i_1 i_2}(t) - \dot{\xi}_{i_1 i_2}(t) - \sum_{|\mathbf{j}|=0}^{NP}\sum_{|\mathbf{k}|=0}^{NP}\sum_{|\mathbf{l}|=0}^{NP} (\bar{\gamma} R_{i_2 j_2 k_2 l_2} + \lambda S_{i_2 j_2 k_2 l_2}) R_{i_1 j_1 k_1 l_1} \dot{\xi}_{j_1 j_2}(t)\eta_{k_1 k_2}(t)\eta_{l_1 l_2}(t) = 0$$

$$|\mathbf{i}| = 0, \cdots, NP \tag{2.35}$$

where R_{ijkl} and S_{ijkl} are defined previously and T_{ij} is given by

$$T_{ij} = E[b' H_i(b') H_j(b')] \tag{2.36}$$

2.6.1 Numerical Examples

The following numerical examples use the same earthquake base excitation employed previously. The damping coefficient and the nonlinear parameter are both assumed to be distributed according to the Ultraspherical distribution, $M = 2$, with a 10% coefficient of variation. All the example results given by the proposed method are based on a third-order approximation.

case (I)

It is well known that for a lightly damped *linear* oscillator, uncertainty in damping and stiffness mainly introduce randomness in the amplitude and phase respectively. Thus, for a moderate-size uncertainty, the response variability due to damping is generally less significant than that due to stiffness. It is of interest to investigate the damping induced response variability under the influence of a nonlinear stiffness.

To provide a primitive comparison in this regard, a linear structure and two nonlinear structures with different levels of softening nonlinearity are selected. These structures are assumed to have the same levels of damping uncertainties given by $\bar{\zeta} = 2\%$ and $\lambda_1 = 0.002$. The results are compared in Fig. 2.13. The long dash lines represent the response statistics of the softening structure with deterministic stiffness characterized by $f_n = 1$ Hz, $\bar{\gamma} = -1$ and $\lambda_2 = 0$. The short dash lines are the response statistics of the structure with a higher level of nonlinearity characterized by $f_n = 1$ Hz, $\bar{\gamma} = -2$ and $\lambda_2 = 0$. The solid lines correspond to the associated linear structure.

As expected, the response standard deviation of the linear structure is confined within a low level. By contrast, the peak value of the standard deviation is nearly four times larger in the nonlinear case $\bar{\gamma} = -1$ and is nearly eight times larger in the stronger nonlinear case $\bar{\gamma} = -2$. For both nonlinear cases, the envelopes of the standard deviation response increase monotonically in time for a period of roughly 10 seconds. The rate of increase is seen to be approximately proportional to the amplitude of the mean response. One possible explanation of this is that the stiffness nonlinearity results in stronger correlation between the amplitude and the phase of the response. The higher the degree of nonlinearity, the stronger the amplitude-phase correlation. Thus, the accumulation of random phase shift in time makes the effect of uncertain damping substantially larger.

case (II)

In this case study, consideration is given to the cases with uncertain nonlinear parameter only and uncertainty in both damping and nonlinear stiffness. The latter case is also validated by the simulation method, where a total 900 samples runs are performed (30 equally-spaced samples in each uncertain parameter) and the response statistics are evaluated by a two-dimensional numerical integration scheme. The response statistics of the these cases of uncertainty are compared in Fig. 2.14.

The mean responses are qualitatively similar. Furthermore, the cases of uncertain nonlinear parameter and uncertain damping have approximately the same influence on the response standard deviation. When both uncertainties are present simultaneously, an additional 20% increase in the response standard deviation is observed.

A comparison with the simulation method is presented in Fig. 2.15. The proposed method solution is in good agreement with the simulation results except for a slight underestimation of the response standard deviation for large time.

2.7 Summary and Conclusions

The dynamic response of structural systems with uncertain parameters is investigated in this chapter. An expansion method based on orthogonal polynomials is proposed for analyzing the response statistics. The superiority of this approach to the perturbation approach is demonstrated through several examples. From the example problems presented, it is observed that response uncertainty depends both on uncertain parameters and the response time history. This dependency reveals the complicated nature of nonlinear problems with parameter uncertainties. The effect of uncertain damping can become substantial when nonlinear stiffness is present.

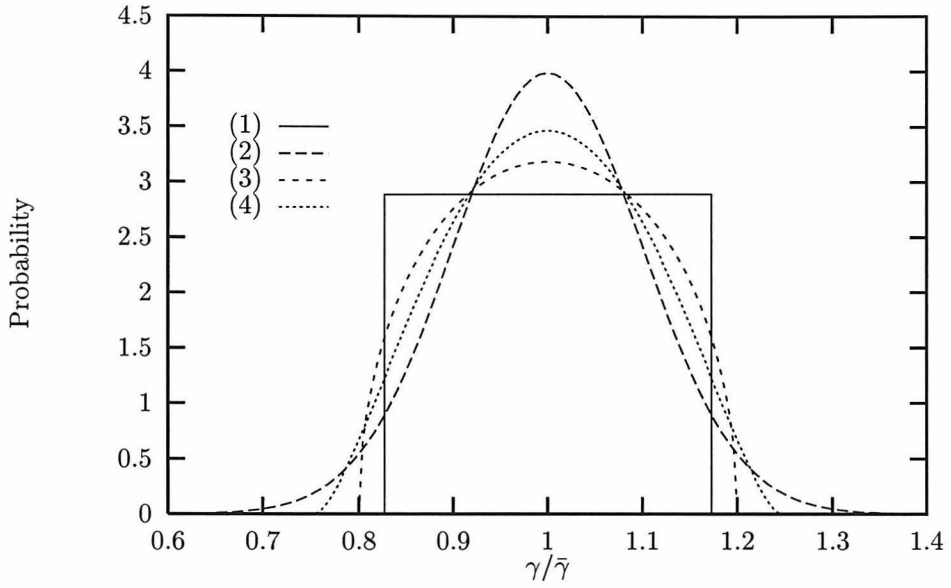

Figure 2.1: Comparison of probability density functions of a random variable γ with 10% coefficient of variance, (1):uniform distribution; (2):normal distribution; (3):Ultraspherical distribution, $M = 1$; (4):Ultraspherical distribution, $M = 2$.

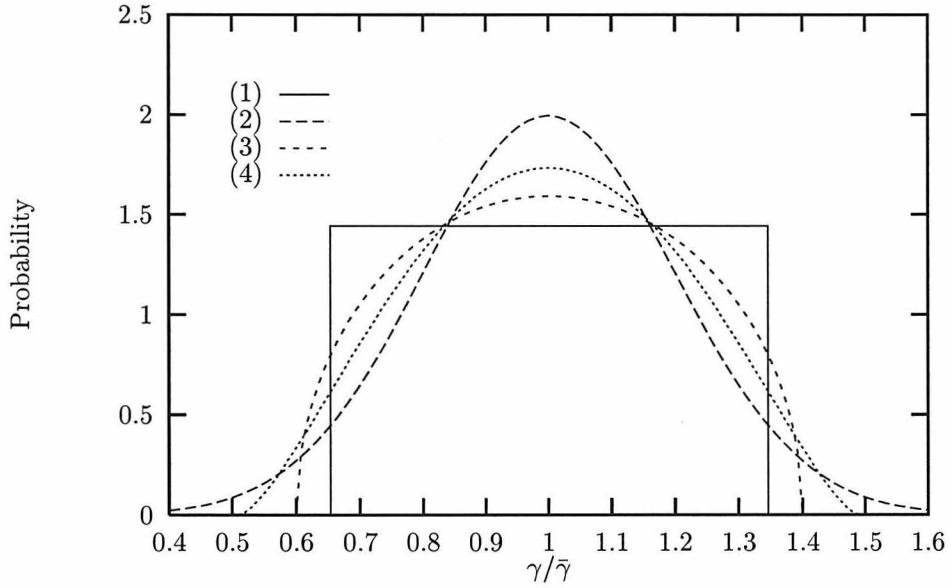

Figure 2.2: Comparison of probability density functions of a random variable γ with 20% coefficient of variance, (1):uniform distribution; (2):normal distribution; (3):Ultraspherical distribution, $M = 1$; (4):Ultraspherical distribution, $M = 2$.

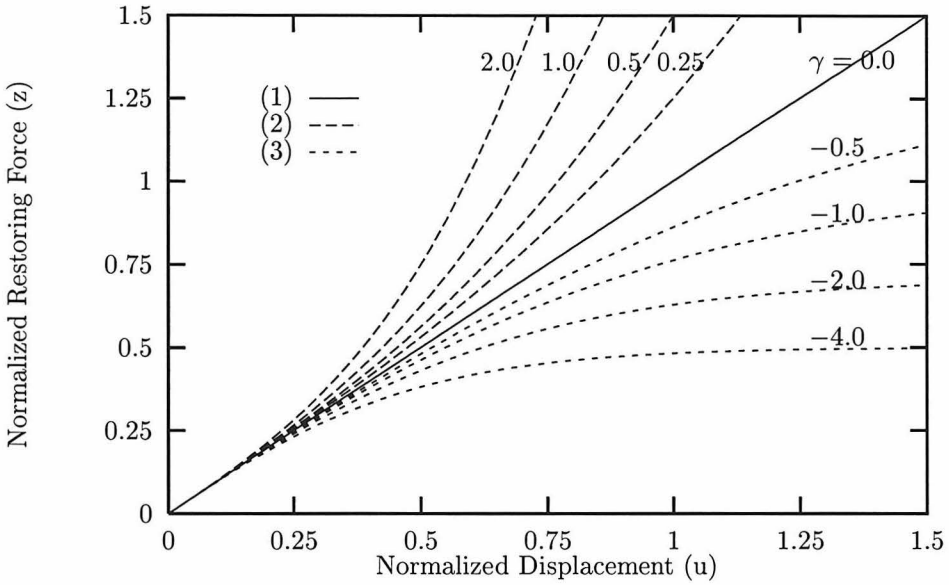

Figure 2.3: Stiffness characteristics of (1): linear system, (2): hardening system, $z = u + \gamma u^3$ and (3): softening system, $dz/du = 1 + \gamma z^2$.

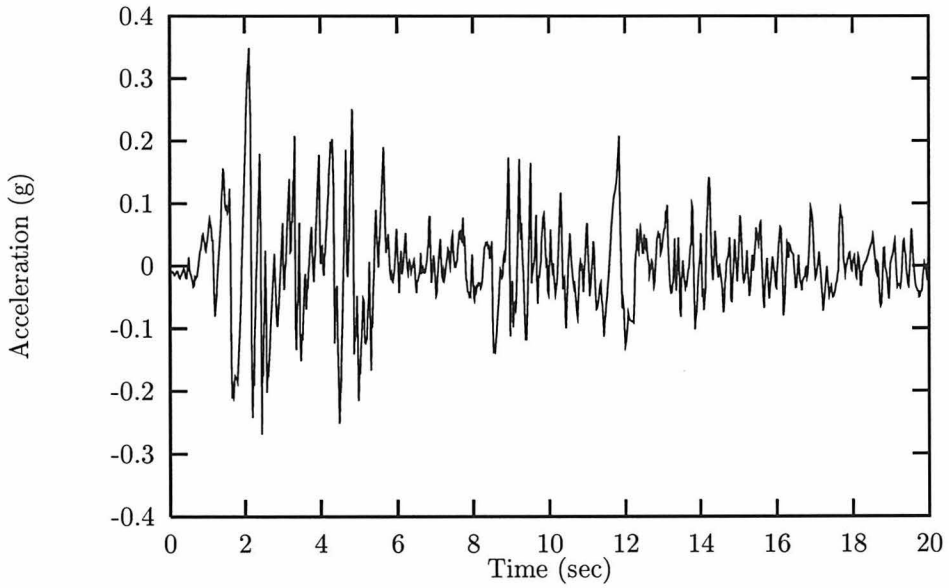

Figure 2.4: N00E component of 1940 El Centro Earthquake.

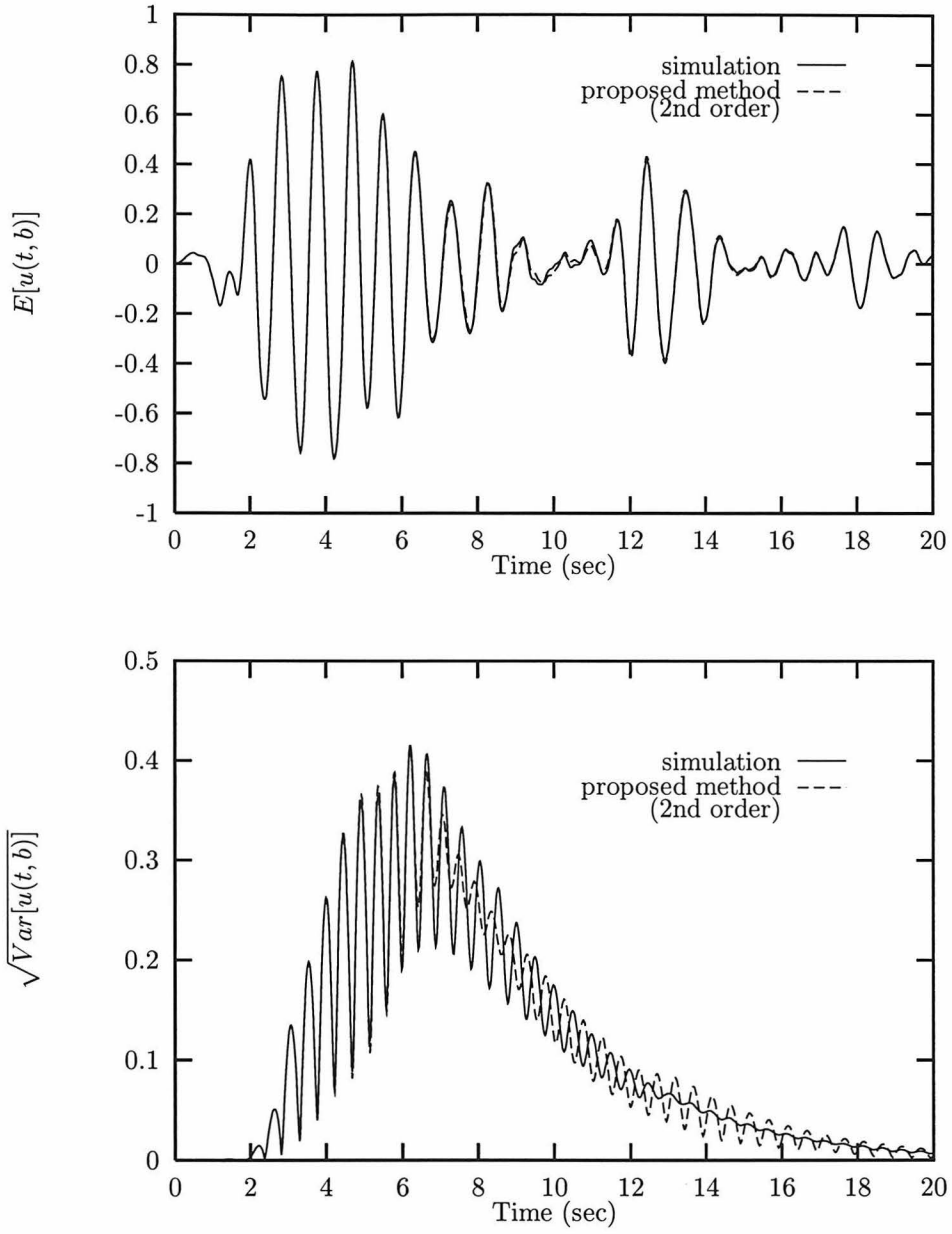

Figure 2.5: Comparison of mean and standard deviation of normalized displacement response (second-order approximation) for a hardening Duffing oscillator subjected to El Centro N00E, $f_n = 1$ Hz, $\zeta = 5\%$, $\bar{\gamma} = 0.5$, $\lambda = 0.25$.

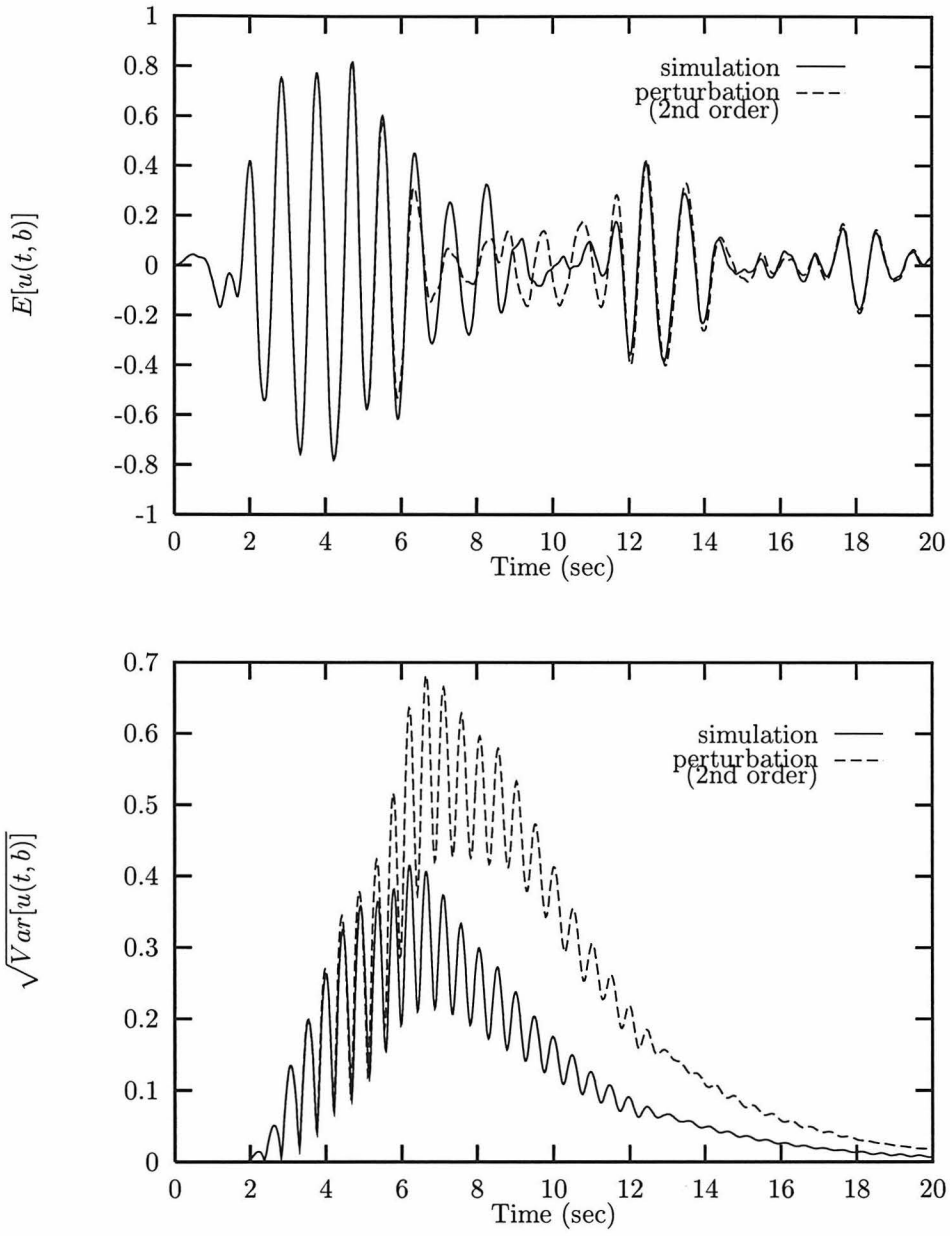

Figure 2.6: Comparison of mean and standard deviation of normalized displacement response (second-order approximation) for a hardening Duffing oscillator subjected to El Centro N00E, $f_n = 1$ Hz, $\zeta = 5\%$, $\bar{\gamma} = 0.5$, $\lambda = 0.25$.

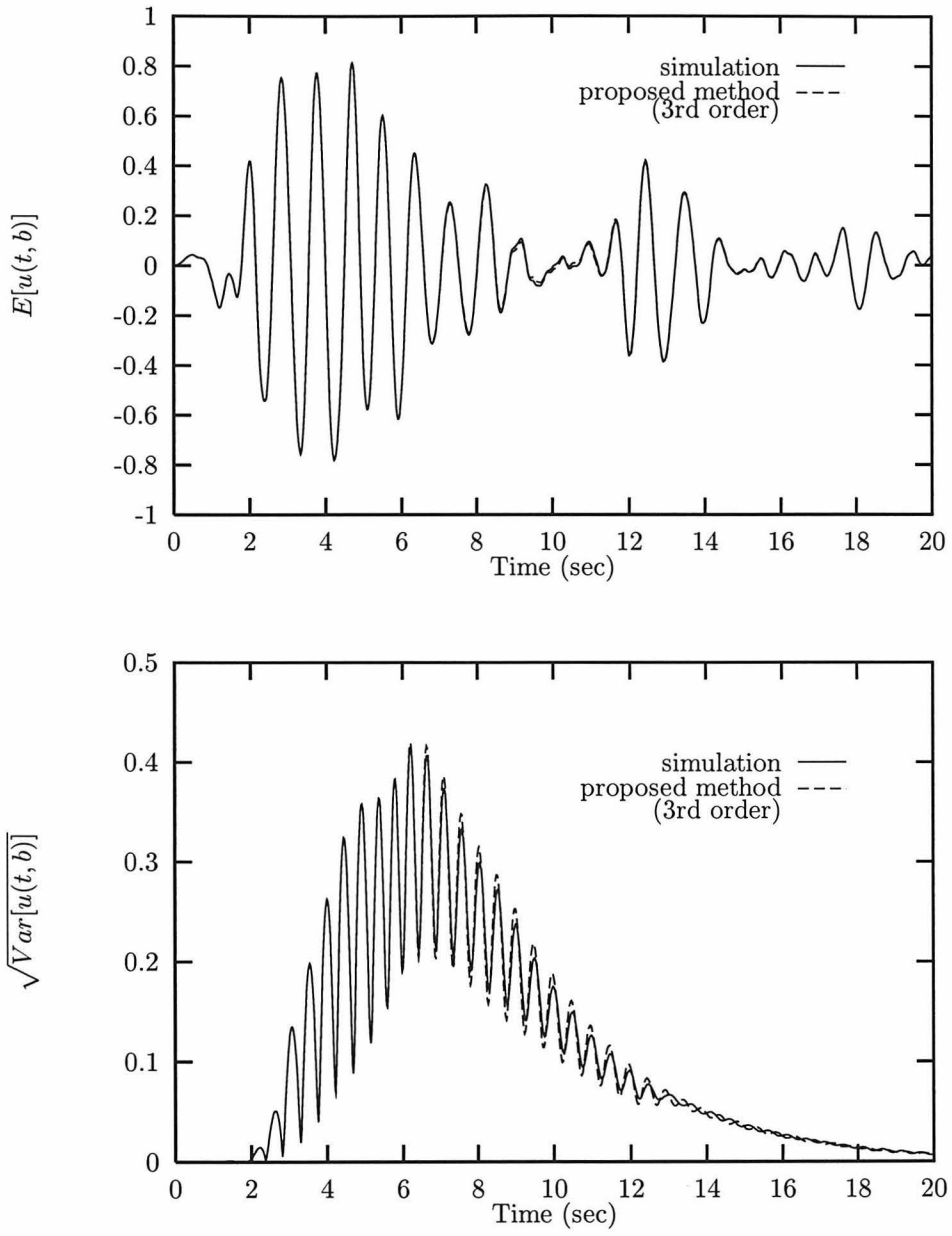

Figure 2.7: Comparison of mean and standard deviation of normalized displacement response (third-order approximation) for a hardening Duffing oscillator subjected to El Centro N00E, $f_n = 1$ Hz, $\zeta = 5\%$, $\bar{\gamma} = 0.5$, $\lambda = 0.25$.

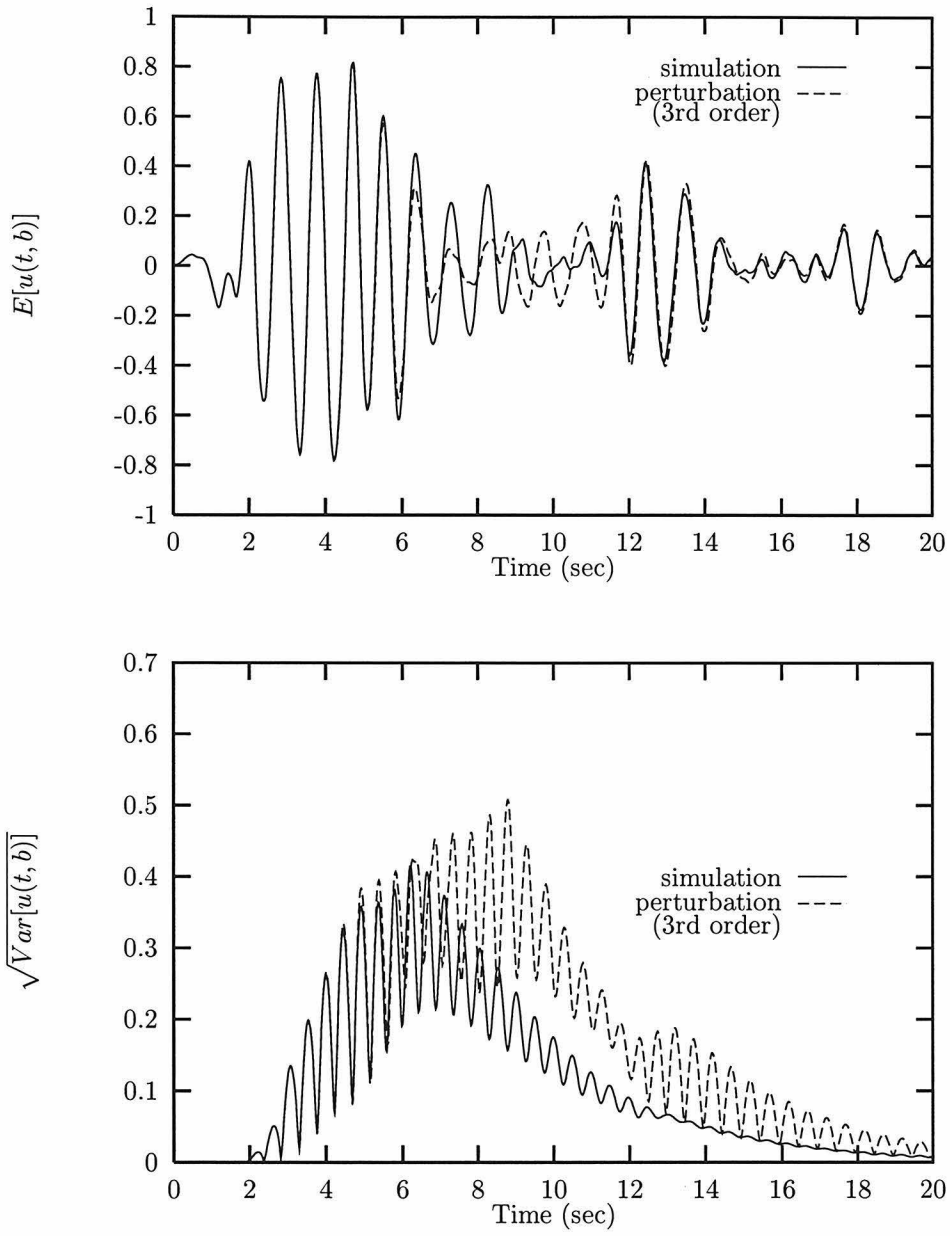

Figure 2.8: Comparison of mean and standard deviation of normalized displacement response (third-order approximation) for a hardening Duffing oscillator subjected to El Centro N00E, $f_n = 1$ Hz, $\zeta = 5\%$, $\bar{\gamma} = 0.5$, $\lambda = 0.25$.

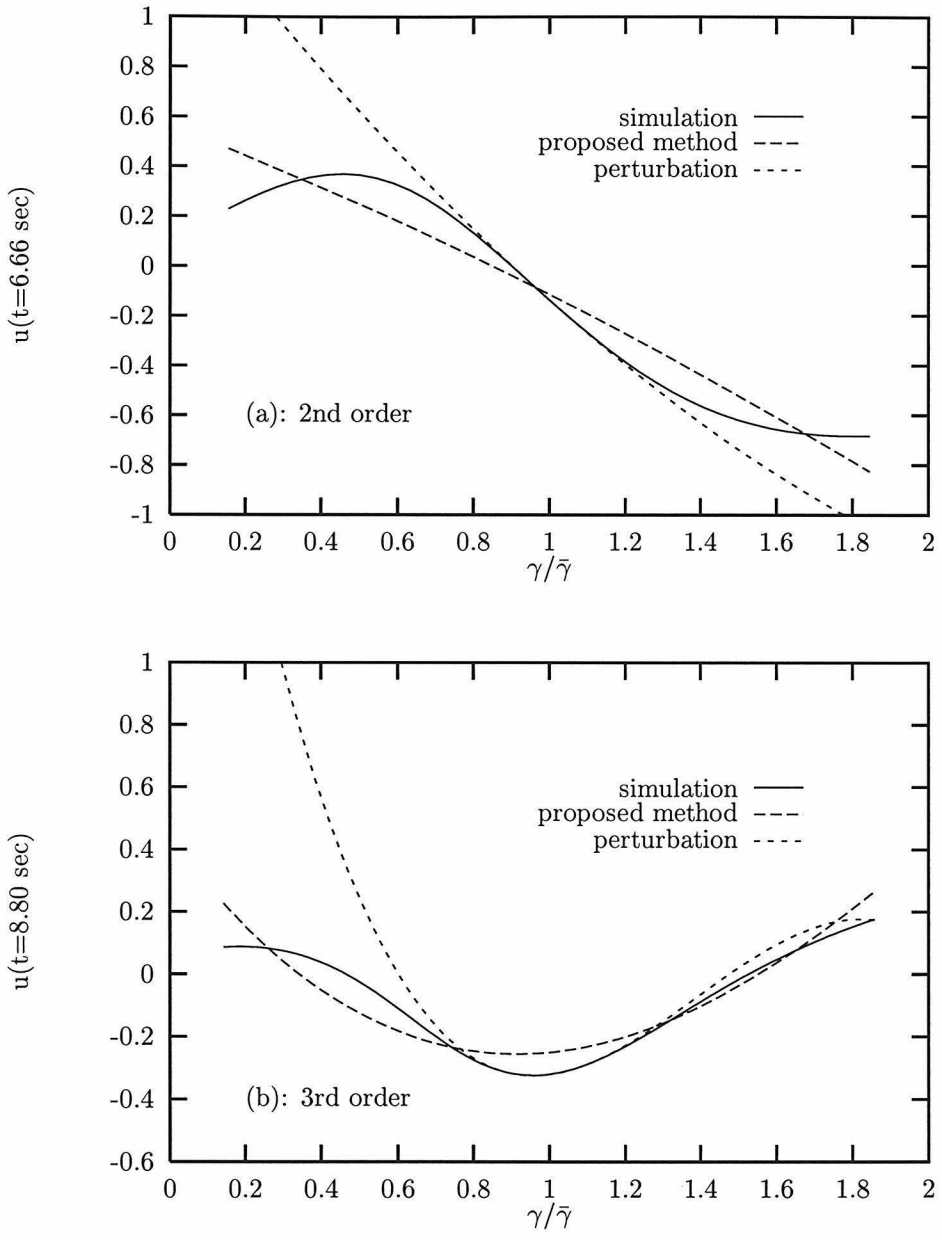

Figure 2.9: Comparison of normalized displacement responses as a function of $\gamma/\bar{\gamma}$ at (a): $t = 6.66$ sec., second-order approximation; (b): $t = 8.80$ sec., third-order approximation.

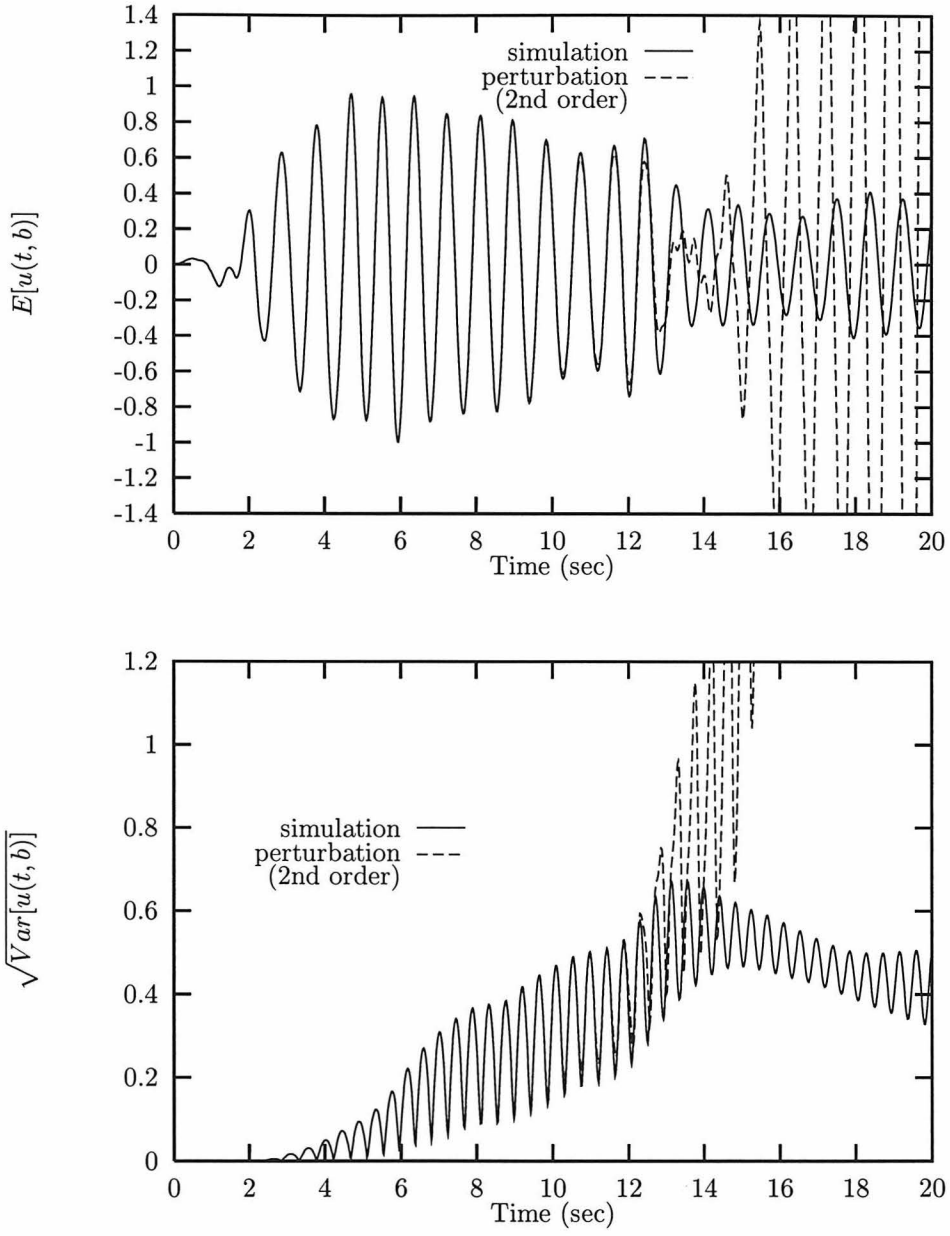

Figure 2.10: Comparison of mean and standard deviation of normalized displacement response (second-order approximation) for a hardening Duffing oscillator subjected to El Centro N00E, $f_n = 1$ Hz, $\zeta = 1\%$, $\bar{\gamma} = 0.5$, $\lambda = 0.05$.

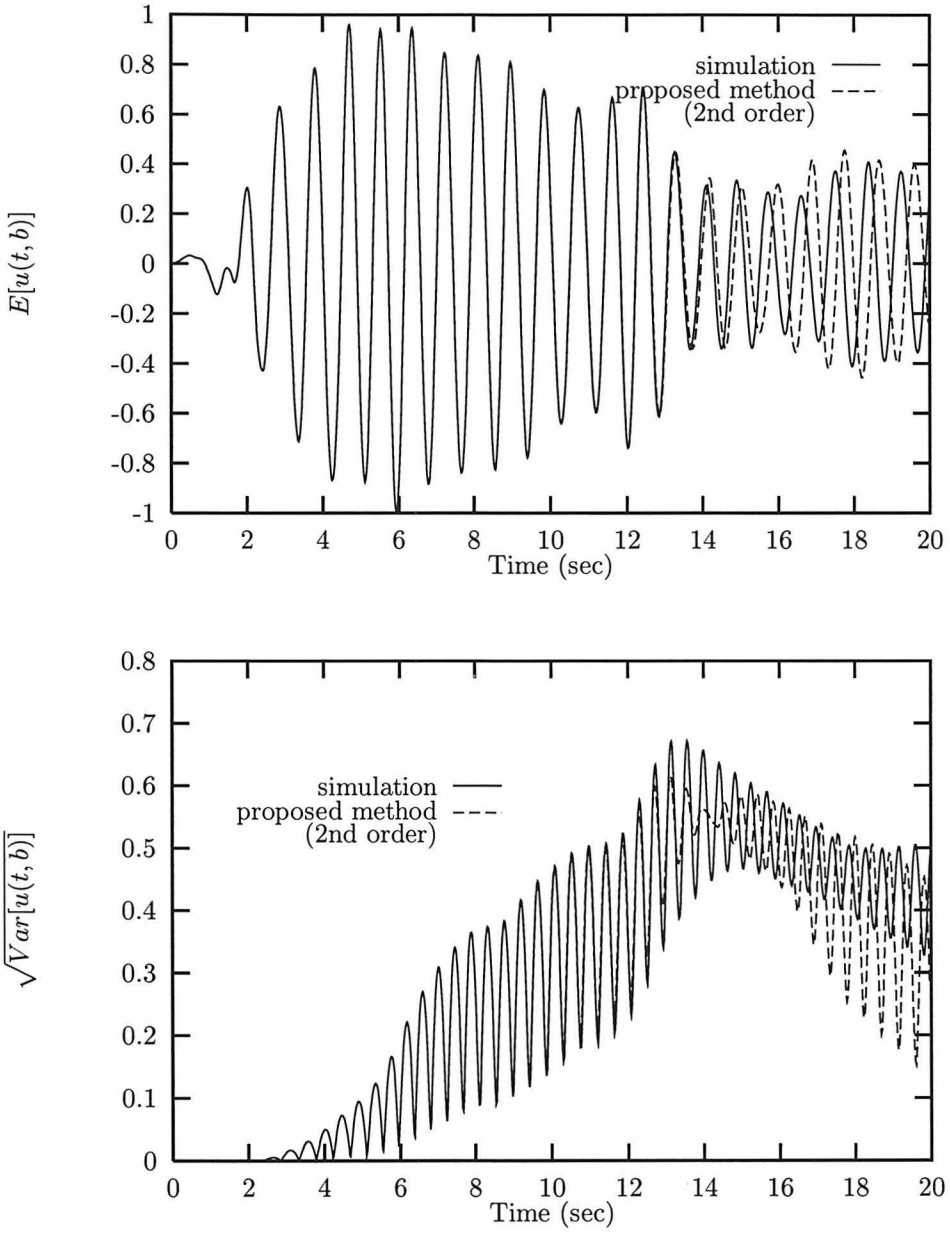

Figure 2.11: Comparison of mean and standard deviation of normalized displacement response (second-order approximation) for a hardening Duffing oscillator subjected to El Centro N00E, $f_n = 1$ Hz, $\zeta = 1\%$, $\bar{\gamma} = 0.5$, $\lambda = 0.05$.

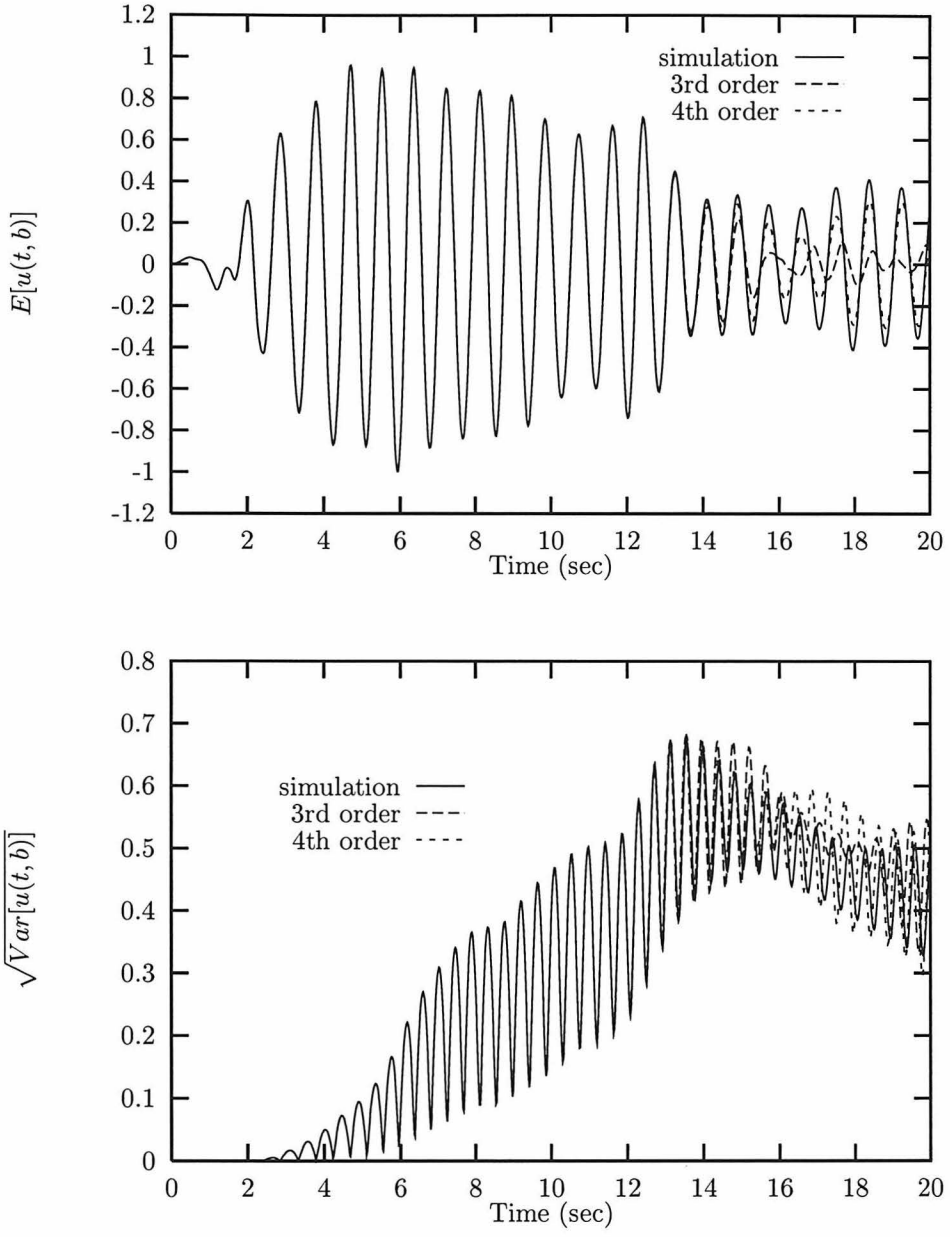

Figure 2.12: Effect of order of approximation for the proposed method. Hardening Duffing oscillator subjected to El Centro N00E, $f_n = 1$ Hz, $\zeta = 1\%$, $\bar{\gamma} = 0.5$, $\lambda = 0.05$.

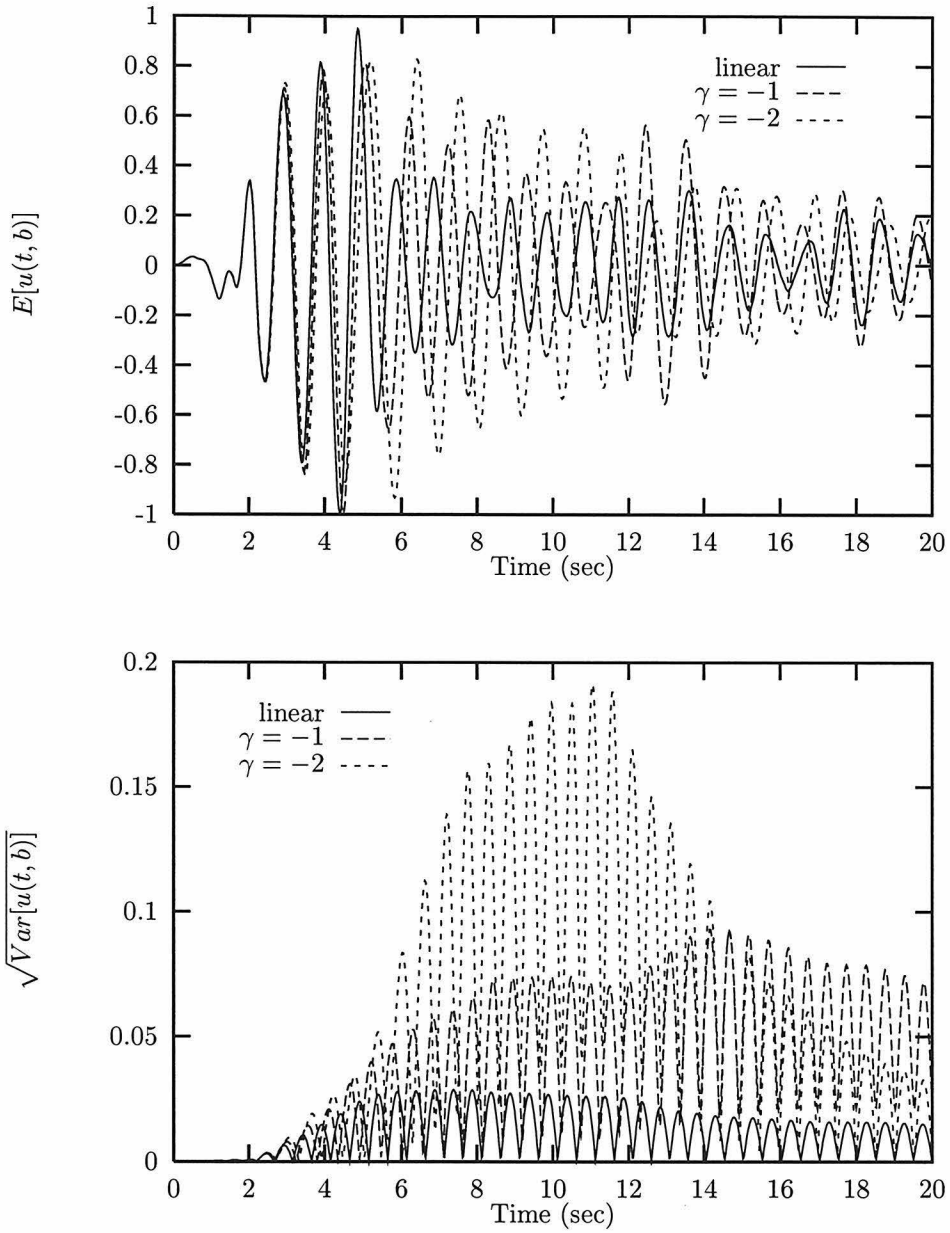

Figure 2.13: Mean and standard deviation of normalized displacement response of linear ($\bar{\gamma} = 0$, $\lambda_2 = 0$) and two softening nonlinear oscillators, ($\bar{\gamma} = -1$, $\lambda_2 = 0$) and ($\bar{\gamma} = -2$, $\lambda_2 = 0$), with damping uncertainty subjected to EL Centro N00E, $f_n = 1$ Hz, $\bar{\zeta} = 2\%$, $\lambda_1 = 0.002$.

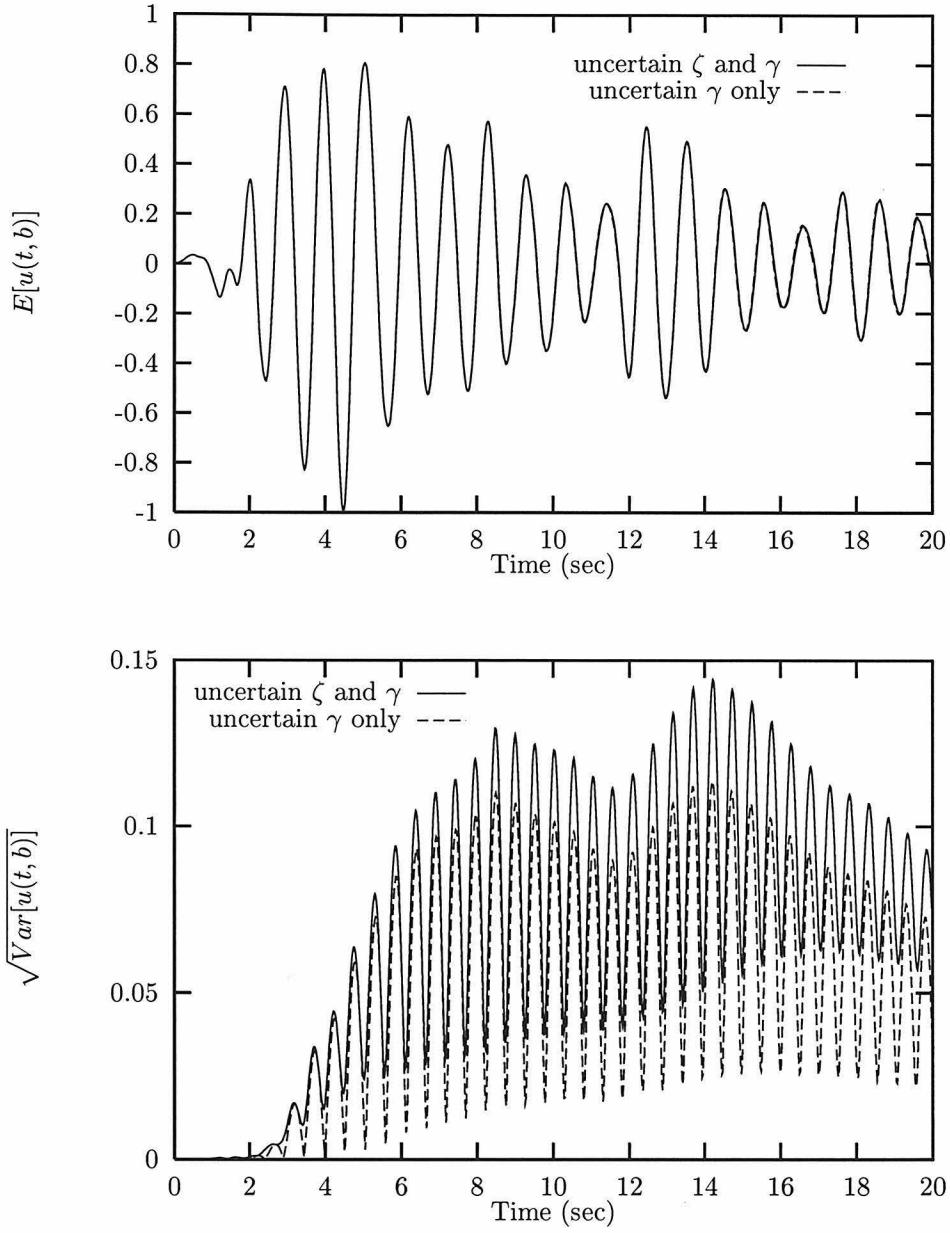

Figure 2.14: Mean and standard deviation of normalized displacement response for softening nonlinear oscillator with uncertain nonlinear parameter, $f_n = 1$ Hz, $\bar{\zeta} = 2\%$, $\bar{\gamma} = -1$, $\lambda_1 = 0$, $\lambda_2 = 0.1$, and both uncertain damping and nonlinear parameter, $f_n = 1$ Hz, $\bar{\zeta} = 2\%$, $\bar{\gamma} = -1$, $\lambda_1 = 0.002$, $\lambda_2 = 0.1$.

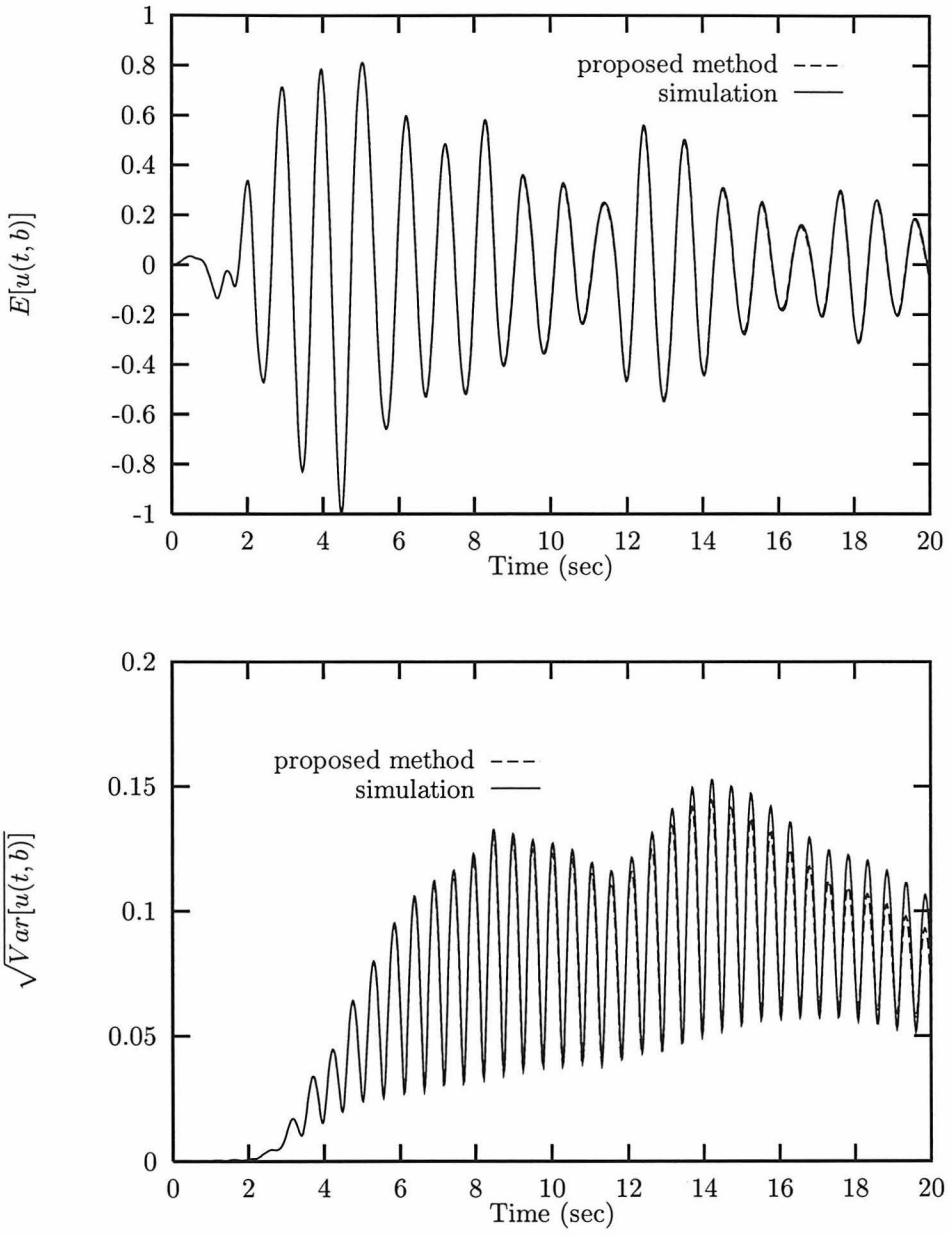

Figure 2.15: Comparison of mean and standard deviation of normalized displacement response for softening nonlinear oscillator with both uncertain damping and nonlinear parameter, $f_n = 1$ Hz, $\bar{\zeta} = 2\%$, $\bar{\gamma} = -1$, $\lambda_1 = 0.002$, $\lambda_2 = 0.1$.

Chapter 3

Nonlinear Continuous Systems with Uncertain Parameters

3.1 Introduction

The dynamic response of continuous systems may be greatly affected by spatial variations of material properties and boundary conditions, as well as the system nonlinearities. The effect of any variation in the above mentioned properties and conditions becomes an important consideration in performing a dynamic analysis for such systems. Due to the fact that most physical properties can not be precisely prescribed, a plausible analysis approach is to introduce a statistical description in an assumed analytical model. A second-moment analysis can then be performed to assess the response variability. Such an analysis approach leads to a dynamic problem defined over a nonlinear random medium, which is potentially challenging to both analytical and numerical solution methods.

In this chapter, a solution method is provided for analyzing the response uncertainty of uncertain nonlinear continuous systems subjected to deterministic dynamic loadings. As an extension of the solution scheme presented in the previous chapter, this method employs the discrete Karhunen-Loève decomposition and a generalized spatial discretization to approximate the nonlinear random continuum by a discrete system with a set of independent random variables. The solution technique developed previously is then applied to the resulting random equations for numerical evaluation

of response statistics. The solution method is illustrated through the formulation of a one-dimensional wave equation with uncertain stiffness parameter fields in the sequel.

3.2 Problem Formulation

Consider a one-dimensional scalar wave equation described by the partial differential equation (PDE)

$$\frac{\partial}{\partial x}\left(\tau(k(x), w)\right) - q(c(x), \dot{w}) = m(x)\ddot{w} + p(x,t) \quad \text{in } \mathcal{D}(x) \tag{3.1}$$

where $w = w(t,x)$ is the dependent variable representing a scalar "displacement" field, $m(\cdot)$ is the "mass" distribution of the system, $q(\cdot,\cdot)$ is the linear "damping" operator, $\tau(\cdot,\cdot)$ is the "stress" operator, $k(\cdot)$ and $c(\cdot)$ are the "stiffness" and "damping" parameter fields, and $p(x,t)$ is the external dynamic loading. The symbol $\mathcal{D}(x)$ denotes the domain in which the PDE is defined. Since the problem is one-dimensional, $\mathcal{D}(x)$ represents a line segment in the x-axis. The PDE is assumed to have zero initial conditions and the following boundary conditions

$$B^g(w) = 0 \quad \text{on } \partial\mathcal{D}(x) \tag{3.2}$$

$$B^n(w) = 0 \quad \text{on } \partial\mathcal{D}(x) \tag{3.3}$$

where B^g and B^n are the geometric and natural boundary conditions respectively.

Eqn. (3.1) together with the initial and boundary conditions form a one-dimensional initial-boundary value problem. This problem arises, for examples, in the studies of the torsional vibration of a shaft, the axial vibration of a rod, the vibration of a string, or the wave propagation in a shear beam.

In many engineering applications, the system is approximately linear for a small amplitude of response. However, the nonlinear effect usually becomes important when

the system undergoes large response. To account for the nonlinear effect, the stress operator τ is assumed to be a nonlinear operator expressible in terms of a sum of a linear stress operator τ^L and a nonlinear stress operator τ^N as

$$\tau(k(x), w) = \tau^L(k^L(x), w) + \tau^N(k^N(x), w) \tag{3.4}$$

where $k^L(x)$ and $k^N(x)$ are respectively the linear and nonlinear "stiffness" parameter fields associated with τ^L and τ^N. This expression accommodates problems with nonlinear stress-strain characteristics and problems with nonlinear strain-displacement relationships.

In the current formulation, the source of uncertainty is assumed to be due to the spatial variations of the linear and/or nonlinear stiffness parameter fields. The manner in which these uncertain parameter fields are introduced determines the model of uncertainty for the system, and consequently implies the pattern of response uncertainty. To illustrate this, consider the case where the nonlinear stiffness parameter field is the only source of uncertainty. Then, the system is deterministic if the response is confined within a linear range, and the uncertainty occurs for a nonlinear response. On the other hand, when both stiffness parameter fields are assumed to be uncertain, response uncertainty is present for all levels of response. The randomness properties of these parameter fields can be appropriately assumed to conform to the physics of problems.

The stiffness parameter fields are idealized as joint second-order Gaussian random fields. The uncertain physical properties, such as the spatial fluctuation, can then be addressed through a mathematical second-moment representation. The statistical properties for a Gaussian random field and a finite representation are described in the next section.

3.3 Random Field and Finite Representation

A second-order Gaussian random field is a random process defined over a spatial space whose statistical properties are fully determined by its first two moments, i.e., the mean and the covariance function. The covariance function is symmetric and positive definite. A random field is said to be *homogeneous* when the statistical properties are invariant under an arbitrary shift of the reference coordinate. In such a case, the covariance function is a function of relative distance only. Otherwise, it is referred to as *inhomogeneous*.

A finite representation of a Gaussian random field is expressed in terms of a set of independent Gaussian random variables with an associated set of deterministic spatial functions. This representation is useful because it permits the continuum of random variables to be represented by a denumerable set of independent random variables. The Karhunen-Loève orthogonal decomposition is a widely used technique to achieve such a finite representation [31]. However, this process requires an eigenvalue-eigenfunction solution to an integral equation with a covariance kernel. The induced mathematical difficulty limits its applications to only a few special cases.

An alternative numerical scheme, referred to as the discrete Karhunen-Loève decomposition [38], is adopted in the present formulation. In this procedure, the continuous random field is sampled at an indexed set of spatial points. The resulting correlated random variables are then transformed into independent random variables using a matrix decomposition of the covariance matrix. Hence, the original infinite dimensional eigenvalue-eigenfunction problem is replaced by a finite dimensional eigenvalue-eigenvector problem. The discretization scheme and its implication are described in the following subsections.

3.3.1 Basis Random Variables

Let $G(x)$ be a one-dimensional second-order Gaussian random field. The random field can be separated into its deterministic mean component and a random fluctuation component by

$$G(x) = \bar{G}(x) + Y(x) \tag{3.5}$$

In the above expression, $\bar{G}(x)$ is the mean value of $G(x)$ given by

$$\bar{G}(x) = E[G(x)] \tag{3.6}$$

where $E[\cdot]$ is the expectation operator, and $Y(x)$ is a zero-mean second-order Gaussian field characterized by a covariance function $R(\xi, \eta)$. That is,

$$E[Y(\xi)Y(\eta)] = R(\xi, \eta) \tag{3.7}$$

Let $Y(x)$ be approximated by $\tilde{Y}(x)$ expressed in terms of a denumerable set of random variables as

$$\tilde{Y}(x) = \sum_{n=1}^{ND} \sum_{m=1}^{ND} b_n S_{nm} \varphi_m(x) \tag{3.8}$$

where $\{b_n\}_{n=1}^{ND}$ is a set of independent random variables with zero means and unit variances, $\{\varphi_m(x)\}_{m=1}^{ND}$ is a set of known deterministic spatial functions, and S_{nm} are unknown constants to be determined. Denote $\tilde{R}$ as the covariance function of the approximate process $\tilde{Y}(x)$. Then, the expression for $\tilde{R}$ is given by

$$\begin{aligned} \tilde{R}(\xi, \eta) &= E[\tilde{Y}(\xi)\tilde{Y}(\eta)] \\ &= \sum_{n=1}^{ND} \sum_{m=1}^{ND} \sum_{s=1}^{ND} S_{nm} S_{ns} \varphi_m(\xi) \varphi_s(\eta) \end{aligned} \tag{3.9}$$

The expressions for the unknown constants S_{nm} are obtained such that the difference of the covariance functions $R(\xi, \eta)$ and $\tilde{R}(\xi, \eta)$ is minimized based on a certain

criterion. To achieved this, the following equations are employed

$$\int_{\mathcal{D}(x)} \int_{\mathcal{D}(x)} w_{ij}(\xi,\eta)[R(\xi,\eta) - \tilde{R}(\xi,\eta)]d\xi d\eta = 0, \quad i,j = 1,\cdots,ND \tag{3.10}$$

where $w_{ij}(\xi,\eta)$ are a set of weighting functions. Several selections for the weighting functions and the known spatial functions are applicable. One convenient selection for $\varphi_m(x)$ is a collection of the Lagrange family of interpolation functions. Let an indexed set of spatial points $\{x_i\}_{i=1}^{ND}$ be associated with the interpolation functions. Then, the interpolation functions satisfy

$$\varphi_m(x_i) = \delta_{mi} \tag{3.11}$$

where δ_{nm} is the Kronecker delta.

The weighting functions can be selected as a set of delta functions placed over the indexed spatial points. The expressions for the weighting functions are given by

$$w_{ij}(\xi,\eta) = w_{ji}(\xi,\eta) = \delta(x_i)\delta(x_j) \tag{3.12}$$

where $\delta(\cdot)$ is the Dirac delta function. Hence, the difference of covariance functions is forced to vanish at each indexed spatial point.

Substituting Eqns. (3.9), (3.11) and (3.12) into Eqn. (3.10) will lead to the following algebraic equations

$$R(x_i,x_j) = \sum_{n=1}^{ND} S_{ni}S_{nj}, \quad i,j = 1,\cdots,ND \tag{3.13}$$

The above equations are equivalent to a matrix equation of the form

$$\mathbf{R} = \mathbf{S}^T\mathbf{S} \tag{3.14}$$

Since the correlation function R is symmetric and positive definite, the correlation

matrix $\mathbf{R}$ is also symmetric and positive definite, which admits a spectral decomposition given by

$$\mathbf{R} = \mathbf{\Psi}\mathbf{\Lambda}\mathbf{\Psi}^T \tag{3.15}$$

where $\mathbf{\Psi}$ is the matrix of eigenvectors satisfying $\mathbf{\Psi}\mathbf{\Psi}^T = \mathbf{I}$, and $\mathbf{\Lambda}$ is a diagonal matrix of the eigenvalues arranged in a decreasing order. It follows that the expression for $\mathbf{S}$ is related to the eigenvalue and eigenvector matrices by

$$\mathbf{S} = \mathbf{\Lambda}^{\frac{1}{2}}\mathbf{\Psi}^T \tag{3.16}$$

With the numerical values of S_{nm}, let $G_n(x)$ be the deterministic spatial functions associated with the random variable b_n defined by

$$G_n(x) = \sum_{m=1}^{ND} S_{nm}\varphi_m(x) \tag{3.17}$$

Combining Eqn. (3.8), Eqn. (3.5) and Eqn. (3.17), the continuous random field is thus represented as

$$G(x) \cong \bar{G}(x) + \sum_{n=1}^{ND} b_n G_n(x) \tag{3.18}$$

Eqn. (3.18) is a finite representation for the random field $G(x)$. This representation involves a set of independent random variables, which is considered as the basis random variables for the system.

3.3.2 Finite Random System

The feasibility and applicability of the finite representation rely on two important statistical properties associated with the random field. The first property is the magnitude of the randomness relative to the mean value of the parameter field. This property is prescribed by the coefficient of variation in the random field model. The second property is the degree of spatial fluctuation relative the size of the domain,

which is characterized by the ratio of the correlation length of the random field to the total length of the physical system. Consider an extreme case where the random field is totally correlated. Then, the system possesses only one degree of randomness. That is, the finite representation contains only one random variable and the associated spatial function is a spatially uniform function. The other extreme case, where the random field is delta-correlated, represents a white noise assumption for the parameter field. In this case, a set of theoretically infinite many random variables is required to represent the random field.

In the subsequent formulations, the correlation distance for the uncertain parameter fields is assumed to be comparatively large to the total length of the problem domain. As a result, the discrete Karhunen-Loève decomposition yields a set of eigen-solutions with rapidly decreasing magnitude. In addition, the randomness is assumed to be "small" which allows one to neglect the relatively small contribution from those random variables with higher indices. With these assumptions, the degree of randomness governing the system can be greatly reduced without significant loss of accuracy for an engineering consideration.

Thus, let the stiffness parameter fields $k^L(x)$ and $k^N(x)$ be represented in terms of the first NR pairs of eigen-solutions by

$$k^L(x) \cong \bar{k}^L(x) + \sum_{n=1}^{NR} b_n k_n^L(x) \tag{3.19}$$

$$k^N(x) \cong \bar{k}^N(x) + \sum_{n=1}^{NR} b_n k_n^N(x) \tag{3.20}$$

where $\bar{k}^L(x)$ and $\bar{k}^N(x)$ denote the mean values of the linear and nonlinear stiffness parameter fields, and $k_n^L(x)$ and $k_n^N(x)$ symbolize the deterministic spatial functions associated with random variable b_n.

It is further assumed that linearity holds for the stress operators with respect to

the basis random variables. Then,

$$\tau^L(k^L(x), w) = \tau^L(\bar{k}^L(x), w) + \sum_{n=1}^{NR} b_n \tau^L(k_n^L(x), w) \tag{3.21}$$

$$\tau^N(k^N(x), w) = \tau^N(\bar{k}^N(x), w) + \sum_{n=1}^{NR} b_n \tau^N(k_n^N(x), w) \tag{3.22}$$

Substituting Eqns. (3.21) and (3.22) into Eqn. (3.1) yields an approximated random PDE as

$$\begin{aligned} &\frac{\partial}{\partial x}\left(\tau^L(\bar{k}^L(x), \hat{w})\right) + \frac{\partial}{\partial x}\left(\tau^N(\bar{k}^N(x), \hat{w})\right) - q(c(x), \dot{\hat{w}}) \\ &+ \sum_{n=1}^{NR} b_n \left\{ \frac{\partial}{\partial x}\left(\tau^L(k_n^L(x), \hat{w})\right) + \frac{\partial}{\partial x}\left(\tau^N(k_n^N(x), \hat{w})\right) \right\} \\ &\qquad = m(x)\ddot{\hat{w}} + p(x,t) \quad \text{in } \mathcal{D}(x) \end{aligned} \tag{3.23}$$

where $\hat{w} = \hat{w}(t, x, \mathbf{b})$ symbolizes the dependent variable of the approximated PDE as a function of t, x and $\mathbf{b} = \{b_1, b_1, \cdots, b_{NR}\}^T$. Hence, the original PDE involving the continuous parameter fields is approximated by a nonlinear PDE with finite random coefficients. Note that the functional dependency of the dependent variable contains the random variable set $\mathbf{b}$. The dependent variable in the boundary conditions given by Eqn. (3.2) are then changed accordingly.

3.4 Generalized Spatial Discretization

This section provides a weak formulation (variational formulation) for the random approximated PDE via a spatial response representation. A set of generalized spatial functions is considered in the formulation. It may represent a spatial Galerkin assumption, as used in a dynamical modal analysis, or may represent a spatial sub-domain discretization, as used in a finite element analysis.

Let the generalized spatial functions be represented as a set of NS basis spatial

functions by

$$\boldsymbol{\phi}(x) = \{\phi_1(x), \phi_2(x), \cdots, \phi_{NS}(x)\}^T \tag{3.24}$$

Associated with the set of spatial functions, introduce a vector of generalized random response variables

$$\mathbf{u}(t, \mathbf{b}) = \{u_1(t, \mathbf{b}), u_2(t, \mathbf{b}), \cdots, u_{NS}(t, \mathbf{b})\}^T \tag{3.25}$$

Then, the dependent variable $\hat{w}(t, x, \mathbf{b})$ is represented as a linear sum of $\boldsymbol{\phi}(x)$ and $\mathbf{u}(t, \mathbf{b})$ by

$$\hat{w}(t, x, \mathbf{b}) = \sum_{j=1}^{NS} u_j(t, \mathbf{b})\phi_j(x) \tag{3.26}$$

Following this response representation, the stress and damping operators are also represented in terms of $\boldsymbol{\phi}(x)$ and $\mathbf{u}(t, \mathbf{b})$ by

$$\tau^L(\cdot, \hat{w}) = \sum_{j=1}^{NS} \hat{\tau}_j^L(\cdot, \boldsymbol{\phi}(x))u_j(t, \mathbf{b}) \tag{3.27}$$

$$q(\cdot, \dot{\hat{w}}) = \sum_{j=1}^{NS} \hat{q}_j(\cdot, \boldsymbol{\phi}(x))\dot{u}_j(t, \mathbf{b}) \tag{3.28}$$

Similarly, the nonlinear stress operator is expressed as

$$\tau^N(\cdot, \hat{w}) = \hat{\tau}^N(\cdot, \boldsymbol{\phi}(x), \mathbf{u}(t, \mathbf{b})) \tag{3.29}$$

Substituting the above response representations into Eqn. (3.23), multiplying the resulting equation by the individual element of the basis spatial functions, and integrating over the spatial domain, a discrete random nonlinear ordinary differential equation can be derived. The equation may be written as

$$\mathbf{M}\ddot{\mathbf{u}} + \mathbf{C}\dot{\mathbf{u}} + \bar{\mathbf{K}}\mathbf{u} + \bar{\mathbf{g}}(\mathbf{u}) + \sum_{n=1}^{NR} b_n[\mathbf{K}_n\mathbf{u} + \mathbf{g}_n(\mathbf{u})] = \mathbf{f}(t) \tag{3.30}$$

where $\mathbf{M}$, $\mathbf{C}$ and $\mathbf{f}(t)$ are the mass matrix, damping matrix and forcing vector respectively; $\bar{\mathbf{K}}$ and $\bar{\mathbf{g}}(\cdot)$ are the mean stiffness matrix and nonlinear stiffness vector respectively; likewise, $\mathbf{K}_n$ and $\mathbf{g}_n(\cdot)$ are the stiffness matrix and nonlinear stiffness vector associated with the random variable b_n respectively.

The expression for the ijth element, indicated with a subscript ij, of these matrices and vectors are given below.

$$M_{ij} = \int_{\mathcal{D}(x)} m(x)\phi_i(x)\phi_j(x)d\mathcal{D}(x) \tag{3.31}$$

$$C_{ij} = \int_{\mathcal{D}(x)} \hat{q}_j^L(c(x), \boldsymbol{\phi}(x))\phi_i(x)d\mathcal{D}(x) \tag{3.32}$$

$$\bar{K}_{ij} = \int_{\mathcal{D}(x)} \hat{\tau}_j^L(\bar{k}(x), \boldsymbol{\phi}(x))\frac{d\phi_i(x)}{dx}d\mathcal{D}(x) \tag{3.33}$$

$$\bar{g}_i(\mathbf{u}^{(e)}) = \int_{\mathcal{D}(x)} \hat{\tau}^N(\bar{k}(x), \boldsymbol{\phi}(x), \mathbf{u})\frac{d\phi_i(x)}{dx}d\mathcal{D}(x) \tag{3.34}$$

$$K_{n_{ij}} = \int_{\mathcal{D}(x)} \hat{\tau}_j^L(k_n(x), \boldsymbol{\phi}(x))\frac{d\phi_i(x)}{dx}d\mathcal{D}(x) \tag{3.35}$$

$$g_{ni}(\mathbf{u}) = \int_{\mathcal{D}(x)} \hat{\tau}^N(k_n(x), \boldsymbol{\phi}(x), \mathbf{u})\frac{d\phi_i(x)}{dx}d\mathcal{D}(x) \tag{3.36}$$

$$f_i(t) = \int_{\mathcal{D}(x)} p(x,t)\phi_i(x)d\mathcal{D}(x) \tag{3.37}$$

$$i, j = 1, \cdots, NS \tag{3.38}$$

3.5 Deterministic Equations

The solution method developed in the previous chapter is employed herein for solving the random multi-degree-of-freedom systems resulting from the generalized spatial discretization. Let the generalized random response be expanded in terms of the orthogonal polynomials as

$$\mathbf{u}(t, \mathbf{b}) = \sum_{|\mathbf{l}|=0}^{NP} \hat{\mathbf{u}}_{l_1 l_2 \cdots l_{NR}}(t) H_{l_1 l_2 \cdots l_{NR}}(\mathbf{b}) \tag{3.39}$$

where $H_{l_1 l_2 \cdots l_{NR}}(\mathbf{b})$ are the set of NR-dimensional orthogonal polynomials satisfying the orthogonality condition

$$E[H_{l_1 l_2 \cdots l_{NR}}(\mathbf{b}) H_{s_1 s_2 \cdots s_{NR}}(\mathbf{b})] = \prod_{i=1}^{NR} \delta_{l_i s_i} \tag{3.40}$$

Since the random variables are Gaussian, these orthogonal polynomials represent the multi-dimensional Hermite polynomials. However, the Gaussian assumption has a theoretically unbounded range of random samples, which implies the possibility of a negative stiffness parameter field. Hence, it may be appropriate to approximate the Gaussian distribution by a bounded distribution, such as the family of Ultraspherical distribution. The various other types of orthogonal polynomials introduced previously are also applicable for the above formulation.

To identify the coupling between the linear terms, it is more convenient to employ the recursive relationship for the orthogonal polynomials [30]. That is,

$$b_n H_{l_n}(b_n) = a_{l_n} H_{l_n - 1}(b_n) + \bar{a}_{l_n} H_{l_n + 1}(b_n) \tag{3.41}$$

To obtain a final deterministic equation, one can first substitute Eqns. (3.41) and (3.39) into Eqn. (3.30) and multiply the resulting equation by the members of orthogonal polynomials. Then, performing the mathematical expectation operator and using the orthogonality condition, a set of deterministic nonlinear differential equations is derived as

$$\begin{aligned} &\mathbf{M}\ddot{\hat{\mathbf{u}}}_{l_1 l_2 \cdots l_{NR}}(t) + \mathbf{C}\dot{\hat{\mathbf{u}}}_{l_1 l_2 \cdots l_{NR}}(t) + \bar{\mathbf{K}}\hat{\mathbf{u}}_{l_1 l_2 \cdots l_{NR}}(t) + E[\bar{\mathbf{g}}(\mathbf{u}(t,\mathbf{b})) H_{l_1 l_2 \cdots l_{NR}}(\mathbf{b})] \\ &\qquad + \sum_{n=1}^{NR} \mathbf{K}_n \left(a_{l_n} \hat{\mathbf{u}}_{l_1 \cdots l_n - 1 \cdots l_{NR}}(t) + \bar{a}_{l_n} \hat{\mathbf{u}}_{l_1 \cdots l_n + 1 \cdots l_{NR}}(t) \right) \\ &+ \sum_{n=1}^{NR} E[\mathbf{g}_n(\mathbf{u}(t,\mathbf{b})) b_n H_{l_1 l_2 \cdots l_{NR}}(\mathbf{b})] = \mathbf{f}(t) \prod_{n=1}^{NR} \delta_{l_n 0}, \quad |\mathbf{l}| = 0, \cdots, NP \end{aligned} \tag{3.42}$$

This is a nonlinear equation set with lightly coupled linear parts and fully coupled nonlinear parts. For an efficient numerical treatment, it is preferred to have a polynomial type of nonlinearity in terms of the response variables. Due to this limitation, the proposed solution scheme can be applied to problems involving nonlinear stress-strain characteristics only on a case-by-case basis.

However, one type of nonlinearity, classified as geometrical nonlinearity, is generally expressed in a polynomial form. The governing equations for this class of nonlinear problems are derived using higher-order strain-displacement relationships [39], which results in a polynomial type of nonlinearity in the final discretized equations. Such problems are more frequently formulated as higher-order nonlinear PDEs with multi-dependent variables. Hence, it should be mentioned that the employed one-dimensional wave equation is mainly for illustration purpose. An extension of the solution scheme to other types of PDEs can be performed in a similar manner to accommodate geometrically nonlinear problems.

Under the above mentioned conditions, the deterministic equation set can be solved numerically using a step-by-step time-integration scheme. Issues related to numerical difficulties and the methods for reducing computational effort are addressed in the previous chapter. After the discrete-time solutions are obtained, the response statistics can be evaluated from

$$E[\hat{w}(t,x,\mathbf{b})] = \sum_{j=1}^{NS} u_{j00\cdots0}(t)\phi_j(x) \tag{3.43}$$

$$Var[\hat{w}(t,x,\mathbf{b})] = \sum_{i=1}^{NS}\sum_{j=1}^{NS}\sum_{|\mathbf{l}|=1}^{NP} u_{i_{l_1}l_2\cdots l_{NR}}(t)u_{j_{l_1}l_2\cdots l_{NR}}(t)\phi_i(x)\phi_j(x) \tag{3.44}$$

Similarly, the statistics of the "strain" response can be evaluated from

$$E[\frac{\partial\hat{w}(t,x,\mathbf{b})}{\partial x}] = \sum_{j=1}^{NS} u_{j00\cdots0}(t)\frac{\partial\phi_j(x)}{\partial x} \tag{3.45}$$

$$Var[\frac{\partial \hat{w}(t,x,\mathbf{b})}{\partial x}] = \sum_{i=1}^{NS}\sum_{j=1}^{NS}\sum_{|\mathbf{l}|=1}^{NP} u_{i_{l_1 l_2 \cdots l_{NR}}}(t) u_{j_{l_1 l_2 \cdots l_{NR}}}(t) \frac{\partial \phi_i(x)}{\partial x}\frac{\partial \phi_j(x)}{\partial x} \tag{3.46}$$

In the next chapter, a specific application of the proposed solution scheme is presented through an analysis of uncertain nonlinear shear beams.

Chapter 4

Application: Nonlinear Uncertain Shear Beam Subjected to Near-Field Earthquake Ground Motion

4.1 Introduction

The dynamic behavior of structures subjected to near-field earthquakes has received increasing attention and has become an important consideration in the process of structural designs. Near-field earthquake ground motion is characterized by its long-period, pulse-like wave form. A tall building subjected to such a pulse can exhibit a wave-type motion propagating along the building. This phenomenon is supported by the recorded response of tall buildings during near-field earthquakes. An important consequence of this type of response is considerable local structural deformations can be developed along the propagating path, and hence damage is likely to occur.

Although the distinct feature of near-field ground motion has long been observed by the seismologists, its impact on modern buildings was not fully appreciated until the recent works by Heaton et al. [40], Hall et al. [41] and Iwan [42]. In the former studies, a detailed nonlinear analysis is performed for a 20-story steel-frame building and a three-story base-isolated structure using both a recorded and a simulated near-field ground motion. The numerical results suggest the possible occurrence of high inter-story drift ratio for the ground motion being considered. Also investigated in this study is the response behavior of multi-story buildings idealized as a uniform shear-beam model under different types of base pulses. Due to the wave-type response of

the shear-beam model, the peak shear strain can be directly related to the peak ground velocity. Calculations show that the peak shear strain may far exceed the elastic limit of most structures even with a moderately peak ground velocity.

As a better indication of the near-field effect on structures, the concept of drift demand spectrum was proposed by Iwan [42] to complement the use of the response spectra as adopted in traditional earthquake engineering practices. The structural response is modeled as a damped wave motion propagating through a simple shear-beam model. The formulation for the local shear strain, or equivalently the inter-story drift ratio, is then derived as a summation of the up-traveling waves from the base and the down-traveling waves reflected from the top of the structure. This study shows that the drift demand spectra for many near-field earthquakes exhibit much larger drift demand than that of far-field earthquakes. However, such a significant difference cannot be fully described from their response spectra. Hence, the near-field effect can be potentially damaging particularly to the local sub-structure in a building.

The objective of this chapter is to investigate the dynamic response of structures exhibiting uncertain material properties to near-field earthquake ground motion. The analytical model considered resembles the shear-beam model employed by Iwan. The randomness of the shear rigidity as well as elastic nonlinear effect are both incorporated into the analysis. The newly developed method for analyzing uncertain continuous systems is then applied to this shear-beam model to perform a second-moment analysis of the shear strain response. This study is based a recorded near-field accelerogram obtained during the Northridge Earthquake of 1994.

4.2 Description of the Physical System

A formulation and physical description of the shear-beam model is given in this section. Consider an undamped nonlinear shear beam described by the equation of motion

$$\frac{\partial}{\partial x}\left(G(x)h(\frac{\partial w}{\partial x})\right) = \rho\ddot{w} + \rho\ddot{q}(t) \quad 0 < x < L \tag{4.1}$$

where $w = w(t,x)$ is the transverse displacement relative to the base, ρ is a constant mass density per unit length, $\ddot{q}(t)$ is the absolute acceleration of the base excitation, $h(\cdot)$ represents a dimensionless nonlinear stress function of its argument, L is the total length of the beam and $G(x)$ is the shear rigidity per unit length. Eqn. (4.1) is assumed to have zero initial conditions subjected to the following boundary conditions

$$w(t,x)|_{x=0} = 0 \qquad \left.\frac{\partial w(t,x)}{\partial x}\right|_{x=L} = 0 \tag{4.2}$$

The configuration and the coordinate system for this shear-beam model are depicted in Fig. 4.1.

To model the uncertainty in its quantitative description, the shear rigidity is idealized as a second-order Gaussian random field with a uniform mean and an assumed slowly varying random fluctuation. The random shear rigidity allows a representation expressible in terms of a set of independent Gaussian random variables and deterministic spatial functions by

$$G(x) \cong \bar{G} + \sum_{n=1}^{NR} b_n G_n(x) \tag{4.3}$$

where $\{b_n\}_{n=1}^{NR}$ is a set of NR Gaussian random variables with zero means and unit variances, $\bar{G}$ is the uniform mean shear rigidity and $G_n(x)$ is the deterministic spatial function associated with the random variable b_n. These deterministic spatial functions are determined through the discrete Karhunen-Loève decomposition of a discretized

covariance function of $G(x)$ as described in the previous chapter.

The nonlinearity of the system is due to the nonlinear stress-strain constitutive relationship described through the dimensionless stress function $h(\frac{\partial w}{\partial x})$. Two types of stress-strain nonlinearity, a hardening type and a softening type, will be considered and formulated separately in Section 4.3 and Section 4.4 respectively.

4.3 Cubic Hardening Nonlinearity

This section considers a stress-strain nonlinearity of the hardening type. The model chosen is the cubic hardening nonlinearity given by

$$h(\frac{\partial w}{\partial x}) = \frac{\partial w}{\partial x} + \gamma(\frac{\partial w}{\partial x})^3 \tag{4.4}$$

where γ is a positive parameter governing the degree of hardening nonlinearity.

Substituting Eqns. (4.4) and (4.3) into Eqn. (4.1) yields an undamped nonlinear wave equation with random coefficients as

$$\bar{G}\frac{\partial}{\partial x}\left(\frac{\partial \hat{w}}{\partial x} + \gamma(\frac{\partial \hat{w}}{\partial x})^3\right) + \sum_{n=1}^{NR} b_n \frac{\partial}{\partial x}\left(G_n(x)(\frac{\partial \hat{w}}{\partial x} + \gamma(\frac{\partial \hat{w}}{\partial x})^3)\right)$$

$$= \rho\ddot{\hat{w}} + \rho\ddot{q}(t) \quad 0 < x < L \tag{4.5}$$

with the boundary conditions

$$\hat{w}(t, x, \mathbf{b})|_{x=0} = 0 \qquad \left.\frac{\partial \hat{w}(t, x, \mathbf{b})}{\partial x}\right|_{x=L} = 0 \tag{4.6}$$

where $\mathbf{b} = \{b_1, b_2, \cdots, b_{NR}\}^T$ and $\hat{w} = \hat{w}(t, x, \mathbf{b})$ is the dependent random response variable. The finite element method (FEM) will be employed to obtain a discrete nonlinear multi-degree-of-freedom (MDOF) system with random coefficients in the next section.

4.3.1 Finite Element Discretization

Let the shear beam be uniformly discretized into NEL elements using the two-node rod element. The basis shape functions are graphically illustrated in Fig. 4.2. The shape functions, $\phi_1^{(e)}$ and $\phi_2^{(e)}$, may be expressed in terms of the local coordinate, $\bar{x}$, as

$$\phi_1^{(e)}(\bar{x}) = 1 - \frac{\bar{x}}{l_e} \qquad \phi_2^{(e)}(\bar{x}) = \frac{\bar{x}}{l_e} \tag{4.7}$$

where $l_e = \frac{L}{NEL}$ is the length of the element and the shape functions are defined over the subdomain $0 \leq \bar{x} \leq l_e$. The resulting FEM mesh is also used for constructing the finite representation of the random shear rigidity.

For this FEM mesh, the random elemental displacement variable $\hat{w}^{(e)}(t, \bar{x}, \mathbf{b})$ is given by

$$\hat{w}^{(e)}(t, \bar{x}, \mathbf{b}) = \phi_1^{(e)}(\bar{x}) u_1^{(e)}(t, \mathbf{b}) + \phi_2^{(e)}(\bar{x}) u_2^{(e)}(t, \mathbf{b}) \tag{4.8}$$

where $u_1^{(e)}(t, \mathbf{b})$ and $u_2^{(e)}(t, \mathbf{b})$ are the random nodal responses. Let $\mathbf{u}^{(e)} = \mathbf{u}^{(e)}(t, \mathbf{b})$ be the random elemental displacement vector given by

$$\mathbf{u}^{(e)}(t, \mathbf{b}) = \left\{ \begin{array}{c} u_1^{(e)}(t, \mathbf{b}) \\ u_2^{(e)}(t, \mathbf{b}) \end{array} \right\} \tag{4.9}$$

Substituting Eqn. (4.8) into Eqn. (4.5) and performing the variational formulation, a discrete random nonlinear ordinary differential equation for $\mathbf{u}^{(e)}$ is derived as

$$\sum_{e=1}^{NEL} \left\{ \mathbf{M}^{(e)} \ddot{\mathbf{u}}^{(e)} + \bar{\mathbf{K}}^{(e)} \mathbf{u}^{(e)} + \bar{\mathbf{g}}^{(e)}(\mathbf{u}^{(e)}) + \sum_{n=1}^{NR} b_n [\mathbf{K}_n^{(e)} \mathbf{u}^{(e)} + \mathbf{g}_n^{(e)}(\mathbf{u}^{(e)})] = \mathbf{f}^{(e)}(t) \right\} \tag{4.10}$$

In the above equation, $\mathbf{M}^{(e)}$ and $\mathbf{f}^{(e)}(t)$ are respectively the elemental mass matrix and

the elemental force vector given by

$$\mathbf{M}^{(e)} = \frac{\rho l_e}{6}\begin{bmatrix} 2 & 1 \\ 1 & 2 \end{bmatrix} \qquad \mathbf{f}^{(e)}(t) = \frac{\rho l_e \ddot{q}(t)}{2}\begin{Bmatrix} 1 \\ 1 \end{Bmatrix} \tag{4.11}$$

The symbols $\bar{\mathbf{K}}^{(e)}$ and $\bar{\mathbf{g}}^{(e)}$ are respectively the mean linear stiffness matrix and nonlinear stiffness vector given by

$$\bar{\mathbf{K}}^{(e)} = \frac{\bar{G}}{l_e}\begin{bmatrix} 1 & -1 \\ -1 & 1 \end{bmatrix} \qquad \bar{\mathbf{g}}^{(e)}(\mathbf{u}^{(e)}) = \gamma\bar{G}(\frac{\triangle u^{(e)}}{l_e})^3\begin{Bmatrix} -1 \\ 1 \end{Bmatrix} \tag{4.12}$$

where $\triangle u^{(e)}$ is the difference of nodal displacement for the element (e) defined as

$$\triangle u^{(e)} \equiv u_2^{(e)} - u_1^{(e)} \tag{4.13}$$

Similar notations $\mathbf{K}_n^{(e)}$ and $\mathbf{g}_n^{(e)}$ stand for the linear stiffness matrix and the nonlinear stiffness vector associated with the random variable b_n given by

$$\mathbf{K}_n^{(e)} = \frac{\bar{G}_n^{(e)}}{l_e}\begin{bmatrix} 1 & -1 \\ -1 & 1 \end{bmatrix} \qquad \mathbf{g}_n^{(e)}(\mathbf{u}^{(e)}) = \gamma\bar{G}_n^{(e)}(\frac{\triangle u^{(e)}}{l_e})^3\begin{Bmatrix} -1 \\ 1 \end{Bmatrix} \tag{4.14}$$

where $\bar{G}_n^{(e)}$ denotes the local average of the nodal values of $G_n(x)$ over the element (e).

Note that the two-node rod element results in an element-wise constant strain given by $\triangle u^{(e)}/l_e$. All the linear and nonlinear stiffness matrices and vectors are directly expressible in terms of the constant strain. Also shown in Eqn. (4.14), the random components of linear and nonlinear stiffness are expressed in terms of the average, $\bar{G}_n^{(e)}$, which represent a constant shear strength for an element. Thus, it seems possible to embody the discretized random equation with a direct physical interpretation.

4.3.2 Discrete Analog to Random Continuous Systems

The elemental mass matrix given by Eqn. (4.11) is usually referred to as the *consistent mass matrix*. Certain difficulties exist in giving a physical interpretation to the off-diagonal terms appeared in the consistent mass matrix. In many FEM applications of structural dynamics, the so-called *lumped mass matrix* is more often used due to its appealing physical interpretation and comparable solution accuracy. By lumping the off-diagonal mass components to the diagonal terms, the lumped mass matrix for Eqn. (4.11) is given by

$$\mathbf{M}_l^{(e)} = \frac{\rho l_e}{2}\begin{bmatrix} 1 & 0 \\ 0 & 1 \end{bmatrix} \tag{4.15}$$

Clearly, this mass matrix represents two lumped mass on the both ends of an element.

By grouping the linear and nonlinear stiffness, a total mean nonlinear restoring vector can be defined as

$$\hat{\mathbf{g}}^{(e)}(\mathbf{u}^{(e)}) = \bar{G}\left(\frac{\triangle u^{(e)}}{l_e} + \gamma(\frac{\triangle u^{(e)}}{l_e})^3\right)\begin{Bmatrix} -1 \\ 1 \end{Bmatrix} \tag{4.16}$$

Similarly, the component of total nonlinear restoring force vector associated with the random variable b_n is defined as

$$\hat{\mathbf{g}}_n^{(e)}(\mathbf{u}^{(e)}) = \bar{G}_n^{(e)}\left(\frac{\triangle u^{(e)}}{l_e} + \gamma(\frac{\triangle u^{(e)}}{l_e})^3\right)\begin{Bmatrix} -1 \\ 1 \end{Bmatrix} \tag{4.17}$$

Combining the consistent mass matrix and the newly introduced nonlinear restoring vectors, an alternative form of the random equation is given by

$$\sum_{e=1}^{NEL}\left\{\mathbf{M}_l^{(e)}\ddot{\mathbf{u}}^{(e)} + \hat{\mathbf{g}}^{(e)}(\mathbf{u}^{(e)}) + \sum_{n=1}^{NR} b_n\hat{\mathbf{g}}_n^{(e)}(\mathbf{u}^{(e)}) = \mathbf{f}^{(e)}(t)\right\} \tag{4.18}$$

Eqn. (4.18) represents a random MDOF nonlinear spring-mass system. This

system may be represented graphically as in Fig. 4.3. It consists of NEL mass blocks inter-connected by a set of deterministic and random springs. Except at the top, each mass block has the same amount of mass which is equal to the total distributed mass in an element. The top mass block has only half the amount of the mass of other elements as a consequence of the mass distribution rule of the FEM analysis. Only the adjacent mass blocks are connected by a set of parallel-arranged nonlinear springs. One of the springs, indicated by a solid line, represents a deterministic nonlinear restoring spring with a cubic hardening force-relative displacement relationship. The rest of the springs represent the random restoring springs. These random restoring springs have random initial slopes but still maintain the same cubic hardening rate as that of the deterministic restoring spring.

The discrete analog not only provides a physical interpretation for the FEM discretization process but also provides insightful guidance when a simulation method is of interest. To see this, again consider the spring-mass system in Fig. 4.3. Note that the vertically aligned random restoring springs are controlled by the same random variable. Hence, a sample value of this random variable will generate a set of sample spring characteristics for those restoring springs. Generalizing this concept, a sample of the random shear rigidity will yield not only vertically but also horizontally arranged restoring springs. By summing up the total spring strength in the same horizontal level, the sample nonlinear structure can be formed.

4.3.3 Deterministic Equation

Let the orthogonal polynomial expansion for the elemental response vector be expressed as

$$\mathbf{u}^{(e)}(t,\mathbf{b}) = \sum_{|\mathbf{l}|=0}^{NP} \hat{\mathbf{u}}^{(e)}_{l_1 l_2 \cdots l_{NR}}(t) H_{l_1 l_2 \cdots l_{NR}}(\mathbf{b}) \tag{4.19}$$

As a result of the Gaussian assumption, the orthogonal polynomial $H_{l_1 l_2 \cdots l_{NR}}(\mathbf{b})$ is the multi-dimensional Hermite polynomial of order $|\mathbf{l}|$.

Along with the above expansion, it is more convenient to denote the associated expansion for the elemental displacement difference by

$$\triangle \hat{u}^{(e)}_{l_1 l_2 \cdots l_{NR}}(t) = \hat{u}^{(e)}_{2_{l_1 l_2 \cdots l_{NR}}}(t) - \hat{u}^{(e)}_{1_{l_1 l_2 \cdots l_{NR}}}(t) \tag{4.20}$$

Applying the method of weighted residuals, the deterministic equation set is derived as

$$\begin{aligned}
\sum_{e=1}^{NEL} \Big\{ & \mathbf{M}_l^{(e)} \ddot{\hat{\mathbf{u}}}^{(e)}_{l_1 l_2 \cdots l_{NR}}(t) + \bar{\mathbf{K}}^{(e)} \hat{\mathbf{u}}^{(e)}_{l_1 l_2 \cdots l_{NR}}(t) + \bar{\mathbf{g}}^{(e)}_{l_1 l_2 \cdots l_{NR}}(\hat{\mathbf{u}}^{(e)}(t)) \\
& + \sum_{n=1}^{NR} \mathbf{K}_n^{(e)} \left(a_{l_n} \hat{\mathbf{u}}^{(e)}_{l_1 \cdots l_n - 1 \cdots l_{NR}}(t) + \bar{a}_{l_n} \hat{\mathbf{u}}^{(e)}_{l_1 \cdots l_n + 1 \cdots l_{NR}}(t) \right) + \mathbf{g}^{(e)}_{n_{l_1 l_2 \cdots l_{NR}}}(\hat{\mathbf{u}}^{(e)}(t)) \\
& = \mathbf{f}^{(e)}(t) \prod_{n=1}^{NR} \delta_{l_n 0} \Big\}, \qquad |\mathbf{l}| = 0, \cdots, NP
\end{aligned} \tag{4.21}$$

where a_{ln} and $\bar{a}_{ln}$ are the constants coefficients defined previously and

$$\begin{aligned}
\bar{\mathbf{g}}^{(e)}_{l_1 l_2 \cdots l_{NR}}(\hat{\mathbf{u}}^{(e)}(t)) = & \frac{\gamma \bar{G}}{{l_e}^3} \sum_{|\mathbf{p}|=0}^{NP} \sum_{|\mathbf{r}|=0}^{NP} \sum_{|\mathbf{s}|=0}^{NP} \triangle \hat{u}^{(e)}_{p_1 p_2 \cdots p_{NR}}(t) \triangle \hat{u}^{(e)}_{r_1 r_2 \cdots r_{NR}}(t) \triangle \hat{u}^{(e)}_{s_1 s_2 \cdots s_{NR}}(t) \\
& \prod_{n=1}^{NR} R_{l_n p_n r_n s_n} \begin{Bmatrix} -1 \\ 1 \end{Bmatrix}
\end{aligned} \tag{4.22}$$

$$\begin{aligned}
\mathbf{g}^{(e)}_{n_{l_1 l_2 \cdots l_{NR}}}(\hat{\mathbf{u}}^{(e)}(t)) = & \frac{\gamma \bar{G}^{(e)}_n}{{l_e}^3} \sum_{|\mathbf{p}|=0}^{NP} \sum_{|\mathbf{r}|=0}^{NP} \sum_{|\mathbf{s}|=0}^{NP} \triangle \hat{u}^{(e)}_{p_1 p_2 \cdots p_{NR}}(t) \triangle \hat{u}^{(e)}_{r_1 r_2 \cdots r_{NR}}(t) \triangle \hat{u}^{(e)}_{s_1 s_2 \cdots s_{NR}}(t) \\
& (a_{l_n} R_{l_n - 1 p_n r_n s_n} + \bar{a}_{l_n} R_{l_n + 1 p_n r_n s_n}) \prod_{\substack{m=1 \\ m \neq n}}^{NR} R_{l_m p_m r_m s_m} \begin{Bmatrix} -1 \\ 1 \end{Bmatrix}
\end{aligned} \tag{4.23}$$

The expression for the constants R_{ijkl} are given by

$$R_{ijkl} = E[H_i(b)H_j(b)H_k(b)H_l(b)] \tag{4.24}$$

In viewing the above equation set, certain numerical difficulties may arise because of the size of the problem and the total number of arithmetic operations involved. This solution scheme may become very inefficient when many random variables are present and a higher-order scheme is used. However, it is frequently the case that only the first few random variables dominate the response uncertainty. In addition, the random variables have a rapidly decreasing rate of contribution as the associated indices increase. This motivates one to define a norm for the orthogonal polynomials such that only a low-order expansion is used in the space spanned by the random variables with high indices. Such considerations can greatly reduce the total size of the problem but still yield the same level of solution accuracy.

Additionally, several other techniques can be implemented to reduce the computational effort. Note that the evaluation of the product terms in Eqns. (4.22) and (4.23) dominates the computations. The coupling between these terms is totally determined by the time-independent constant product $\prod_{n=1}^{NR} R_{l_n p_n r_n s_n}$. It is observed that a large number of these constants are identically equal to zero and hence the corresponding solution variables have no contribution. Therefore, these constants can be evaluated *a priori* and only the nonzero constants are retained and tabulated. Using the symmetry property between the triple products of the solution variables and the corresponding constants, the required arithmetic operations can be further effectively reduced.

4.4 Arctangent Softening Nonlinearity

This section considers a shear-beam model with a softening stress-strain nonlinearity. The particular stress-strain model employed is the arctangent softening type given by

$$h(\frac{\partial w}{\partial x}) = \frac{2h_y}{\pi}\tan^{-1}(\frac{\pi}{2h_y}\frac{\partial w}{\partial x}) \tag{4.25}$$

where h_y is an "yielding" level of the dimensionless stress function. This stress function has an unit initial slope as a function of the strain field. Since the shear stress is the product of the random shear rigidity $G(x)$ and the stress function h, a variation in the shear rigidity will result in both the variation of the initial shear stiffness and the ultimate yielding shear stress.

Using Eqn. (4.25) and the discrete representation of the random shear rigidity, an approximated random PDE for this case is obtained as

$$\bar{G}\frac{\partial}{\partial x}\left(\frac{2h_y}{\pi}\tan^{-1}(\frac{\pi}{2h_y}\frac{\partial \hat{w}}{\partial x})\right) + \sum_{n=1}^{NR} b_n \frac{\partial}{\partial x}\left(G_n(x)\frac{2h_y}{\pi}\tan^{-1}(\frac{\pi}{2h_y}\frac{\partial \hat{w}}{\partial x})\right)$$

$$= \rho\ddot{\hat{w}} + \rho\ddot{q}(t) \quad 0 < x < L \tag{4.26}$$

subject to the same boundary conditions as given in Eqn. (4.6).

4.4.1 FEM Discretization and Nonlinear MDOF System

The previously applied FEM discretization will also be implemented for this random softening system. Again adopting the two-node rod element and the lumped mass approach, the discretized equation can be shown to be given by

$$\sum_{e=1}^{NEL}\left\{\mathbf{M}_l^{(e)}\ddot{\mathbf{u}}^{(e)} + \hat{\mathbf{g}}^{(e)}(\mathbf{u}^{(e)}) + \sum_{n=1}^{NR} b_n \hat{\mathbf{g}}_n^{(e)}(\mathbf{u}^{(e)}) = \mathbf{f}^{(e)}(t)\right\} \tag{4.27}$$

where $\mathbf{M}_l^{(e)}$ and $\mathbf{f}^{(e)}$ are as defined previously. The expressions for $\hat{\mathbf{g}}^{(e)}$ and $\hat{\mathbf{g}}_n^{(e)}$ are obtained through the variational formulation. Since the shape functions selected imply a constant strain in each element, the expressions for $\hat{\mathbf{g}}^{(e)}$ and $\hat{\mathbf{g}}_n^{(e)}$ are greatly simplified to the followings:

$$\hat{\mathbf{g}}^{(e)}(\mathbf{u}^{(e)}) = \bar{G}h(\frac{\triangle u^{(e)}}{l_e})\begin{Bmatrix} -1 \\ 1 \end{Bmatrix} \qquad \hat{\mathbf{g}}_n^{(e)}(\mathbf{u}^{(e)}) = \bar{G}_n^{(e)}h(\frac{\triangle u^{(e)}}{l_e})\begin{Bmatrix} -1 \\ 1 \end{Bmatrix} \tag{4.28}$$

where l_e and $\triangle u^{(e)}$ are as defined previously.

The FEM discretization of a shear beam with an arctangent stiffness constitutive relationship also possesses a direct discrete analog. An examination of Eqn. (4.27) and Eqn. (4.18) shows a similarity between the hardening and softening shear beams. Therefore, the schematic diagram shown in Fig. 4.3 and the discussion given for the hardening beam are both applicable except only for the difference in the spring characteristics.

However, it is more difficult to apply the proposed solution method to the softening system due to the non-polynomial type of nonlinearity. To cope with this difficulty, introduce a vector of elemental state variables $\mathbf{z}^{(e)}$ which satisfies the relationship

$$\hat{\mathbf{g}}^{(e)}(\mathbf{u}^{(e)}) = \bar{\mathbf{K}}^{(e)}\mathbf{z}^{(e)} \tag{4.29}$$

Then, Eqn. (4.27) can be arranged as

$$\sum_{e=1}^{NEL}\left\{\mathbf{M}^{(e)}\ddot{\mathbf{u}}^{(e)} + \bar{\mathbf{K}}^{(e)}\mathbf{z}^{(e)} + \sum_{n=1}^{NR} b_n\mathbf{K}_n^{(e)}\mathbf{z}^{(e)} = \mathbf{f}^{(e)}(t)\right\} \tag{4.30}$$

Furthermore, introduce a negative parameter γ defined by

$$\gamma \equiv -\left(\frac{\pi}{2h_y}\right)^2 \tag{4.31}$$

The case that $\gamma = 0$ implies an infinite high "yield" stress and is therefore the case of a linear constitutive law. Decreasing the value of γ will decrease the "yielding" value, h_y, and therefore increase the degree of softening nonlinearity.

The dynamics of the newly defined vector $\mathbf{z}^{(e)}$ is then governed by an auxiliary equation

$$\left(1 - \gamma \left(\frac{\triangle u^{(e)}}{l_e}\right)^2\right) \triangle \dot{z}^{(e)} = \triangle \dot{u}^{(e)} \tag{4.32}$$

The random equation Eqn. (4.30) together with the nonlinear auxiliary equation set Eqn. (4.32) will be used to obtain a set of deterministic equations.

4.4.2 Deterministic Equations

Let the expansion of nodal response vectors be expanded as

$$\mathbf{u}^{(e)}(t, \mathbf{b}) = \sum_{|\mathbf{l}|=0}^{NP} \hat{\mathbf{u}}^{(e)}_{l_1 l_2 \cdots l_{NR}}(t) H_{l_1 l_2 \cdots l_{NR}}(\mathbf{b}) \tag{4.33}$$

$$\mathbf{z}^{(e)}(t, \mathbf{b}) = \sum_{|\mathbf{l}|=0}^{NP} \hat{\mathbf{z}}^{(e)}_{l_1 l_2 \cdots l_{NR}}(t) H_{l_1 l_2 \cdots l_{NR}}(\mathbf{b}) \tag{4.34}$$

The final deterministic equations are given by

$$\sum_{e=1}^{NEL} \left\{ \mathbf{M}^{(e)} \ddot{\hat{\mathbf{u}}}^{(e)}_{l_1 l_2 \cdots l_{NR}}(t) + \bar{\mathbf{K}}^{(e)} \hat{\mathbf{z}}^{(e)}_{l_1 l_2 \cdots l_{NR}}(t) + \sum_{n=1}^{NR} \mathbf{K}^{(e)}_n \left(a_{l_n} \hat{\mathbf{z}}^{(e)}_{l_1 \cdots l_n - 1 \cdots l_{NR}}(t) \right.\right.$$
$$\left.\left. + \bar{a}_{l_n} \hat{\mathbf{z}}^{(e)}_{l_1 \cdots l_n + 1 \cdots l_{NR}}(t) \right) = \mathbf{f}^{(e)}(t) \prod_{n=1}^{NR} \delta_{l_n 0} \right\}, \qquad |\mathbf{l}| = 0, \cdots, NP \tag{4.35}$$

with an auxiliary equation

$$\sum_{|\mathbf{s}|=0}^{NP} \left(\prod_{i=1}^{NR} \delta_{l_i s_i} - \frac{\gamma}{l_e^2} \sum_{|\mathbf{p}|=0}^{NP} \sum_{|\mathbf{r}|=0}^{NP} \triangle \hat{u}^{(e)}_{p_1 p_2 \cdots p_{NR}}(t) \triangle \hat{u}^{(e)}_{r_1 r_2 \cdots r_{NR}}(t) \right.$$
$$\left. \prod_{n=1}^{NR} R_{l_n p_n r_n s_n} \right) \triangle \dot{\hat{z}}^{(e)}_{s_1 s_2 \cdots s_{NR}}(t) = \triangle \dot{\hat{u}}^{(e)}_{r_1 r_2 \cdots r_{NR}}(t) \tag{4.36}$$

Eqn. (4.35) is linear and can be solved numerically very efficiently. However, in Eqn. (4.36), given the elemental response difference $\dot{\hat{u}}^{(e)}_{r_1 r_2 \cdots r_{NR}}(t)$ and $\hat{u}^{(e)}_{r_1 r_2 \cdots r_{NR}}(t)$, the time derivative of $\hat{z}^{(e)}_{l_1 l_2 \cdots l_{NR}}(t)$ must be solved via a matrix equation. The size of the matrix is the same as the total number of orthogonal polynomials employed. Hence, this becomes a major drawback for this solution scheme when a system with many random variables is analyzed.

4.5 Consideration of the Damping Matrix

The formulations given in the previous sections are based on an undamped shear-beam model. The energy dissipation of the system is assumed to be deterministic and its relation to the FEM formulation is addressed in this section. Quite often, the system damping is provided as a damping field in the governing wave equation. The FEM is then applied to the damping field to obtain the correspond damping matrix. Alternatively, the FEM discretization can be first applied to an undamped equation of motion. Then, the damping matrix is artificially generated using the resulting mass and stiffness matrices. The latter approach using a Rayleigh type of damping matrix is employed in the formulation.

The Rayleigh damping matrix is a linear combination of the mass matrix and the stiffness matrix. As to the random system being considered, the Rayleigh damping is expressed as

$$\mathbf{C} = \sum_{e=1}^{NEL} \left\{ \alpha_1 \mathbf{M}_l^{(e)} + \alpha_2 \bar{\mathbf{K}}^{(e)} \right\} \tag{4.37}$$

where $\mathbf{C}$ is the global damping matrix for the discretized system, $\mathbf{M}_l^{(e)}$ is the elemental lumped mass matrix, $\bar{\mathbf{K}}^{(e)}$ is the mean elemental linear stiffness matrix and α_1 and α_2 are two constants to be selected according to a specific engineering need.

Using the property that the global mass matrix, linear mean stiffness matrix and the Rayleigh damping matrix can be diagonalized simultaneously, Eqn. (4.37) gives

the following expression for the ith linearized modal damping ratio.

$$\zeta_i = \frac{1}{2}(\frac{\alpha_1}{\omega_i} + \alpha_2\omega_i) \tag{4.38}$$

where ω_i is the undamped natural frequency for the ith mode. Let ζ_i and ζ_j be two desired damping ratios for the ith and jth modes respectively. This leads to two algebraic equations for the parameters α_1 and α_2. Solving the resulting algebraic equation yields the following expressions for α_1 and α_2.

$$\alpha_1 = \frac{2(\zeta_i\omega_j - \zeta_j\omega_i)}{\omega_j/\omega_i - \omega_i/\omega_j} \qquad \alpha_2 = \frac{2(\zeta_i\omega_i - \zeta_j\omega_j)}{\omega_j^2 - \omega_i^2} \tag{4.39}$$

Hence, the global damping matrix can be constructed using the desired modal damping ratios, ζ_i and ζ_j, and the associated modal frequencies, ω_i and ω_j.

The Rayleigh damping matrix also possesses a direct physical interpretation. When α_1 vanishes, the resulting damping matrix is also referred to as the *stiffness proportional* damping matrix. Applying the spring-mass analog given previously, this case provides a set of viscous damped dashpots inter-connected in the same way as the deterministic restoring springs are arranged. Likewise, when α_2 vanishes, it is referred to as the *mass proportional* damping matrix. In this case, it corresponds to a set of dashpots connected from the mass blocks to the ambient. When both constants are present, the corresponding physical system is then the combined arrangement in the both cases. Finally, the incorporation of the damping matrix to the deterministic equation set becomes straightforward and will not be elaborated.

4.6 Numerical Examples

As mentioned earlier, the shear-beam model used in the current analysis resembles the one employed by Iwan in obtaining the drift spectrum. In this model, a single

parameter, T, the linear fundamental period of the shear beam, is used to determine the height and the mean shear wave velocity. From the Uniform Building Code (ICBO 1994) for a steel structure [43], the total length of the shear beam L, measured in meters, is related to T by

$$T = 0.0853L^{3/4} \tag{4.40}$$

Further using the linear fundamental modal equation, the mean shear wave velocity $\sqrt{\bar{G}/\rho}$ is related to T and L by

$$T = \frac{4L}{\sqrt{\bar{G}/\rho}} \tag{4.41}$$

The random fluctuation component of the shear rigidity is assumed to be homogeneous and to follow the exponential correlation function

$$R(\xi) = \bar{G}^2\sigma^2 e^{-(\frac{\xi}{\mu L})^2} \tag{4.42}$$

where σ represents the coefficient of variation and μ represents the ratio of the correlation distance to the total length L.

Unless otherwise specified, the shear-beam model is uniformly discretized into ten elements for the cases examined. The resulting global mass matrix and the linear mean stiffness matrix are used to evaluate the modal natural frequencies and a subsequent construction of the Rayleigh damping matrix. A 5% model damping ratio for the first two modes is assumed in most of the examples presented.

The input base excitation chosen is the N-S acceleration component recorded at Rinaldi Receiving Station during the 1994 Northridge Earthquake. The recorded data are processed using a special base-line correction technique developed by Iwan and Chen [44]. Figs. 4.6 and 4.7 shows the corrected acceleration and velocity time histories where the peak velocity reaches around 170 cm/sec. The time history shows a significant "pulse-like" ground motion due to the near-field effects.

4.6.1 Linear Deterministic Drift Spectrum

It is recognized that a wave-propagation based solution approach is more appropriate in analyzing the response of a shear beam subjected to a pulse-like ground motion due to the fact that the local deformation may be derived from contributions of all modal responses. It is therefore necessary to validate the multi-modal solution approach as resulted from the FEM discretization prior to a full-scale nonlinear uncertain analysis. This allows one to estimate the size of the error and to understand the nature of the error due to the finite discretization of the continuum. Furthermore, a suitable size of FEM mesh for the problem can be selected. With these objectives, the case of a linear model with a uniform deterministic shear rigidity is first examined using a mesh size of 10 elements and 20 elements. An exact solution for the continuous linear shear-beam model has been obtained by Iwan based on a nondispersive damped wave solution technique. These solutions are compared through the drift spectrum to emphasize the peak local deformation response. The term *drift ratio* is equivalent to the local shear strain in the subsequent discussions.

Fig. 4.8 and Fig. 4.9 are the 2% and 5% damped drift spectra obtained by the damped wave solution and by the FEM model respectively. It shows two large peak drift ratios at a period about 1.0 second and 1.4 second. The spectral curves then gradually decrease as the period increased. For the period range less than 2 seconds, both results agree well except for a slight underestimation in the results of FEM model. However, for higher period range, the FEM model yields smaller values on the peak drift ratio. Only a little improvement in the difference is achieved when the mesh size is refined as 20 elements for both the 2% and 5% damped solutions.

This discrepancy is believed to be caused by the different types of damping assumed. The Rayleigh damping as employed in the FEM model yields a highly damped high modal response because of an increasing damping ratio as the modal number increases. On the other hand, the damped wave solution has an effectively decreasing

theoretical modal damping ratio as the effective modal number increases. Therefore, less solution difference is observed when the response is strongly dominated by the fundamental mode. In general, the FEM model yields more conservative results when the participation of higher modal response is substantial.

Despite its slightly conservative nature, the FEM model yields a good estimation of both the spectral shape and the drift magnitude. In addition, the employed Rayleigh damping also provides an alternative damping mechanism in modeling the energy dissipation of the shear-beam model.

In the subsequent nonlinear uncertain analysis, a ten-element finite element model using the Rayleigh damping will be used to evaluate the response for a fundamental period range of 0.5 second to 2.5 seconds. The selected mesh size is believed to be capable of providing reasonable accuracy for the selected period range.

4.6.2 Nonlinear Statistical Drift Spectrum (Effect of γ)

The response uncertainty due to the effects of the uncertain shear rigidity and structural nonlinearity is examined in this and the next subsections. In order to investigate the combined effects of the natural frequency, nonlinearity and uncertain shear rigidity, the study results are presented through a *nonlinear statistical drift spectrum.* The mean shear strain as well as the mean plus one standard deviation of the shear strain are considered as the representative response statistics. For each selected fundamental period T, the peak elemental response statistics are evaluated first. Then, the maximum of these peak elemental statistics is plotted as a function of T.

In this subsection, an infinite correlation length, $\mu = \infty$, is assumed for the correlation function $R(\xi)$. Such an assumption gives a fully correlated shear rigidity in the axial direction. The uncertain shear rigidity therefore has a spatially uniform value controlled by only one random variable. The randomness of the shear rigidity is assumed to have 10% coefficient of variation given by $\sigma = 0.1$.

Recall that the sign of γ determined the hardening or softening type of nonlinearity. The effect of γ on the stress function-strain characteristics is illustrated in Fig. 4.4. Four representative cases of nonlinearity are chosen. The case $\gamma = 500$ represents a hardening stress-strain relationship. The case $\gamma = 0$ represents the linear structural characteristics. Two levels of softening nonlinearity are given by $\gamma = -500$ and $\gamma = -2000$. The latter case results in half of the linear stiffness when the strain reaches around 5%.

Figs. 4.10-4.13 show the resulting nonlinear statistical drift spectra where a third-order approximation is used, except in the case $\gamma = -2000$ where a fifth-order approximation is required for acceptable accuracy. These results are verified at selected data points using a simulation technique. Also shown are the results associated with the nonlinear shear beam with a uniform deterministic shear rigidity represented by $\sigma = 0$.

From these drift spectra, it is clear that the peak drift statistics increase as the degree of softening nonlinearity increased. For the case, $\gamma = -2000$, the peak mean drift reaches about 4.7% and the peak mean plus one standard deviation exceeds 5.5%. These statistics are much higher than the values observed in the linear case. By contrast, the case with hardening nonlinearity has relatively low mean strain and low standard deviation over the entire range of the fundamental period considered. The deterministic solution for all cases is all seen to be bounded by the mean and mean plus one standard deviation solutions.

To further examine the influence of nonlinearity on the spectral shape of the drift spectrum, the peak statistics for selected values of γ are plotted simultaneously in Fig. 4.14 and Fig. 4.15. This comparison shows a significant shift in the period of peak drift demand when the nonlinearity takes effect. In addition, this shift in period is accompanied by a change in the level of drift. The presence of a softening nonlinearity causes the period to shift toward a lower period range with an increasing

response level, while a hardening nonlinearity causes the opposite effect. Applying the notion of nonlinear modal analysis, the local strain is directly related to the dominant nonlinear modal response. Hence the variation of the period of maximal response may be interpreted in terms of the variation of the nominal effective modal period due to the nonlinear effect.

To better describe the above observation, the time history of the drift statistics for the case, $\gamma = -2000$, $T = 0.75$, is given in Figs. 4.16-4.19. These figures correspond respectively to the response of the first four elements numbered sequentially from the base. The effective period lengthening is clearly evident in the mean drift response for the time duration of 2-4 seconds. The period of oscillation is approximately equal to one second which is about the same as the period of peak drift observed in the linear drift spectrum. The phases of these mean drift responses are approximately the same. The base element is seen to have the largest strain statistics, and the response magnitude gradually decreases away from the base. Hence a modal-like response and the mean nonlinear mode shape can be imagined.

4.6.3 Nonlinear Statistical Drift Spectrum (Effect of μ)

This subsection considers a correlated random shear rigidity given by the exponential correlation function with $\mu = 0.5$ and $\sigma = 0.1$. This assumed correlation function can be found in Fig. 4.5. Due to the finite correlation distance, more than one random variable is required to appropriately represent the governing randomness. By numerically solving the resulting eigenvalue-eigenvector problem, the deterministic spatial functions associated with the first three random variables are plotted in Fig. 4.20. This plot shows that as the index of a random variable increases, the associated spatial function has a decreasing overall magnitude and an increasing degree of fluctuation.

The response variability under the presence of individual random variables is first

examined using the model, $\gamma = -2000$, $T = 0.75$ sec. The results for the first four elements are shown in Figs. 4.21-4.24. These plots demonstrate a rapidly decreasing response variability for random variables of higher indices. Hence, the contribution from these random variables rapidly becomes negligible. Due to the preceding analysis, only the first three random variables are taken into account.

The nonlinear statistical drift spectra for the cases $\gamma = -2000$ and $\gamma = -500$ are given in Fig. 4.25 and Fig. 4.26. Great similarity is observed in the spectral curves for the case $\mu = 0.5$ and the case $\mu = \infty$, especially in those structures having large drift response. Only a slight difference can be seen in the mean plus one standard deviation curves for a period higher than about 1.5 second. This indicates that the effect of spatial variation is not significant in the considered case and a uniformly correlated random rigidity can be a good approximation in evaluating the peak response statistics.

Finally, time histories of statistics for the structure with $T = 0.75$ second and $\gamma = -2000$ are shown in Figs. 4.27 - 4.30 along with simulation results. The proposed method well predicts the response statistics for all time. The strain statistics for the base element is less accurate as compared to the other locations. This is because the base element exhibits a higher degree of response variation over the random parameter space.

4.7 Remarks

In the presented examples, two different levels of correlation ratio, $\mu = \infty$ and $\mu = 0.5$, are assumed for the random shear rigidity. For these levels of correlation ratio, it is appropriate to perform an analysis using only a few random variables. However, for problems with relatively small correlation ratio, the analysis must be based on a further refined FEM mesh and a large number of random variables. Due to its prohibitive size,

the simulation technique may become more appropriate for such problems. Further research to develop an efficient simulation technique is considered to be valuable.

An auxiliary equation is herein employed for handling the arctangent type softening nonlinearity. Such an approximation yields satisfactory results but also results in a degree of computational inefficiency. The task of developing a solution method which can efficiently handle a non-polynomial nonlinearity and yield accurate results remains challenging. An extension to the proposed solution method that both allows a general nonlinearity to be treated and a higher-order approximation to be performed would prove very beneficial in analyzing the dynamic response of a nonlinear continuum with random parameter fields.

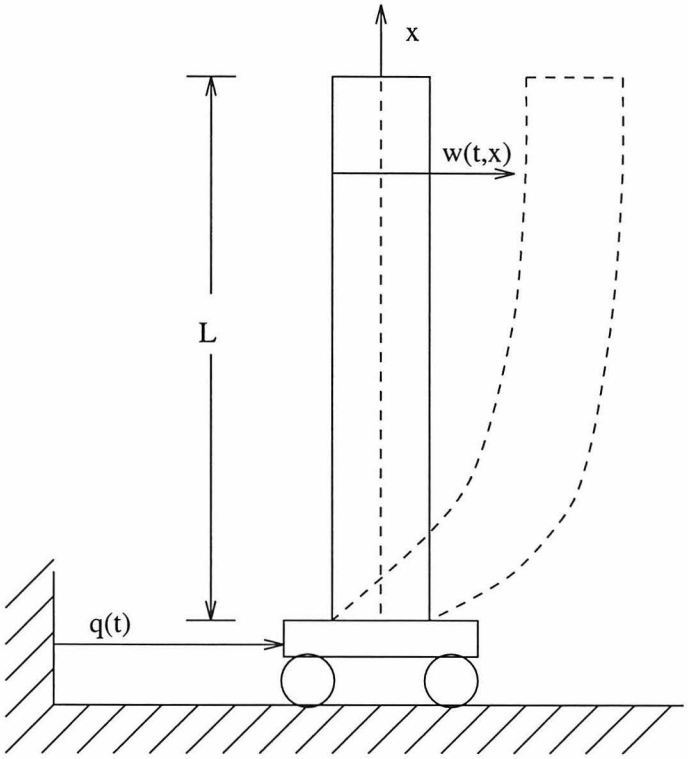

Figure 4.1: Shear-beam model subjected to base excitation.

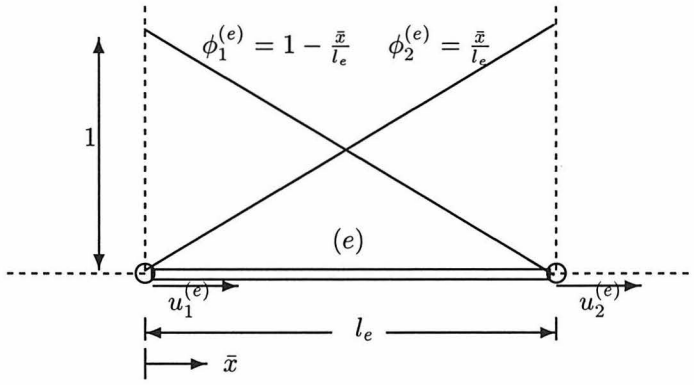

Figure 4.2: Shape functions of two-node rod element.

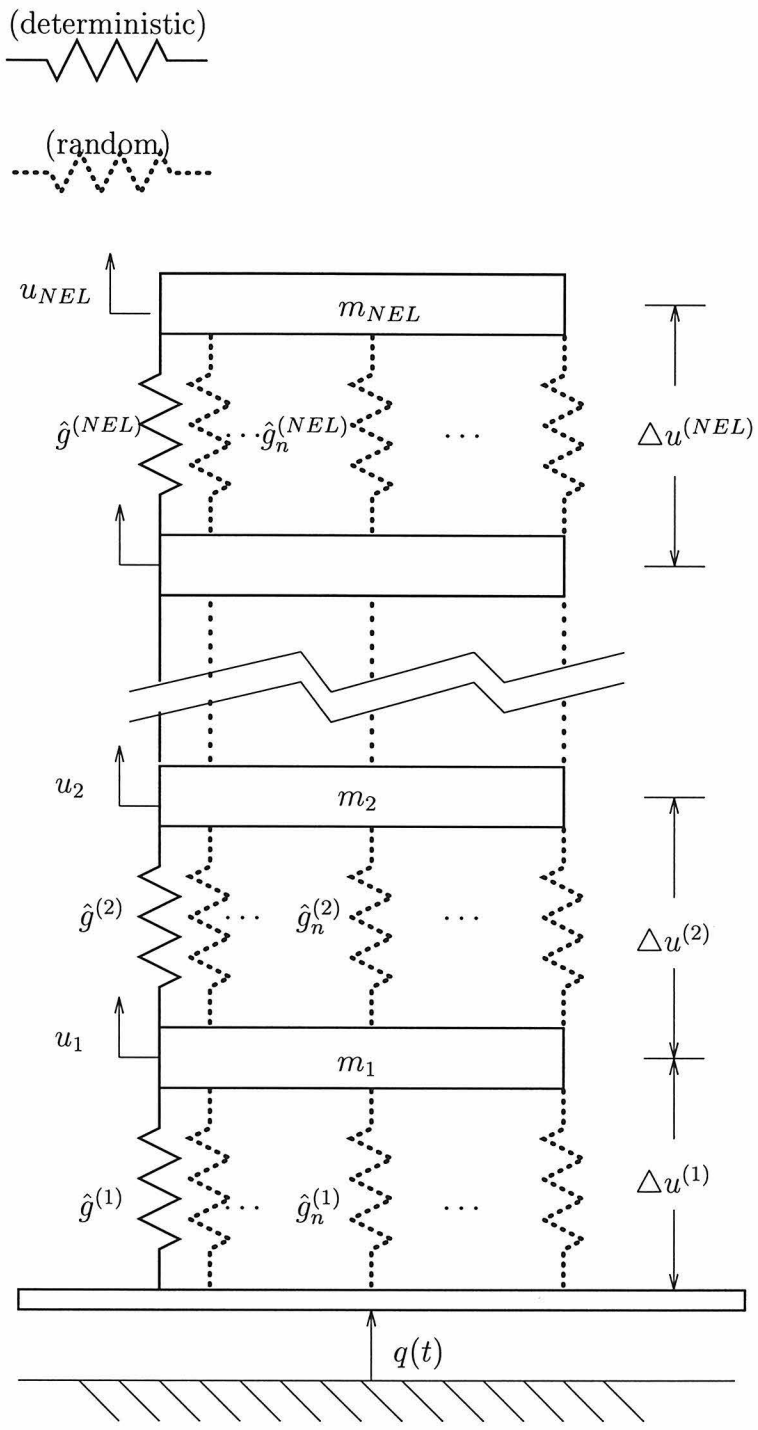

Figure 4.3: Discrete analog to uncertain nonlinear shear beam, deterministic springs: $\hat{g}^{(e)} = \bar{G}_n^{(e)} h(\frac{\triangle u^{(e)}}{l_e})$, random springs: $b_n \hat{g}_n^{(e)} = b_n \bar{G}_n^{(e)} h(\frac{\triangle u^{(e)}}{l_e})$.

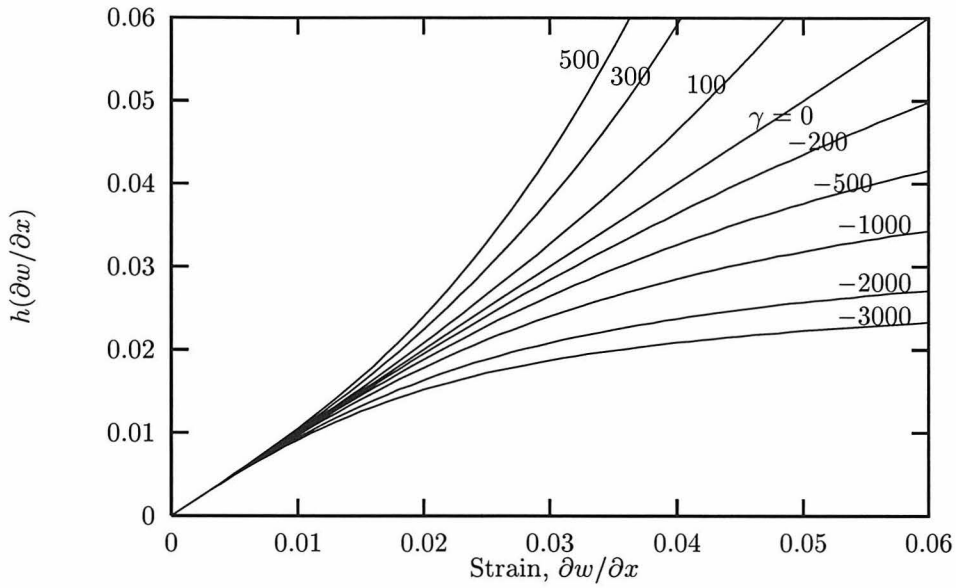

Figure 4.4: Nonlinear Stress-Strain Curves.

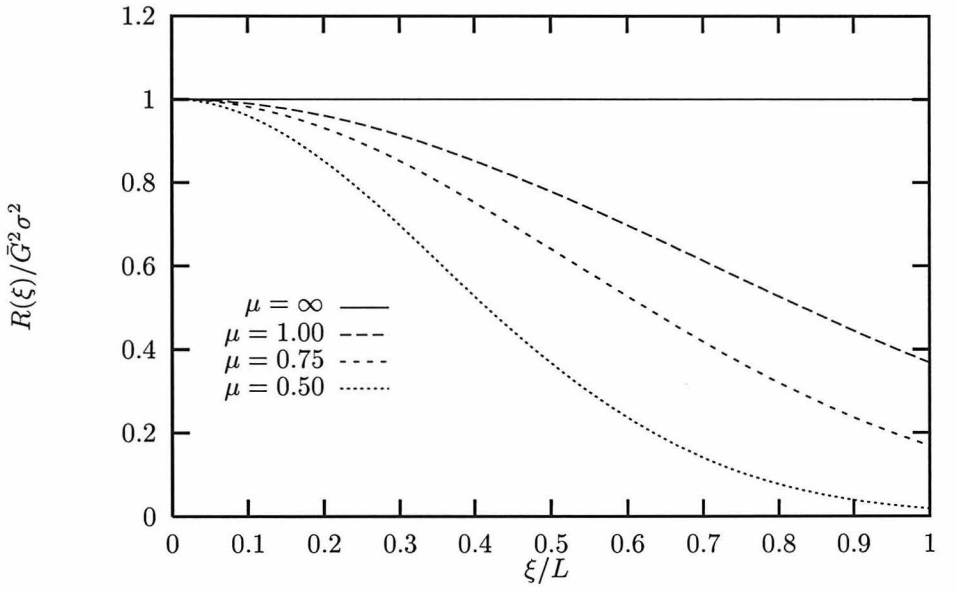

Figure 4.5: Exponential correlation function, $R(\xi) = \bar{G}^2\sigma^2 e^{-(\frac{\xi}{\mu L})^2}$.

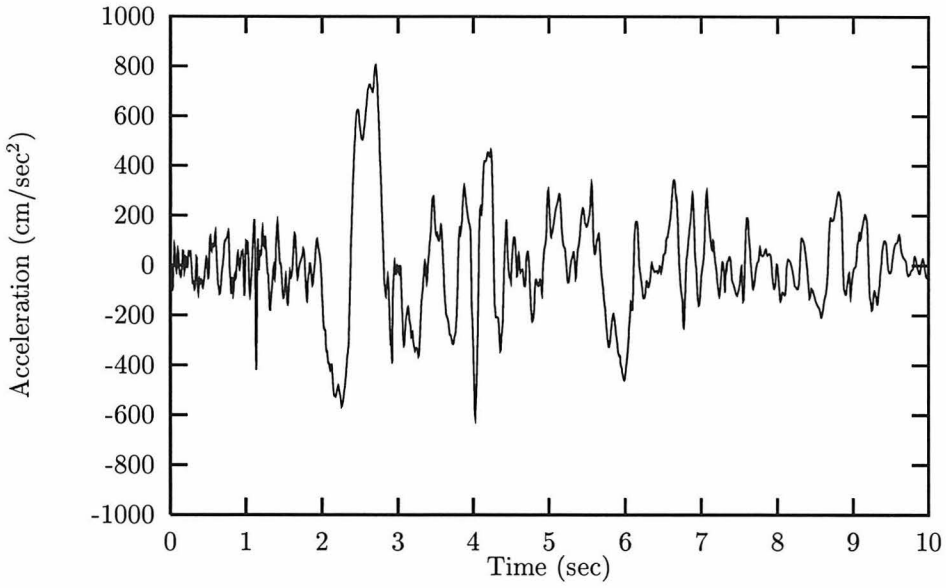

Figure 4.6: N-S component of acceleration time history of Rinaldi Receiving Station, 1994 Northridge Earthquake.

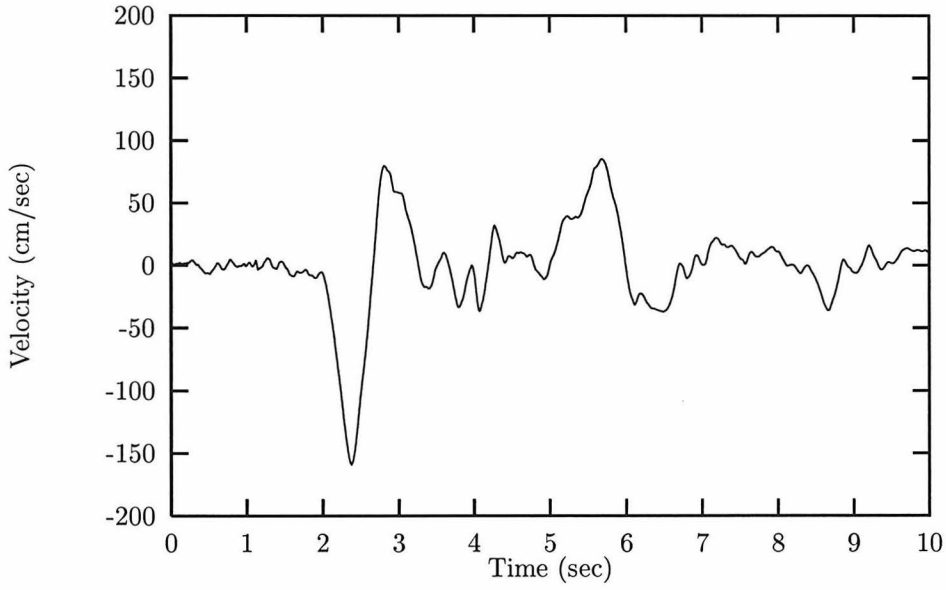

Figure 4.7: N-S component of velocity time history of Rinaldi Receiving Station, 1994 Northridge Earthquake.

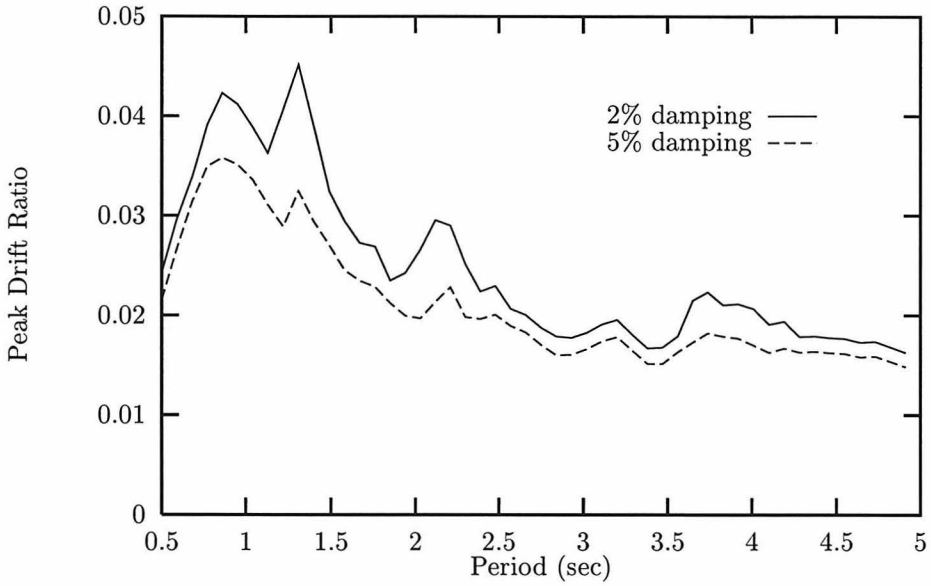

Figure 4.8: Drift spectrum obtained using damped wave approach.

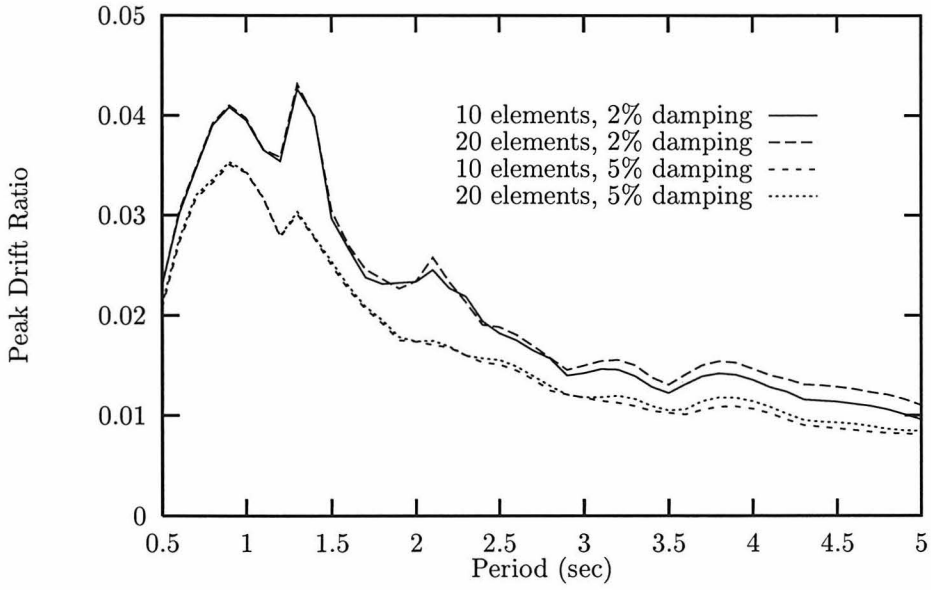

Figure 4.9: Drift spectrum obtained using FEM model.

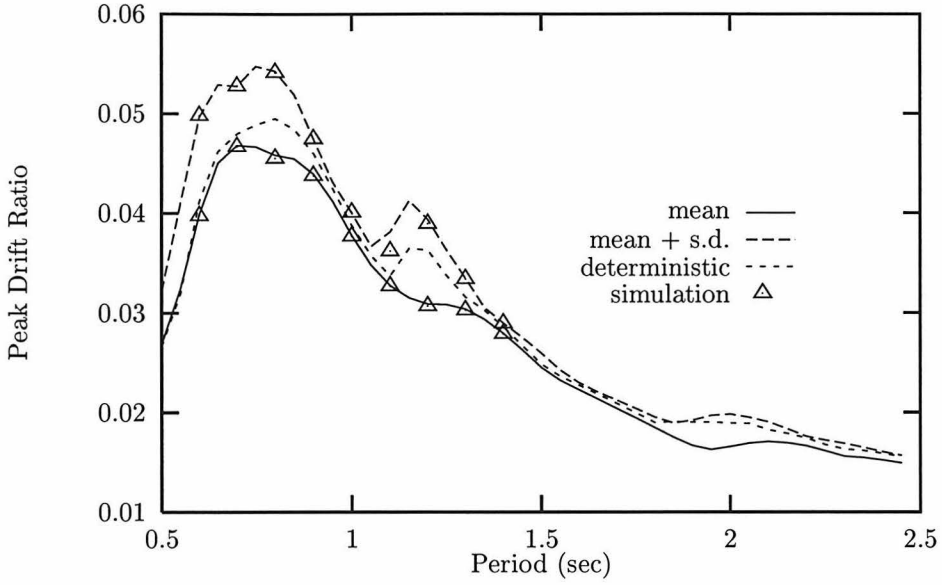

Figure 4.10: Nonlinear statistical drift spectrum, $\gamma = -2000$, $\mu = \infty$, $\sigma = 0.1$.

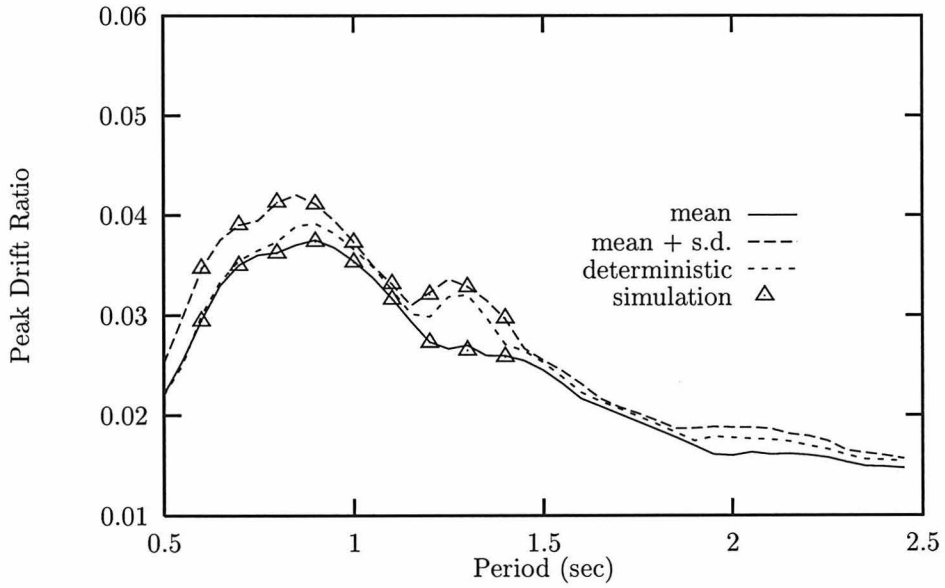

Figure 4.11: Nonlinear statistical drift spectrum, $\gamma = -500$, $\mu = \infty$, $\sigma = 0.1$.

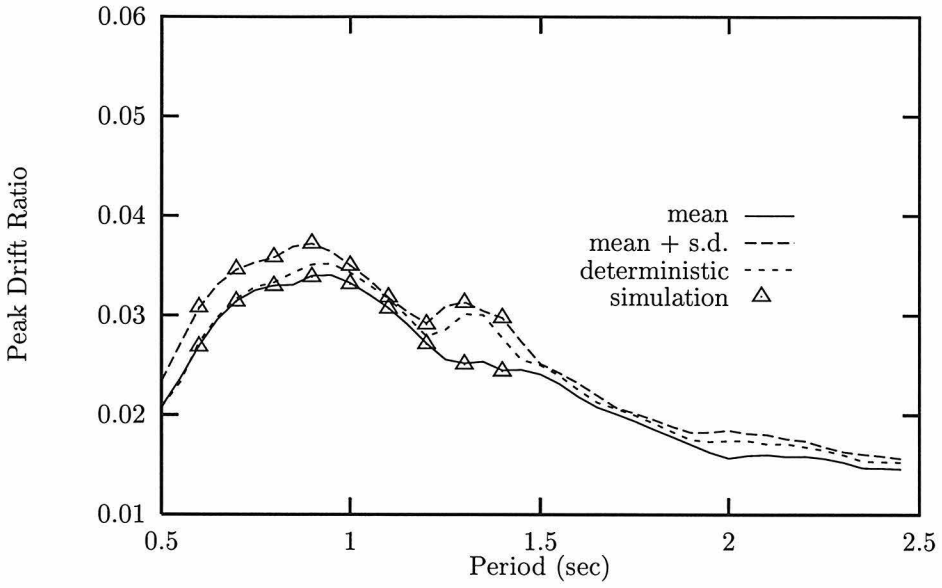

Figure 4.12: Nonlinear statistical drift spectrum, $\gamma = 0$, $\mu = \infty$, $\sigma = 0.1$.

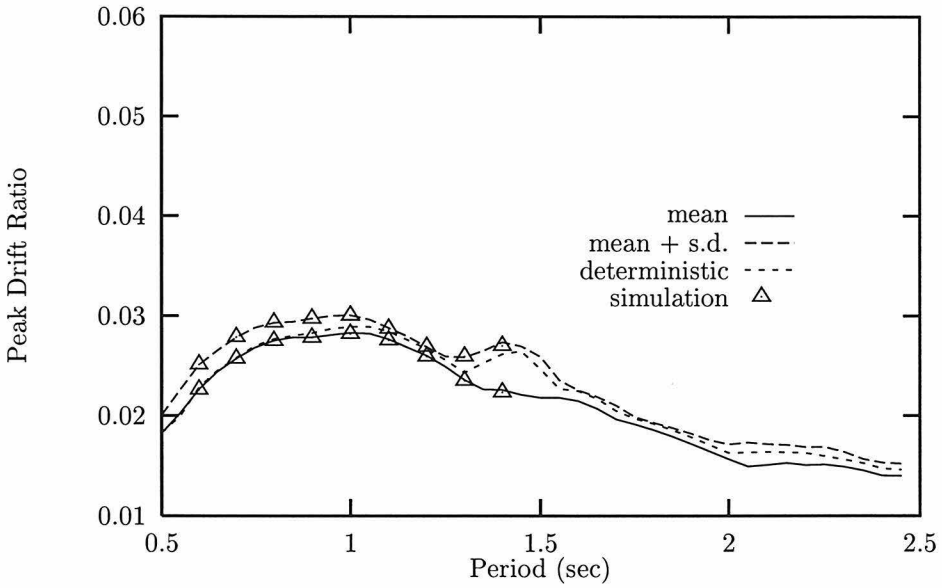

Figure 4.13: Nonlinear statistical drift spectrum, $\gamma = 500$, $\mu = \infty$, $\sigma = 0.1$.

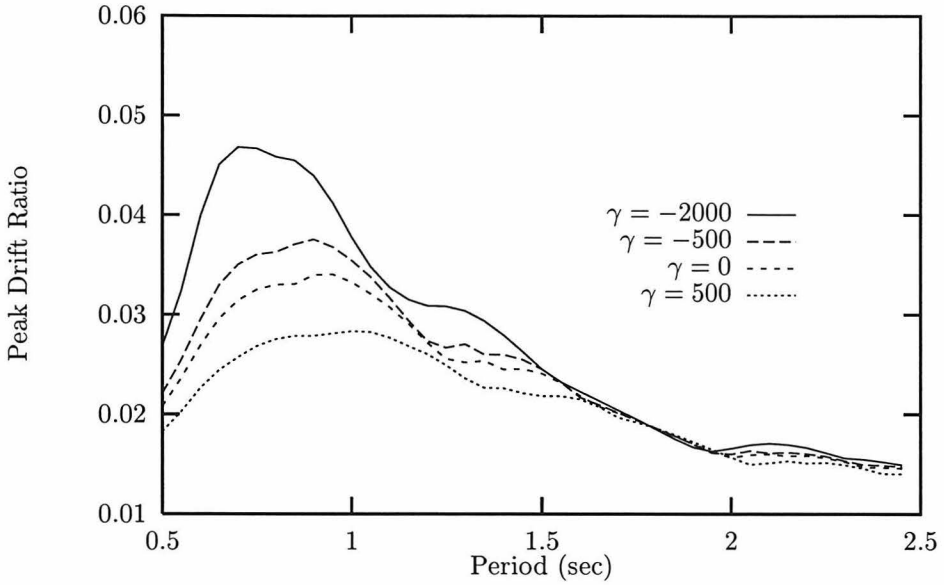

Figure 4.14: Comparison of mean drift ratio for various values of γ.

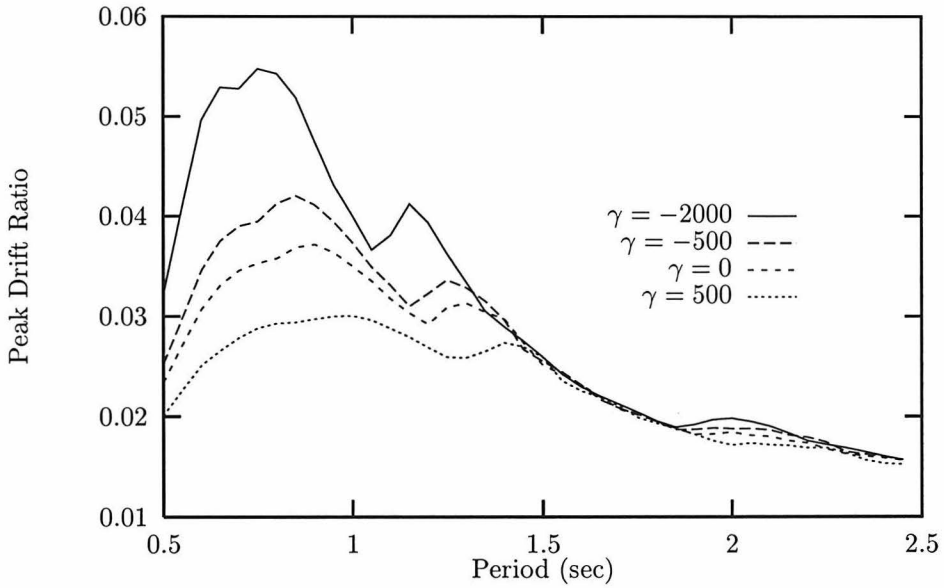

Figure 4.15: Comparison of mean plus one standard deviation of drift ratio for various values of γ.

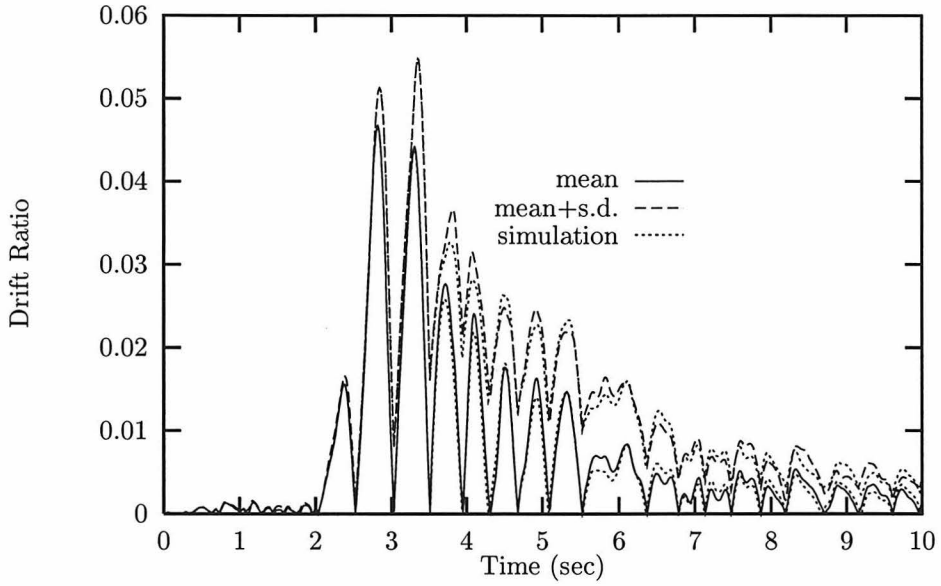

Figure 4.16: Drift statistics time history of the base element, $T = 0.75$, $\sigma = 0.1$, $\gamma = -2000$, $\mu = \infty$.

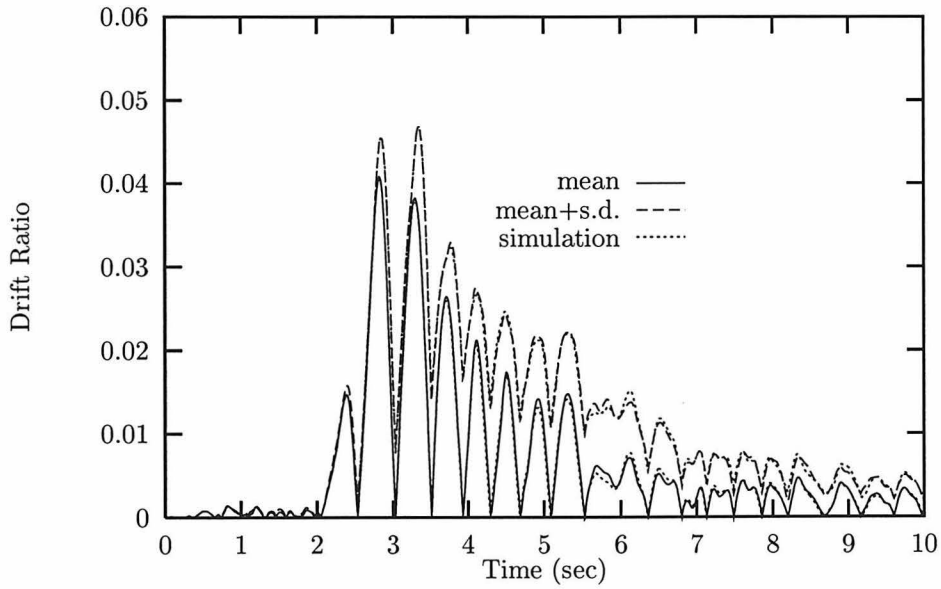

Figure 4.17: Drift statistics time history of the second element, $T = 0.75$, $\sigma = 0.1$, $\gamma = -2000$, $\mu = \infty$.

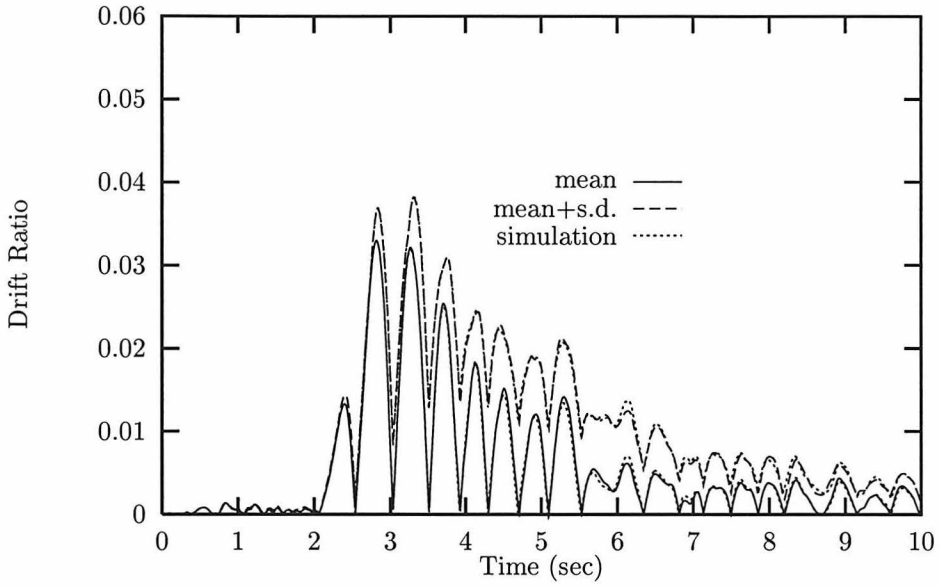

Figure 4.18: Drift statistics time history of the third element, $T = 0.75$, $\sigma = 0.1$, $\gamma = -2000$, $\mu = \infty$.

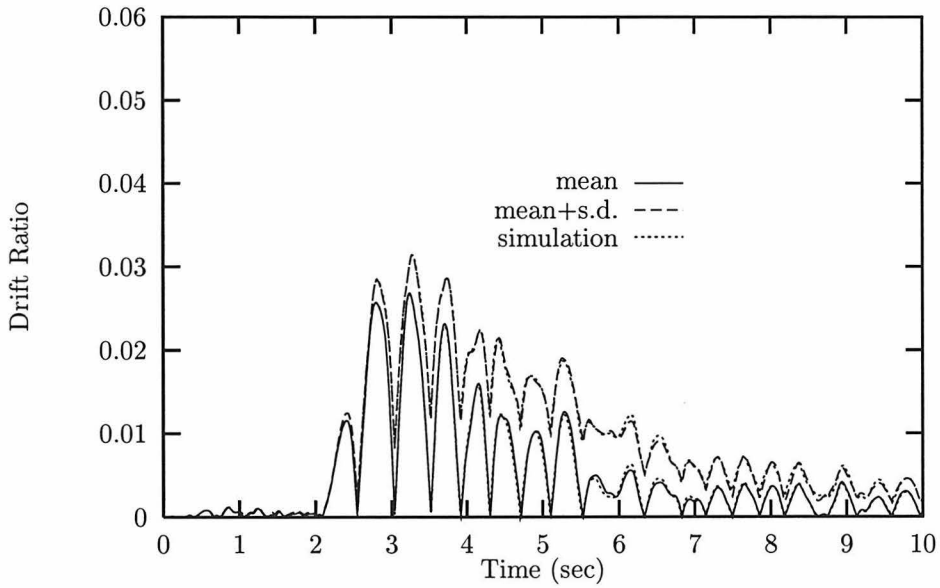

Figure 4.19: Drift statistics time history of the fourth element, $T = 0.75$, $\sigma = 0.1$, $\gamma = -2000$, $\mu = \infty$.

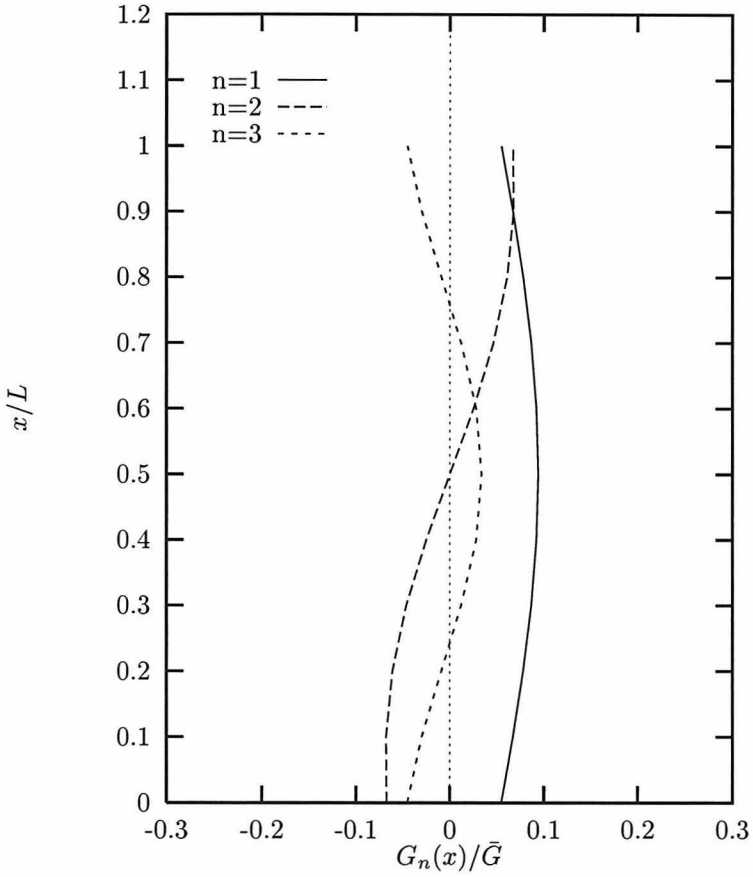

Figure 4.20: Comparison of deterministic spatial functions associated with the first three random variables, $\mu = 0.5$, $\sigma = 0.1$.

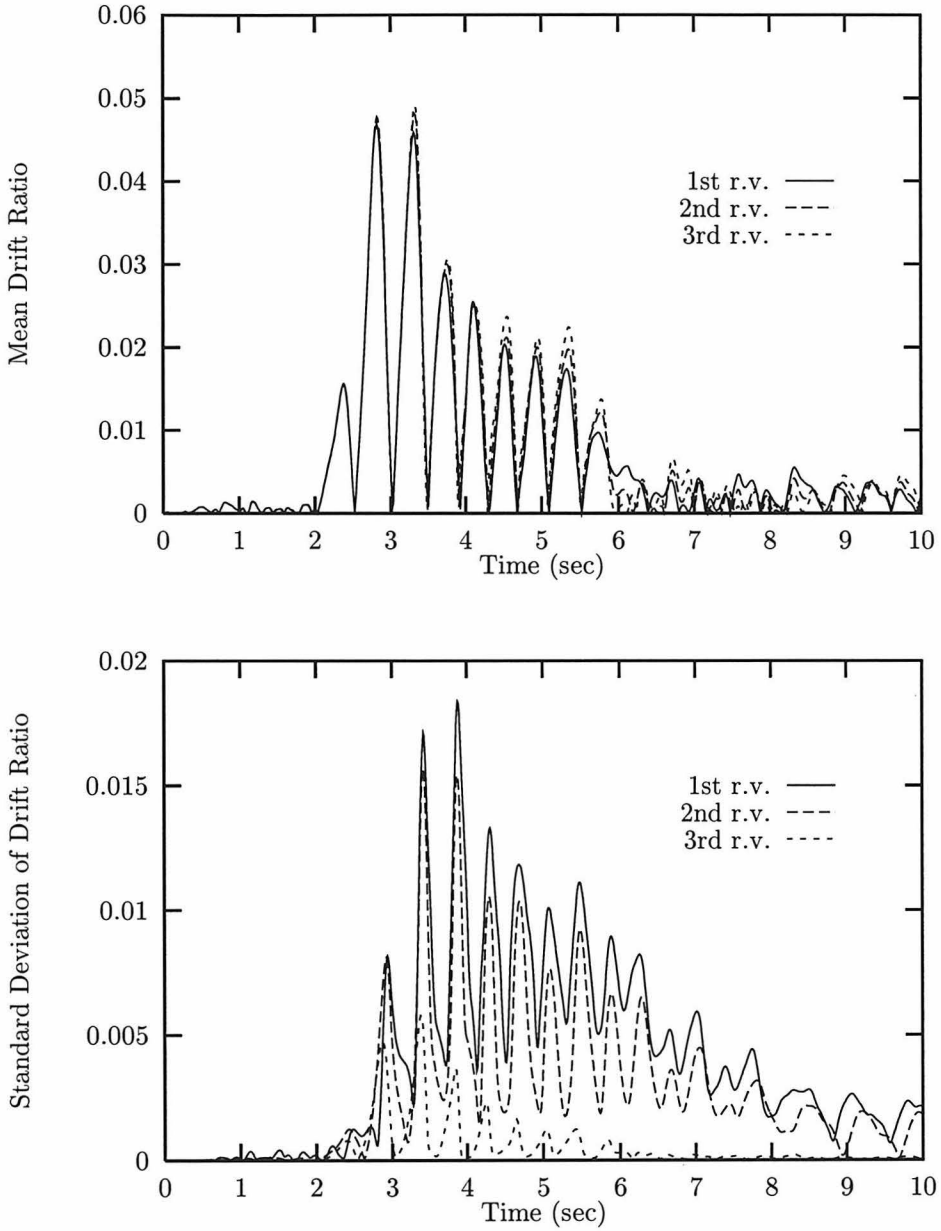

Figure 4.21: Comparison of response variability in the base element due to the first three random variables, $T = 0.75$, $\gamma = -2000$, $\mu = 0.5$.

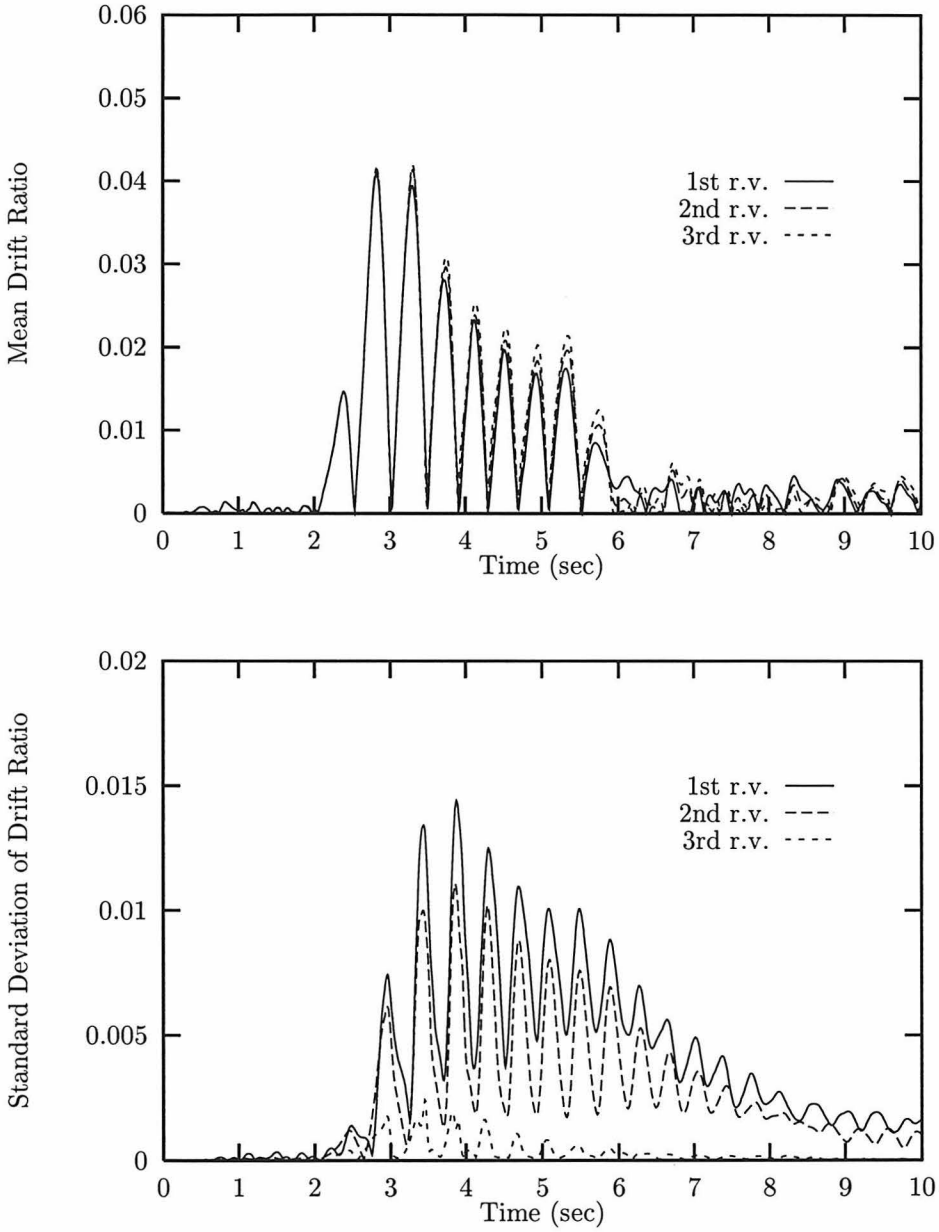

Figure 4.22: Comparison of response variability in the second element due to the first three random variables, $T = 0.75$, $\gamma = -2000$, $\mu = 0.5$.

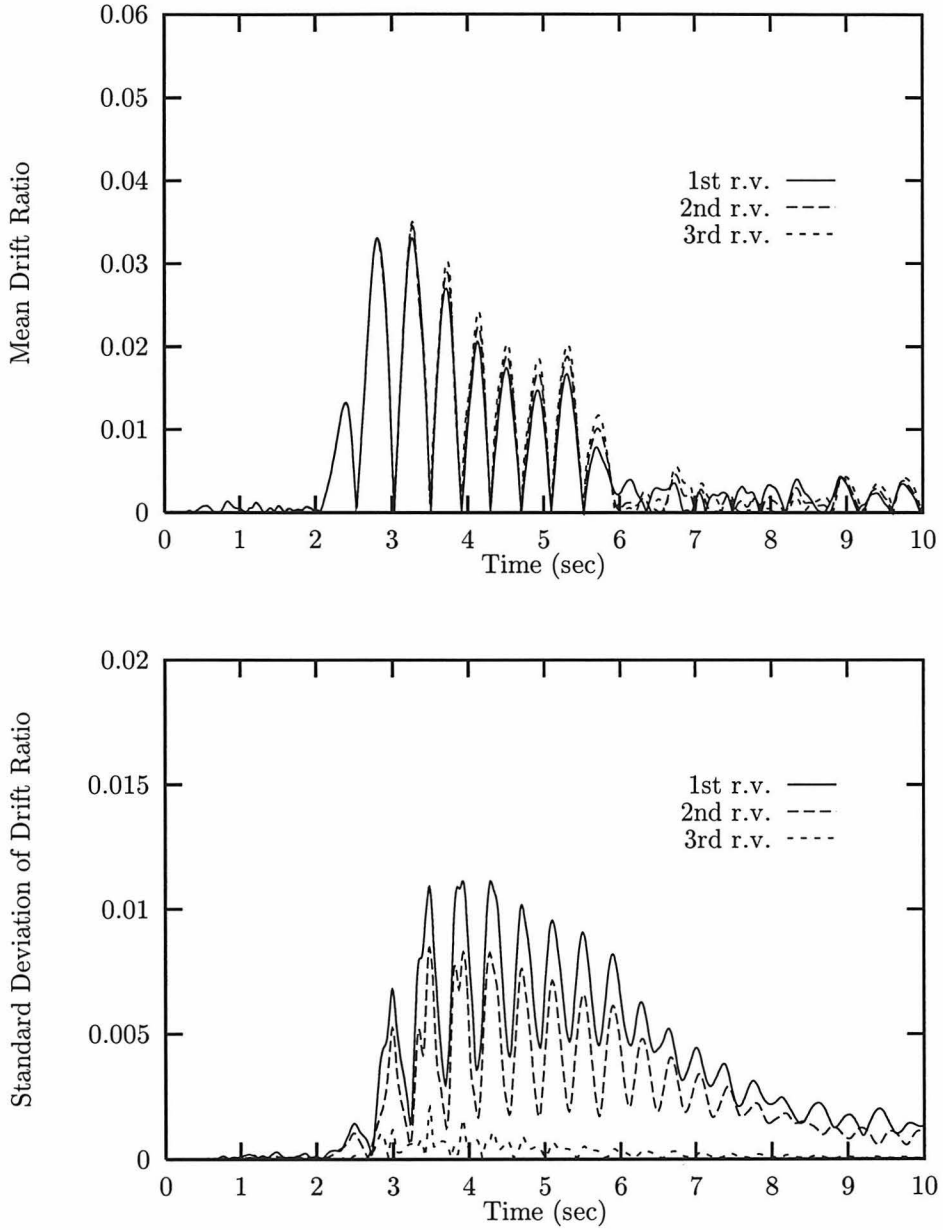

Figure 4.23: Comparison of response variability in the third element due to the first three random variables, $T = 0.75$, $\gamma = -2000$, $\mu = 0.5$.

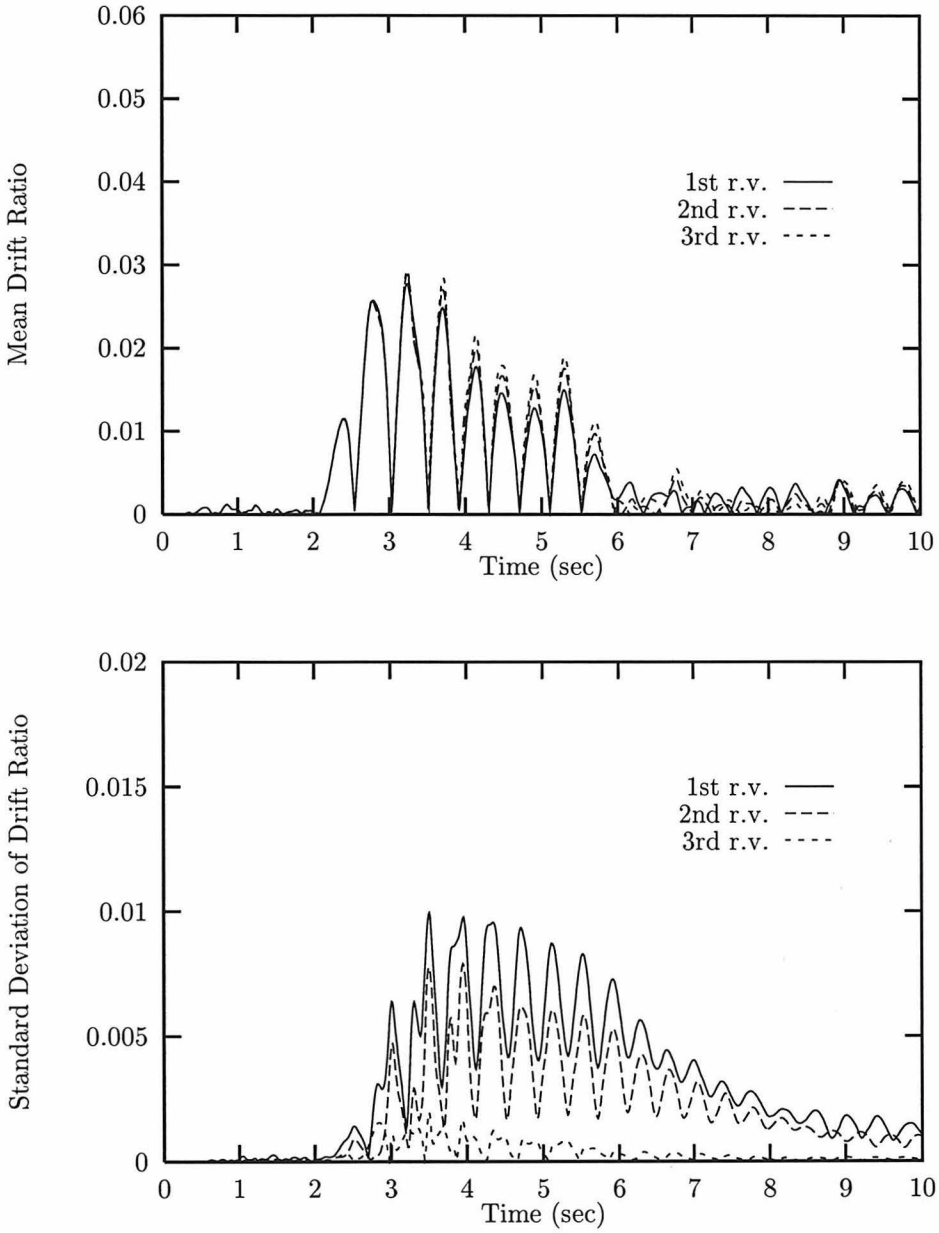

Figure 4.24: Comparison of response variability in the fourth element due to the first three random variables, $T = 0.75$, $\gamma = -2000$, $\mu = 0.5$.

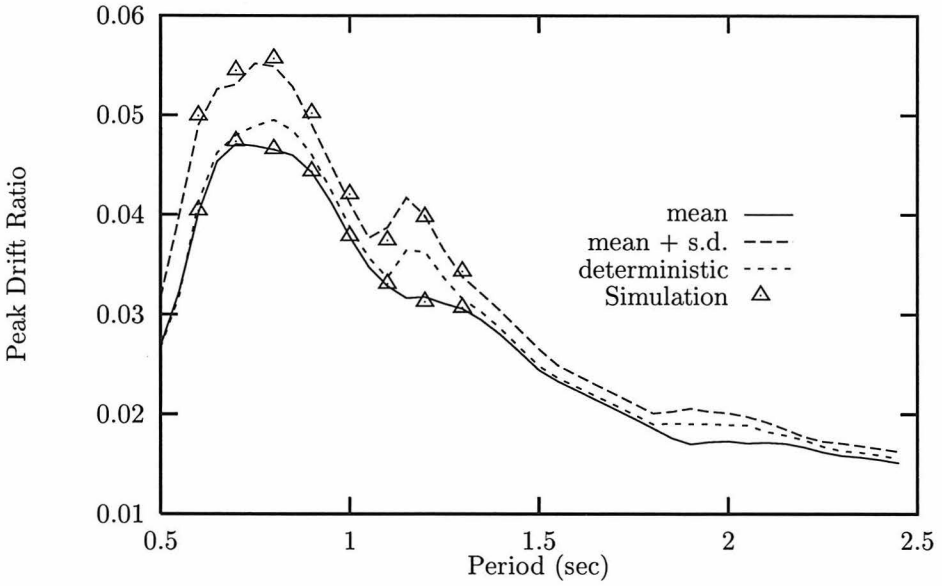

Figure 4.25: Nonlinear statistical drift spectrum, $\mu = 0.5, \gamma = -2000$, sample size of simulation $= 20 \times 20 \times 10$.

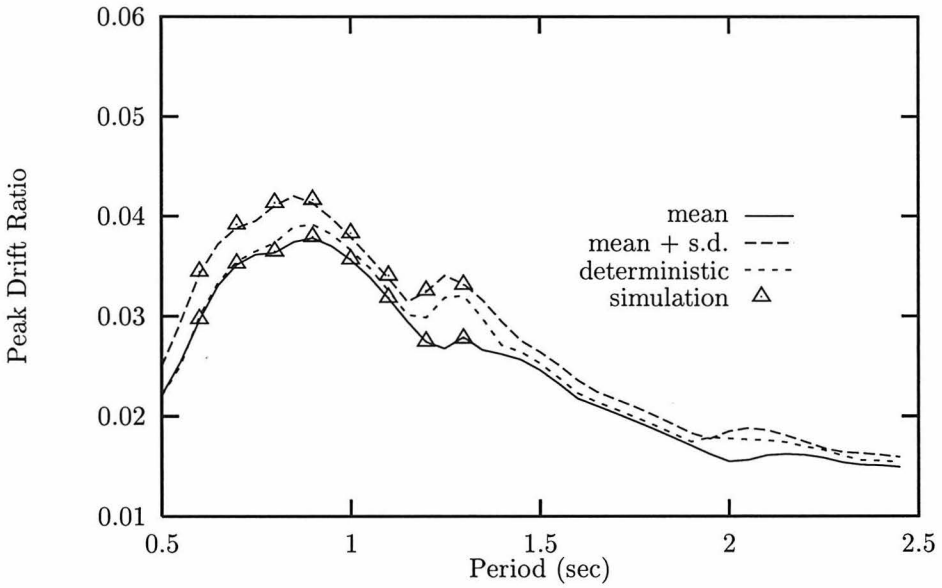

Figure 4.26: Nonlinear statistical drift spectrum, $\mu = 0.5, \gamma = -500$, sample size of simulation $= 20 \times 20 \times 10$.

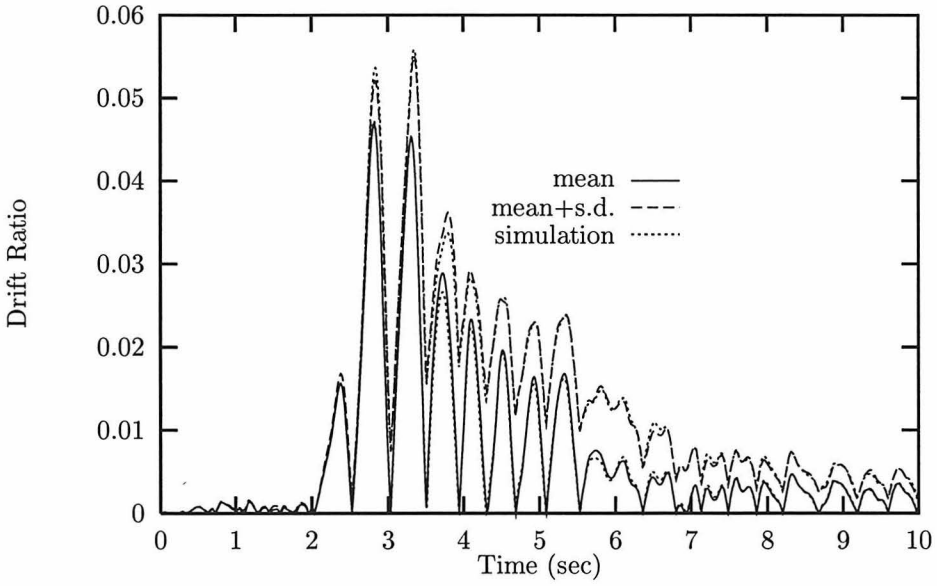

Figure 4.27: Drift statistics time history of the base element, $T = 0.75$, $\sigma = 0.1$, $\gamma = -2000$, $\mu = 0.5$.

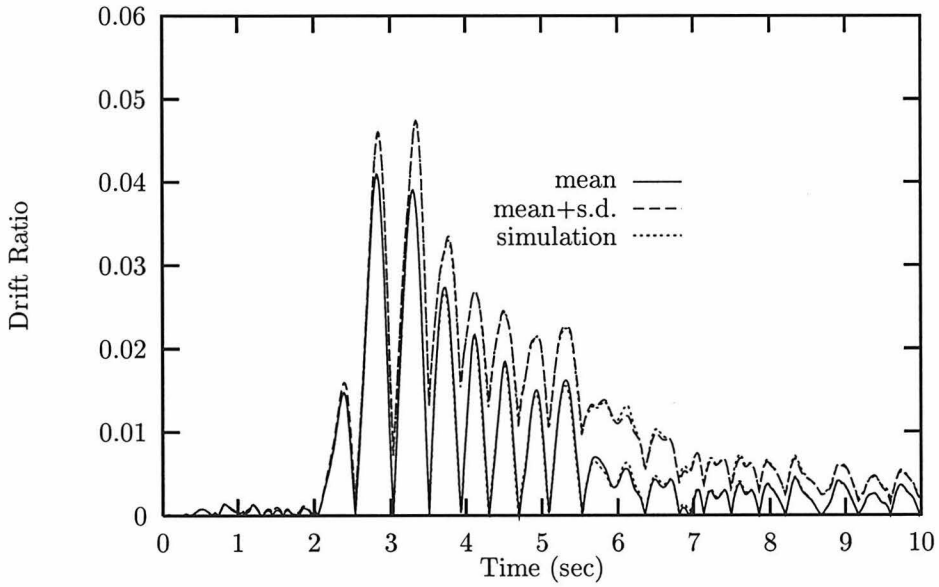

Figure 4.28: Drift statistics time history of the second element, $T = 0.75$, $\sigma = 0.1$, $\gamma = -2000$, $\mu = 0.5$.

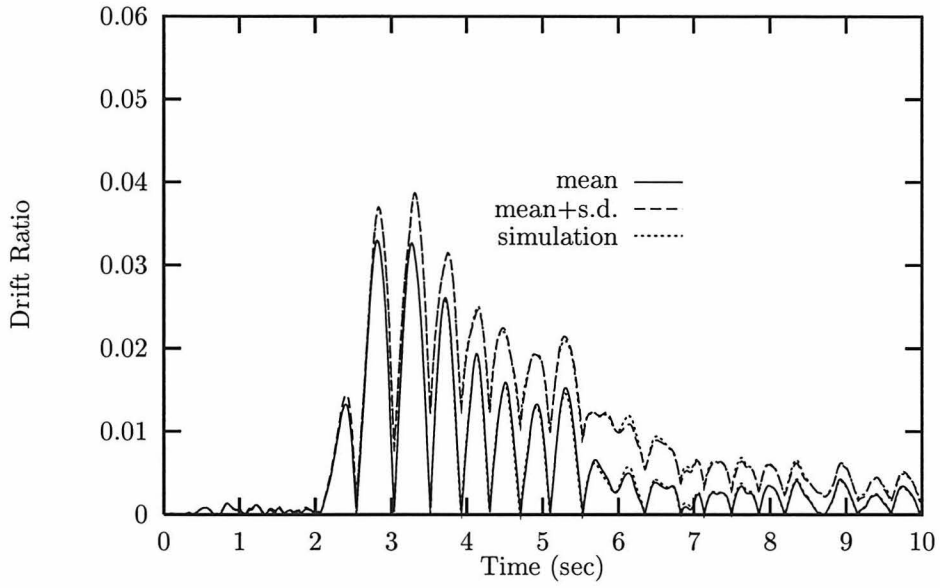

Figure 4.29: Drift statistics time history of the third element, $T = 0.75$, $\sigma = 0.1$, $\gamma = -2000$, $\mu = 0.5$.

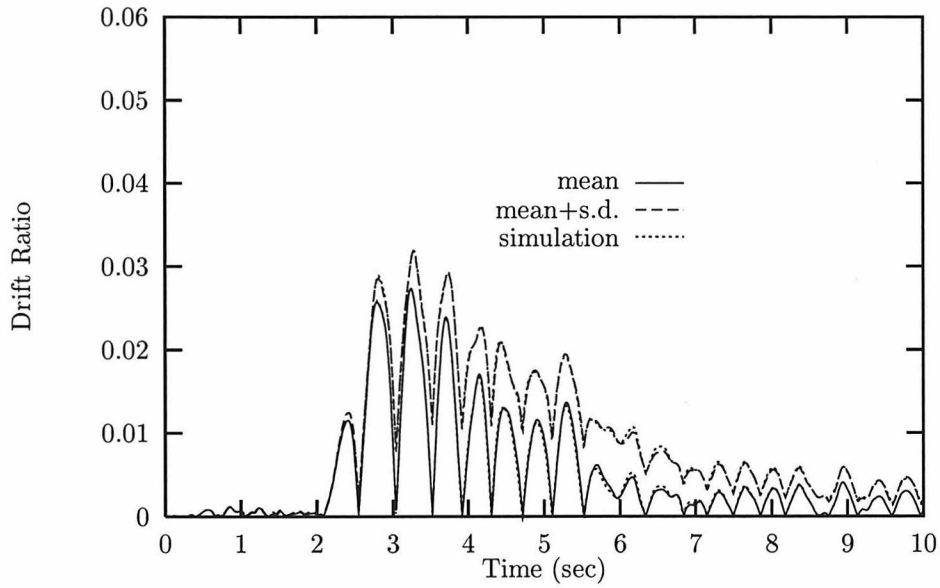

Figure 4.30: Drift statistics time history of the fourth element, $T = 0.75$, $\sigma = 0.1$, $\gamma = -2000$, $\mu = 0.5$.

Chapter 5

Nonlinear Random Vibration with Parameter Uncertainty

5.1 Introduction

Many important engineering problems are prescribed under inherently uncertain dynamical environments. Such problems arise from, for example, the response evaluation of off-shore structures under wave excitation, or the dynamical analysis of buildings subjected to some types of earthquakes, etc. To account for the excitation uncertainty, stochastic excitation models, representing a statistical generalization of deterministic excitation, are more often used as the input sources for the systems being analyzed.

In this chapter, the uncertainty due to excitation sources will also be incorporated in studying the dynamic response of uncertain nonlinear systems. The objective of this chapter is to provide a solution framework within which both the excitation uncertainty and the parameter uncertainty are treated simultaneously. The scope of study is extended to general nonlinear multi-degree-of-freedom systems with an emphasis on the nonstationary response. In this solution framework, the equivalent linearization technique is adopted to construct random equivalent systems. The solution procedure is illustrated via a general formulation for an uncertain multi-degree-of-freedom system subjected to external white noise excitation in the sequel.

5.2 Problem Formulation

Consider a nonlinear dynamical system with a set of N uncertain parameters subjected to random input excitation idealized as a modulated white noise process. The equation of motion may be written as

$$\mathbf{M}\ddot{\mathbf{x}}(t) + \mathbf{g}(\dot{\mathbf{x}}(t), \mathbf{x}(t), \boldsymbol{\gamma}) = \boldsymbol{\theta}(t)n(t) \tag{5.1}$$

where $\mathbf{M}$ is the mass matrix which is assumed to be deterministic, $\mathbf{x}(t)$, $\dot{\mathbf{x}}(t)$ and $\ddot{\mathbf{x}}(t)$ are the displacement, velocity and acceleration response vectors, $\boldsymbol{\theta}(t)$ is a vector of deterministic envelop functions, $\boldsymbol{\gamma} = \{\gamma_1, \gamma_2, \cdots, \gamma_N\}^T$ is a vector of uncertain parameters and $n(t)$ signifies a zero-mean Gaussian white process with a constant power spectrum density S_0. The autocorrelation function of $n(t)$ is given by

$$E[n(t)n(t+\tau)] = 2\pi S_0 \delta(\tau) \tag{5.2}$$

where $E[\cdot]$ denotes the expectation operator and $\delta(\cdot)$ is the Dirac delta function.

Without loss of generality, the uncertain parameters are assumed to be time-independent and are idealized as independent random variables. For convenience, $\boldsymbol{\gamma}$ is represented in terms of a set of zero-mean, unit-variance independent random variables, $\mathbf{b} = \{b_1, b_2, \cdots, b_N\}^T$, by the relation

$$\boldsymbol{\gamma} = \bar{\boldsymbol{\gamma}} + \boldsymbol{\Lambda}\mathbf{b} \tag{5.3}$$

where $\bar{\boldsymbol{\gamma}} = E[\boldsymbol{\gamma}]$, $\boldsymbol{\Lambda} = \text{diag}[\lambda_1, \lambda_2, \cdots, \lambda_N]$ and λ_i is the variance of the uncertain parameter γ_i. Substituting Eqn. (5.3) into Eqn. (5.1) and suppressing the deterministic arguments gives

$$\mathbf{M}\ddot{\mathbf{x}}(t, \mathbf{b}) + \mathbf{g}(\dot{\mathbf{x}}(t, \mathbf{b}), \mathbf{x}(t, \mathbf{b}), \mathbf{b}) = \boldsymbol{\theta}(t)n(t) \tag{5.4}$$

The randomness governing Eqn. (5.4) comes from two statistically independent sources: randomness due to the parameter uncertainty represented as time-independent discrete random variables, and randomness due to the driving force uncertainty represented as a continuum of random variables in time. Denote $\Omega_{\mathbf{b}}$ and Ω_t as the sample spaces of the parameter uncertainty and driving force uncertainty respectively. The response vectors $x(t, \mathbf{b})$ and $\dot{x}(t, \mathbf{b})$ are therefore random processes defined on the space product $\Omega_{\mathbf{b}} \times \Omega_t$. Traditional analyses for random vibration problems with deterministic parameters provide the response moments averaged over the sample space Ω_t. Under the presence of uncertain parameters, these response moments are still random quantities defined over the sample space $\Omega_{\mathbf{b}}$. Thus, the objective of studying random vibration problems with parameter uncertainty may be aimed at providing a measure of these random response moments. In the current study, this task is accomplished by performing the unconditional mean and variance analyses of the random moments.

When a stationary nonlinear response is of interest, exact closed-form solutions exist for some single-degree-of-freedom systems [14, 13, 15]. The statistics of moments can then be evaluated by either a numerical integration or a mathematical integration with the possibility of closed-form moment statistics. Yet, great difficulties have been encountered in pursuing exact analyses for the cases of nonstationary response or for systems with more than one degree-of-freedom. To the best knowledge of the author, no exact solution has been obtained so far for the types of problems mentioned above. Lacking an explicit solution, approximation techniques have to be adopted in both aspects of the random sources. In particular, the notion of equivalent linearization is employed in the formulation. In the next section, the traditional linearization scheme is further generalized to accommodate the problems with random parameters.

5.3 Equivalent Random System

The basic framework of equivalent linearization is to approximate an unknown nonlinear solution with the aid of an auxiliary linear system. Due to the linear assumption, this solution technique can also be interpreted as a Gaussian approximation method when the driving force is Gaussian. By prescribing a measure of the equation error, the principle of minimization is then applied over the entire class of linear solutions. This results in a set of partial differentiation procedures for obtaining the expression of the equivalent linear parameters. Special consideration is required when the system parameters are assumed to be random. This is due to the fact that the presence of parameter uncertainty yields the randomness in $\Omega_{\mathbf{b}} \times \Omega_t$ of the response vectors and so does the equation error. Therefore, the equation error becomes a random functional. The following is a theoretical supplement of the linearization scheme for the transition from problems with deterministic parameters to problems with random parameters.

Let the candidate equivalent system to Eqn. (5.4) be described by

$$\mathbf{M}\ddot{\mathbf{x}}(t,\mathbf{b}) + \mathbf{C}_{eq}(\mathbf{Q}(t,\mathbf{b}),\mathbf{b})\dot{\mathbf{x}}(t,\mathbf{b}) + \mathbf{K}_{eq}(\mathbf{Q}(t,\mathbf{b}),\mathbf{b})\mathbf{x}(t,\mathbf{b}) = \boldsymbol{\theta}(t)n(t) \tag{5.5}$$

where $\mathbf{Q}(t,\mathbf{b})$ denotes the time-varying covariance matrix. The randomness of the equivalent damping matrix and stiffness matrix are implicitly declared in their argument lists. Denote the equation difference as $\boldsymbol{\epsilon}(t,\mathbf{b})$. A comparison of Eqn. (5.4) and (5.5) then yields

$$\boldsymbol{\epsilon}(t,\mathbf{b}) = \mathbf{C}_{eq}(\mathbf{Q}(t,\mathbf{b}),\mathbf{b})\dot{\mathbf{x}}(t,\mathbf{b}) + \mathbf{K}_{eq}(\mathbf{Q}(t,\mathbf{b}),\mathbf{b})\mathbf{x}(t,\mathbf{b}) - \mathbf{g}(\dot{\mathbf{x}}(t,\mathbf{b}),\mathbf{x}(t,\mathbf{b}),\mathbf{b}) \tag{5.6}$$

Let J be the objective function to be minimized and define J as the unconditional

mean square equation error giving by

$$J = E\left[\int_0^\tau \boldsymbol{\epsilon}^T(t,\mathbf{b})\boldsymbol{\epsilon}(t,\mathbf{b})dt\right] \tag{5.7}$$

where τ is an arbitrary instant of time. Following the fundamental properties of probability theory, the expectation operator in Eqn. (5.7) can be conditioned on the sample vector of $\mathbf{b}$ as

$$J = \int_{\Omega_\mathbf{b}} P(\boldsymbol{\beta})E\left[\int_0^\tau \boldsymbol{\epsilon}^T(t,\mathbf{b})\boldsymbol{\epsilon}(t,\mathbf{b})dt|\mathbf{b}=\boldsymbol{\beta}\right]d\boldsymbol{\beta} \tag{5.8}$$

where $\boldsymbol{\beta}$ is a vector of the sample values of the random parameters $\mathbf{b}$. Given the condition $\mathbf{b} = \boldsymbol{\beta}$, the equation error is statistically independent of the random parameters. Further using the commutation of the expectation operator and the integration operator, Eqn. (5.8) may be rewritten as

$$J = \int_{\Omega_\mathbf{b}}\int_0^\tau P(\boldsymbol{\beta})E\left[\boldsymbol{\epsilon}^T(t,\boldsymbol{\beta})\boldsymbol{\epsilon}(t,\boldsymbol{\beta})\right]dtd\boldsymbol{\beta} \tag{5.9}$$

The integrand of Eqn. (5.9) involves only a deterministic set of the elements of the equivalent stiffness and damping matrices. Hence, regular calculus of variation can be directly applied for obtaining an optimal function representation.

Let

$$\delta J = 0 \tag{5.10}$$

Then, two independent Euler equations are derived as

$$\frac{\partial E[\boldsymbol{\epsilon}^T(t,\boldsymbol{\beta})\boldsymbol{\epsilon}(t,\boldsymbol{\beta})]}{\partial \mathbf{C}_{eq}^{(ij)}(\mathbf{Q}(t,\boldsymbol{\beta}),\boldsymbol{\beta})} = 0 \quad t\in[0,\tau], \quad \boldsymbol{\beta}\in\Omega_\mathbf{b} \tag{5.11}$$

$$\frac{\partial E[\boldsymbol{\epsilon}^T(t,\boldsymbol{\beta})\boldsymbol{\epsilon}(t,\boldsymbol{\beta})]}{\partial \mathbf{K}_{eq}^{(ij)}(\mathbf{Q}(t,\boldsymbol{\beta}),\boldsymbol{\beta})} = 0 \quad t\in[0,\tau], \quad \boldsymbol{\beta}\in\Omega_\mathbf{b} \tag{5.12}$$

where the superscript (ij) denotes the ijth element of a matrix. These equation sets are used to determine the equivalent system parameters. It has been shown by Atalik [21] that under the Gaussian assumption and certain required smooth conditions, the $\mathbf{C}_{eq}$ and $\mathbf{K}_{eq}$ take the expressions

$$\mathbf{C}_{eq}(\mathbf{Q}(t,\boldsymbol{\beta}),\boldsymbol{\beta}) = E\left[\frac{\partial \mathbf{g}(\dot{\mathbf{x}}(t,\boldsymbol{\beta}),\mathbf{x}(t,\boldsymbol{\beta}),\boldsymbol{\beta})}{\partial \dot{\mathbf{x}}(t,\boldsymbol{\beta})}\right] \tag{5.13}$$

$$\mathbf{K}_{eq}(\mathbf{Q}(t,\boldsymbol{\beta}),\boldsymbol{\beta}) = E\left[\frac{\partial \mathbf{g}(\dot{\mathbf{x}}(t,\boldsymbol{\beta}),\mathbf{x}(t,\boldsymbol{\beta}),\boldsymbol{\beta})}{\partial \mathbf{x}(t,\boldsymbol{\beta})}\right] \tag{5.14}$$

This indicates that the optimal $\mathbf{C}_{eq}$ and $\mathbf{K}_{eq}$ that minimize Eqn. (5.7) depend only on the instantaneous covariance matrix and the sample point of the random parameters being conditioned. This observation agrees with the postulated equivalent system given in Eqn. (5.5). In addition, the expressions given by Eqn. (5.13) and (5.14) are identical to what is given for the problems with deterministic parameters, and these expressions indeed minimize the unconditional mean square equation error. Note that the vector argument $\boldsymbol{\beta}$ is defined in the random sample space $\Omega_{\mathbf{b}}$. Therefore, the randomness of these matrices is automatically defined.

5.4 Random Liapunov Equation

As indicated previously, the response vector of the equivalent system is a zero-mean Gaussian process when the excitation is zero-mean Gaussian, and the statistical properties of any Gaussian process are fully characterized by its first two moments. The first moment response is identically equal to zero and is therefore independent to the parameter uncertainty. It can then be concluded that a random second-moment equation alone serves as an alternative statement for the response process under the linearized scheme. This observation motivates a process of partially suppressing the response randomness in Ω_t as the first step toward the solution of the random equi-

valent system. As a result, a Liapunov equation with random parameters governing the covariance matrix is derived. Using the state-space formulation, the derivation for the random Liapunov equation is given below.

Let $\mathbf{s}(t, \mathbf{b})$ be a vector of m state variables defined by

$$\mathbf{s}(t, \mathbf{b}) = \left\{ \begin{array}{c} \mathbf{x}(t, \mathbf{b}) \\ \dot{\mathbf{x}}(t, \mathbf{b}) \end{array} \right\} \tag{5.15}$$

and $\mathbf{f}(t)$ be the corresponding forcing vector given by

$$\mathbf{f}(t) = \left\{ \begin{array}{c} \mathbf{0} \\ \mathbf{M}^{-1}\boldsymbol{\theta}(t) \end{array} \right\} \tag{5.16}$$

Eqn. (5.5) is then converted into a first-order state-space equation by

$$\dot{\mathbf{s}}(t, \mathbf{b}) = \mathbf{A}_{eq}(t, \mathbf{b})\mathbf{s}(t, \mathbf{b}) + \mathbf{f}(t)n(t) \tag{5.17}$$

where $\mathbf{A}_{eq}(t, \mathbf{b})$ denotes the time-varying equivalent system matrix given by

$$\mathbf{A}_{eq}(t, \mathbf{b}) = \left[\begin{array}{cc} \mathbf{0} & \mathbf{I} \\ -\mathbf{M}^{-1}\mathbf{K}_{eq}(t, \mathbf{b}) & -\mathbf{M}^{-1}\mathbf{C}_{eq}(t, \mathbf{b}) \end{array} \right] \tag{5.18}$$

Let the symbol $E_t(\cdot)$ be the average operator over the random space of the driving force Ω_t. Post-multiplying Eqn. (5.17) by $\mathbf{s}^T$, premultiplying the transpose of Eqn. (5.17) by $\mathbf{s}$ and then performing the E_t operator on the sum of resulting equations yields

$$\begin{aligned} \dot{\mathbf{Q}}(t, \mathbf{b}) \;=\; & \mathbf{A}_{eq}(t, \mathbf{b})\mathbf{Q}(t, \mathbf{b}) + \mathbf{Q}(t, \mathbf{b})\mathbf{A}_{eq}^T(t, \mathbf{b}) + \\ & E_t[\mathbf{s}(t, \mathbf{b})n(t)]\mathbf{f}^T(t) + \mathbf{f}(t)E_t[\mathbf{s}^T(t, \mathbf{b})n(t)] \end{aligned} \tag{5.19}$$

where $\mathbf{Q}(t, \mathbf{b}) = E_t[\mathbf{s}(t, \mathbf{b})\mathbf{s}^T(t, \mathbf{b})]$.

Eqn. (5.19) can be further simplified by considering the correlation between the response vector $\mathbf{s}(t, \mathbf{b})$ and the white noise excitation $n(t)$. Noting that $\mathbf{s}(t, \mathbf{b})$ is the solution of the linear equation Eqn. (5.17), there exists a random principle matrix $\Phi(t, \mathbf{b})$ satisfying the following two conditions

$$\dot{\Phi}(t, \mathbf{b}) = \mathbf{A}_{eq}(t, \mathbf{b})\Phi(t, \mathbf{b}) \tag{5.20}$$

$$\Phi(0, \mathbf{b}) = \mathbf{I} \tag{5.21}$$

Then, the response $\mathbf{s}(t, \mathbf{b})$ is expressed in terms of the principle matrix and white noise excitation as

$$\mathbf{s}(t, \mathbf{b}) = \Phi(t, \mathbf{b})\mathbf{s}(0, \mathbf{b}) + \Phi(t, \mathbf{b}) \int_0^t \Phi^{-1}(\tau, \mathbf{b})\mathbf{f}(\tau)n(\tau)d\tau \tag{5.22}$$

Multiplying Eqn. (5.22) by $n(t)$ and then performing E_t operator gives

$$E_t[\mathbf{s}(t, \mathbf{b})n(t)] = \Phi(t, \mathbf{b}) \int_0^t \Phi^{-1}(\tau, \mathbf{b})\mathbf{f}(\tau)E_t[n(\tau)n(t)]d\tau. \tag{5.23}$$

Recall that the white process $n(t)$ is delta-correlated satisfying

$$E_t[n(t)n(\tau)] = 2\pi S_0\delta(t - \tau) \tag{5.24}$$

Substituting Eqn. (5.24) into Eqn. (5.23) yields

$$E_t[\mathbf{s}(t, \mathbf{b})n(t)] = \pi S_0\mathbf{f}(t) \tag{5.25}$$

Substituting Eqn. (5.25) and its transpose into Eqn. (5.19) gives a random Liapunov

equation of the form

$$\dot{\mathbf{Q}}(t,\mathbf{b}) = \mathbf{A}_{eq}(t,\mathbf{b})\mathbf{Q}(t,\mathbf{b}) + \mathbf{Q}(t,\mathbf{b})\mathbf{A}_{eq}^{T}(t,\mathbf{b}) + 2\pi S_0 \mathbf{f}(t)\mathbf{f}^{T}(t) \tag{5.26}$$

Eqn. (5.26) is a matrix equation representing a set of $m \times m$ equations. Since the random covariance matrix is symmetric, there are only $\frac{m(m+1)}{2}$ independent equations out of the m^2 equations. Alternatively, Eqn. (5.26) can be expressed as a vector form where only the independent equations are involved.

5.5 Approximation of the Random System Matrix

Given a random instantaneous covariance matrix, the $\mathbf{C}_{eq}$ and $\mathbf{K}_{eq}$ can be approximated as quadratic functions of $\mathbf{b}$. Let $\mathbf{D}(\mathbf{b})$ be a matrix of functions $\mathbf{b}$, and denote the nth partial derivative coefficient matrix as $\mathbf{D}_{i\cdots j}^{[n]}$. Then,

$$\mathbf{D}_{\underbrace{i\cdots j}_{n}}^{[n]} = \left.\frac{\partial^n \mathbf{D}(\mathbf{b})}{\underbrace{\partial b_i \cdots \partial b_j}_{n}}\right|_{\mathbf{b}=\mathbf{0}} \tag{5.27}$$

A second-order Taylor expansion of the instantaneous equivalent damping and stiffness matrices takes the forms

$$\begin{aligned}
\mathbf{C}_{eq}(\mathbf{Q}(t,\mathbf{b}),\mathbf{b}) &\approx \mathbf{C}^{[0]}(t) + \sum_{i=1}^{N} \mathbf{C}_i^{[\mathrm{I}]}(t) b_i + \frac{1}{2}\sum_{i=1}^{N}\sum_{j=1}^{N} \mathbf{C}_{ij}^{[\mathrm{II}]}(t) b_i b_j \\
\mathbf{K}_{eq}(\mathbf{Q}(t,\mathbf{b}),\mathbf{b}) &\approx \mathbf{K}^{[0]}(t) + \sum_{i=1}^{N} \mathbf{K}_i^{[\mathrm{I}]}(t) b_i + \frac{1}{2}\sum_{i=1}^{N}\sum_{j=1}^{N} \mathbf{K}_{ij}^{[\mathrm{II}]}(t) b_i b_j
\end{aligned} \tag{5.28}$$

where the time-dependent nth-order variation matrices are obtained through the chain rule of partial differentiation of the covariance matrix and the random variables. The variation matrices may contain functions of the covariance matrix up to the nth-order

as indicated by the following symbolic expressions

$$\mathbf{C}^{[n]}_{i\cdots j}(t) = \mathbf{C}^{[n]}_{i\cdots j}[\mathbf{Q}^{[0]}(t), \mathbf{Q}^{[\mathrm{I}]}_{i}(t), \cdots, \mathbf{Q}^{[n]}_{i\cdots j}(t)] \tag{5.29}$$

$$\mathbf{K}^{[n]}_{i\cdots j}(t) = \mathbf{K}^{[n]}_{i\cdots j}[\mathbf{Q}^{[0]}(t), \mathbf{Q}^{[\mathrm{I}]}_{i}(t), \cdots, \mathbf{Q}^{[n]}_{i\cdots j}(t)] \tag{5.30}$$

Denote $\mathbf{A}^{[0]}(t)$, $\mathbf{A}^{[\mathrm{I}]}_{i}(t)$ and $\mathbf{A}^{[\mathrm{II}]}_{ij}(t)$ as the zero, first and second-order time-varying matrices respectively. These matrices are defined as

$$\mathbf{A}^{[n]}_{i\cdots j}(t) = \begin{bmatrix} \mathbf{0} & \mathbf{I} \\ -\mathbf{M}^{-1}\mathbf{K}^{[n]}_{i\cdots j}(t) & -\mathbf{M}^{-1}\mathbf{C}^{[n]}_{i\cdots j}(t) \end{bmatrix} \tag{5.31}$$

Then a second-order approximation of the random system matrix, denoted as $\mathbf{A}(t, \mathbf{b})$, is given by

$$\mathbf{A}(t, \mathbf{b}) = \mathbf{A}^{[0]}(t) + \sum_{i=1}^{N} \mathbf{A}^{[\mathrm{I}]}_{i}(t) b_i + \frac{1}{2} \sum_{i=1}^{N} \sum_{j=1}^{N} \mathbf{A}^{[\mathrm{II}]}_{ij}(t) b_i b_j \tag{5.32}$$

The approximated random Liapunov equation thus becomes

$$\dot{\mathbf{Q}}(t, \mathbf{b}) = \mathbf{A}(t, \mathbf{b})\mathbf{Q}(t, \mathbf{b}) + \mathbf{Q}(t, \mathbf{b})\mathbf{A}^{T}(t, \mathbf{b}) + 2\pi S_0 \mathbf{f}(t)\mathbf{f}^{T}(t) \tag{5.33}$$

where the expression for the matrix $\mathbf{A}(t, \mathbf{b})$ is given in Eqn. (5.32)

Note that, except for the twice-differentiable condition with respect to $\mathbf{b}$ of the equivalent system matrix, no additional assumption is made on the type of system nonlinearity or the way the uncertain parameters appear in the equation of motion. Also note that the random variable set is extracted explicitly up to the second order. Thus, there is great advantage in converting the random Liapunov equation into a deterministic one.

5.6 Deterministic Liapunov Equation

To solve Eqn. (5.33), the covariance matrix is expanded in terms of the set of orthogonal polynomials as

$$\mathbf{Q}(t,\mathbf{b}) \cong \sum_{|\mathbf{l}|=\mathbf{0}}^{NP} \hat{\mathbf{Q}}_{l_1 l_2 \cdots l_N}(t) H_{l_1 l_2 \cdots l_N}(\mathbf{b}) \tag{5.34}$$

where $|\mathbf{l}|$ denotes the norm which can take

$$|\mathbf{l}| = \sum_{i=1}^{N} l_i \tag{5.35}$$

Recall that the set of orthogonal polynomials $\{H_{l_1 l_2 \cdots l_N}(\mathbf{b})\}_{|\mathbf{l}|=0}^{\infty}$ satisfy the orthogonality condition

$$E\left[H_{l_1 l_2 \cdots l_N}(\mathbf{b}) H_{m_1 m_2 \cdots m_N}(\mathbf{b})\right] = \prod_{i=1}^{N} \delta_{l_i m_i} \tag{5.36}$$

Note that the system matrices involve the evaluation of up to the nth-order Taylor coefficient matrices of the covariance matrix. With the orthogonal polynomial solution basis, these Taylor coefficient matrices can be evaluated explicitly by

$$\begin{aligned} \hat{\mathbf{Q}}^{[n]}_{i\cdots j}(t) &= \sum_{|\mathbf{l}|=0}^{NP} \hat{\mathbf{Q}}_{l_1 l_2 \cdots l_N}(t) \left.\frac{\partial^n H_{l_1 l_2 \cdots l_N}(\mathbf{b})}{\partial b_i \cdots \partial b_j}\right|_{\mathbf{b}=\mathbf{0}} \\ &= \sum_{|\mathbf{l}|=0}^{NP} \hat{\mathbf{Q}}_{l_1 l_2 \cdots l_N}(t) H^{[n]}_{l_1 l_2 \cdots l_N, i\cdots j} \end{aligned} \tag{5.37}$$

where $H^{[n]}_{l_1 l_2 \cdots l_N, i\cdots j}$ are constant coefficients which can be evaluated efficiently and tabulated. Thus, the system matrices becomes

$$\hat{\mathbf{A}}^{[n]}_{i\cdots j}(t) = \mathbf{A}^{[n]}_{i\cdots j}[\hat{\mathbf{Q}}^{[0]}(t), \hat{\mathbf{Q}}^{[\mathrm{I}]}_{i}(t), \cdots, \hat{\mathbf{Q}}^{[n]}_{i\cdots j}(t)] \tag{5.38}$$

In the preceding formulations, the instantaneous stiffness and damping matrices are approximated by quadratic random functions. These quadratic random functions

are expressed explicitly in terms of the power of the random variables. It is useful to apply the recursive relationships of the orthogonal polynomials for subsequent derivations. For a symmetric probability density function, the recursive relationships may be expressed as

$$b_i H_{l_i}(b_i) = a_{-1}^{l_i} H_{l_i-1}(b_i) + a_1^{l_i} H_{l_i+1}(b_i) \tag{5.39}$$

$$b_i^2 H_{l_i}(b_i) = \bar{a}_{-2}^{l_i} H_{l_i-2}(b_i) + \bar{a}_0^{l_i} H_{l_i}(b_i) + \bar{a}_2^{l_i} H_{l_i+2}(b_i) \tag{5.40}$$

where the coefficients in Eqn. (5.40) are derived from Eqn. (5.39). Their relations are given by

$$\begin{aligned} \bar{a}_{-2}^{l_i} &= a_{-1}^{l_i} a_{-1}^{l_i-1} \\ \bar{a}_0^{l_i} &= a_{-1}^{l_i} a_1^{l_i-1} + a_1^{l_i} a_{-1}^{l_i+1} \\ \bar{a}_2^{l_i} &= a_1^{l_i} a_1^{l_i+1} \end{aligned} \tag{5.41}$$

To obtain the final deterministic equations, first substitute Eqn. (5.38) and Eqn. (5.34) into Eqn. (5.33) and multiply the resulting equation with individual orthogonal polynomials. Applying the expectation operator and using the recursive relationships will lead to a coupled set of deterministic Liapunov equations as

$$\begin{aligned} \dot{\hat{\mathbf{Q}}}_{l_1 l_2 \cdots l_N}(t) &= \hat{\mathbf{A}}^{[0]}(t)\hat{\mathbf{Q}}_{l_1 l_2 \cdots l_N}(t) + \hat{\mathbf{Q}}_{l_1 l_2 \cdots l_N}(t)\hat{\mathbf{A}}^{[0]^T}(t) + 2\pi S_0 \mathbf{f}(t)\mathbf{f}^T(t) \prod_{i=1}^{N} \delta_{0 l_i} \\ &+ \sum_{i=1}^{N} \sum_{r=-1,1} a_r^{l_i} \left(\hat{\mathbf{A}}_i^{[\mathrm{I}]}(t)\hat{\mathbf{Q}}_{l_1 \cdots l_i+r \cdots l_N}(t) + \hat{\mathbf{Q}}_{l_1 \cdots l_i+r \cdots l_N}(t)\hat{\mathbf{A}}_i^{[\mathrm{I}]^T}(t) \right) \\ &+ \frac{1}{2} \sum_{i=1}^{N} \sum_{r=-2,0,2} \bar{a}_r^{l_i} \left(\hat{\mathbf{A}}_{ii}^{[\mathrm{II}]}(t)\hat{\mathbf{Q}}_{l_1 \cdots l_i+r \cdots l_N}(t) + \hat{\mathbf{Q}}_{l_1 \cdots l_i+r \cdots l_N}(t)\hat{\mathbf{A}}_{ii}^{[\mathrm{II}]^T}(t) \right) \\ &+ \frac{1}{2} \sum_{i,j=1}^{N} \sum_{r,s=-1,1} a_r^{l_i} a_s^{l_j} \left(\hat{\mathbf{A}}_{ij}^{[\mathrm{II}]}(t)\hat{\mathbf{Q}}_{l_1 \cdots l_i+r \cdots l_j+s \cdots l_N}(t) + \hat{\mathbf{Q}}_{l_1 \cdots l_i+r \cdots l_j+s \cdots l_N}(t)\hat{\mathbf{A}}_{ij}^{[\mathrm{II}]^T}(t) \right) \\ &\qquad |\mathbf{l}| = 0, NP \end{aligned} \tag{5.42}$$

Eqn. (5.42) can be solved numerically in time to obtain the nonstationary covari-

ance response. The nonstationary response statistics can then be calculated using

$$\begin{aligned} E\left[\mathbf{Q}^{(ij)}(t,\mathbf{b})\right] &= \hat{\mathbf{Q}}^{(ij)}_{0\cdots 0}(t) \\ Var\left[\mathbf{Q}^{(ij)}(t,\mathbf{b})\right] &= \sum_{|\mathbf{l}|=1}^{NP} \hat{\mathbf{Q}}^{(ij)^2}_{l_1\cdots l_N}(t) \end{aligned} \tag{5.43}$$

where the bracketed superscript, (ij), denotes the ijth element of the covariance matrix.

Chapter 6

Application: Hardening and Softening SDOF Systems

In this chapter, the newly developed solution technique for obtaining the statistics of nonstationary response moments is applied to several uncertain nonlinear single-degree-of-freedom systems subjected to modulated white noise excitation.

6.1 Formulation

Consider a nonlinear uncertain single-degree-of-freedom system subjected to a modulated white noise excitation formulated by the equation of motion

$$\ddot{x}(t,\mathbf{b}) + g(\dot{x}(t,\mathbf{b}), x(t,\mathbf{b}), \mathbf{b}) = \theta(t)n(t) \tag{6.1}$$

In the above equation, $n(t)$ is a Gaussian white noise process with a constant power spectral density S_0, $\theta(t)$ is a deterministic envelop function, $\mathbf{b}$ denotes a vector of N independent random variables with zero means and unit variances, and $x(t,\mathbf{b})$ and $\dot{x}(t,\mathbf{b})$ are the random displacement and velocity responses respectively.

In terms of the state-space formulation, the state vector contains the displacement and velocity response. The covariance matrix for the system becomes a 2-by-2 matrix with three independent random response moments. Define the vector of these random

moments by

$$\mathbf{q}(t,\mathbf{b}) = \left\{ \begin{array}{c} q_{xx}(t,\mathbf{b}) \\ q_{x\dot{x}}(t,\mathbf{b}) \\ q_{\dot{x}\dot{x}}(t,\mathbf{b}) \end{array} \right\} = E_t \left\{ \begin{array}{c} x^2(t,\mathbf{b}) \\ x(t,\mathbf{b})\dot{x}(t,\mathbf{b}) \\ \dot{x}^2(t,\mathbf{b}) \end{array} \right\} \tag{6.2}$$

where the operator $E_t(\cdot)$ is the average operator over the sample space of the random driving force. Then, the equivalent linear system is expressed in terms of $\mathbf{q}(t,\mathbf{b})$ as

$$\ddot{x}(t,\mathbf{b}) + c_{eq}(\mathbf{q}(t,\mathbf{b}),\mathbf{b})\dot{x}(t,\mathbf{b}) + k_{eq}(\mathbf{q}(t,\mathbf{b}),\mathbf{b})x(t,\mathbf{b}) = \theta(t)n(t) \tag{6.3}$$

As a special case of the nonlinear matrix equations derived in the previous chapter, the equations governing the evolutionary covariance matrix can be rearranged and represented as three independent sets of nonlinear moment equations for this single-degree-of-freedom system. These equation sets are given by

$$\dot{q}_{xx,l_1 l_2 \cdots l_N}(t) = 2q_{x\dot{x},l_1 l_2 \cdots l_N}(t) \tag{6.4}$$

$$\begin{aligned} \dot{q}_{x\dot{x},l_1 l_2 \cdots l_N}(t) &= q_{\dot{x}\dot{x},l_1 l_2 \cdots l_N}(t) - \left(k^{[0]}(t) q_{xx,l_1 l_2 \cdots l_N}(t) + c^{[0]}(t) q_{x\dot{x},l_1 l_2 \cdots l_N}(t)\right) \\ &\quad - \sum_{i=1}^{N} \sum_{r=-1,1} a_r^{l_i} \left(k_i^{[\mathrm{I}]}(t) q_{xx,l_1 \cdots l_i+r \cdots l_N}(t) + c_i^{[\mathrm{I}]}(t) q_{x\dot{x},l_1 \cdots l_i+r \cdots l_N}(t)\right) \\ &\quad - \frac{1}{2} \sum_{i=1}^{N} \sum_{r=-2,0,2} \bar{a}_r^{l_i} \left(k_{ii}^{[\mathrm{II}]}(t) q_{xx,l_1 \cdots l_i+r \cdots l_N}(t) + c_{ii}^{[\mathrm{II}]}(t) q_{x\dot{x},l_1 \cdots l_i+r \cdots l_N}(t)\right) \\ &\quad - \frac{1}{2} \sum_{i,j=1}^{N} \sum_{r,s=-1,1} a_r^{l_i} a_s^{l_i} \left(k_{ij}^{[\mathrm{II}]}(t) q_{xx,l_1 \cdots l_i+r \cdots l_j+s \cdots l_N}(t) + c_{ij}^{[\mathrm{II}]}(t) q_{x\dot{x},l_1 \cdots l_i+r \cdots l_j+s \cdots l_N}(t)\right) \end{aligned} \tag{6.5}$$

$$\begin{aligned} \dot{q}_{\dot{x}\dot{x},l_1 l_2 \cdots l_N}(t) &= -2\left(k^{[0]}(t) q_{xx,l_1 l_2 \cdots l_N}(t) + c^{[0]}(t) q_{x\dot{x},l_1 l_2 \cdots l_N}(t)\right) + 2\pi S_0 \theta^2(t) \prod_{n=0}^{N} \delta_{0 l_n} \\ &\quad - 2\sum_{i=1}^{N} \sum_{r=-1,1} a_r^{l_i} \left(k_i^{[\mathrm{I}]}(t) q_{x\dot{x},l_1 \cdots l_i+r \cdots l_N}(t) + c_i^{[\mathrm{I}]}(t) q_{\dot{x}\dot{x},l_1 \cdots l_i+r \cdots l_N}(t)\right) \end{aligned}$$

$$-\sum_{i=1}^{N}\sum_{r=-2,0,2}\bar{a}_r^{l_i}\left(k_{ii}^{[\mathrm{II}]}(t)q_{x\dot{x},l_1\cdots l_i+r\cdots l_N}(t)+c_{ii}^{[\mathrm{II}]}(t)q_{\dot{x}\dot{x},l_1\cdots l_i+r\cdots l_N}(t)\right)$$
$$-\sum_{i,j=1}^{N}\sum_{r,s=-1,1}a_r^{l_i}a_s^{l_i}\left(k_{ij}^{[\mathrm{II}]}(t)q_{x\dot{x},l_1\cdots l_i+r\cdots l_j+s\cdots l_N}(t)+c_{ij}^{[\mathrm{II}]}(t)q_{\dot{x}\dot{x},l_1\cdots l_i+r\cdots l_j+s\cdots l_N}(t)\right)$$
$$\sum_{i=1}^{N}l_i=0,1,2 \tag{6.6}$$

In the above equation sets, the subscription $(\cdot)_{,l_1l_2\cdots l_N}$ indicates various orders of the orthogonal polynomial expansion associated with the moment response as usual. The constant coefficients a_r^l and $\bar{a}_r^l$ are given previously and their values depend on the type of probability density function of the random parameters.

The above equation set represents a general solution format for a problem expressible in the forms given by Eqn. (6.1) and Eqn. (6.3). It encompasses a wide-class of uncertain nonlinear single-degree-of-freedom random vibration problems including some types of uncertain hysteretic systems. Under this solution format, the feature of nonlinearity and parameter uncertainty is provided through the second-order Taylor coefficients of the equivalent stiffness and damping by the following formulations.

$$k^{[0]}=k_{eq}|_{\mathbf{b}=0}\quad k_i^{[\mathrm{I}]}=\left.\frac{\partial k_{eq}}{\partial b_i}\right|_{\mathbf{b}=0}\quad k_{ij}^{[\mathrm{II}]}=\left.\frac{\partial^2 k_{eq}}{\partial b_i\partial b_j}\right|_{\mathbf{b}=0}\quad i,j=1,\cdots,N \tag{6.7}$$

$$c^{[0]}=c_{eq}|_{\mathbf{b}=0}\quad c_i^{[\mathrm{I}]}=\left.\frac{\partial c_{eq}}{\partial b_i}\right|_{\mathbf{b}=0}\quad c_{ij}^{[\mathrm{II}]}=\left.\frac{\partial^2 c_{eq}}{\partial b_i\partial b_j}\right|_{\mathbf{b}=0}\quad i,j=1,\cdots,N \tag{6.8}$$

The proposed solution scheme will be applied to uncertain nonlinear systems with uncertain hardening and softening stiffnesses in the following sections. For validation and comparison purposes, other solution schemes are also considered and introduced in the next section.

6.2 Existing Solution Methods

Three other approximation methods for obtaining the moment statistics are investigated. These methods are presented and described below.

A second-order perturbation method using a set of random moment equations is considered herein as the first method for comparison. These random moment equations are derived from the nonstationary equivalent linearization technique. In an alternative viewpoint, these random moment equations represent a set of coupled nonlinear equations with random parameters. Hence, the response moments can be perturbed about the means of the random parameters and the moment statistics can then be evaluated using the numerical solutions of the resulting perturbed equations. This moment-equation based perturbation scheme is referred to as the MEP method in later use.

A simulation method based on the same set of nonlinear random moment equations is also considered. This method first generates a set of samples of the uncertain parameters. For each sample, the corresponding set of moment equations is evaluated numerically. The statistics of the moment response are then calculated. This moment-equation based simulation method is referred to as the MES method. For a large number of samples combined with a sophisticated numerical integration scheme, the MES method can accurately provide the moment statistics given by the nonstationary equivalent linearization. Hence, MES will be used to verify the accuracy of the expansion technique employed in the proposed method.

In addition to these moment-equation based approximations, a Monte-Carlo type of simulation method, referred to as the MCS method, is also provided. In MCS, two groups of random samples are generated which are associated with the random system parameters and random driving force. The driving force samples are a fixed set of simulated white noise processes. For each sample of the uncertain system parameters, the resulting nonlinear system is sequentially excited by the set of white

noise processes. Due to the theoretical zero first moment, only the second moment is calculated and stored. This process continues until the second moments for all samples of system parameters are evaluated. The final statistics of the moment response are then evaluated. MCS can provide the highest accuracy but at the expense of extremely extensive computations.

6.3 Examples of Uncertain Hardening Systems

Consider the Duffing oscillator subjected to white noise random excitation expressed as

$$\ddot{x} + 2\zeta\omega_0\dot{x} + \omega_0^2(x + \gamma x^3) = \theta(t)n(t) \tag{6.9}$$

where ζ and ω_0 are the linear damping ratio and undamped natural frequency respectively, γ is a positive nonlinear parameter indicating the degree of nonlinearity, and $\theta(t)$ is a deterministic envelop function chosen as the unit step function. The arguments of the response x are suppressed for simplicity.

The equivalent stiffness of the system is well-known to be

$$k_{eq} = \omega_0^2(1 + 3\gamma q_{xx}) \tag{6.10}$$

The implementation and performance of the proposed method are illustrated through two different types of uncertain hardening restoring force by assuming uncertain γ and uncertain ω_0 respectively. For each numerical example, the MEP, MES and MCS methods are also employed for comparison. For both types of uncertainty, the solution results are presented in terms of the mean moment response and the mean plus one standard deviation. The statistics for both the displacement moment and velocity moment will be given. The cross correlation of the displacement and velocity response is in general small and will not be presented. To facilitate the discussion,

the abbreviated notations $\bar{q}_{xx}$ and $\bar{q}^{+}_{xx}$ will stand for the mean value of q_{xx} and the mean plus one standard deviation of q_{xx}. Similar notations, $\bar{q}_{\dot{x}\dot{x}}$ and $\bar{q}^{+}_{\dot{x}\dot{x}}$, are used for the statistics of velocity moments. The example with uncertain nonlinear parameter γ is first presented in the next subsection.

6.3.1 Uncertain Hardening Nonlinear Parameter

In this subsection, the system is assumed to have uniformly distributed uncertain γ represented by

$$\gamma = \bar{\gamma} + \lambda b \tag{6.11}$$

Substituting Eqn. (6.11) and Eqn. (6.10) into Eqn. (6.7) yields the following expressions

$$\begin{aligned} k^{[0]} &= \omega_0^2(1 + 3\bar{\gamma}q^{[0]}_{xx}) \\ k^{[\mathrm{I}]}_1 &= 3\omega_0^2(\lambda q^{[0]}_{xx} + \bar{\gamma}q^{[\mathrm{I}]}_{xx,1}) \\ k^{[\mathrm{II}]}_{11} &= 3\omega_0^2(2\lambda q^{[\mathrm{I}]}_{xx,1} + \bar{\gamma}q^{[\mathrm{II}]}_{xx,11}) \end{aligned} \tag{6.12}$$

The only nonzero damping component in Eqn. (6.8) is given by

$$c^{[0]} = 2\zeta\omega_0 \tag{6.13}$$

Substituting Eqn. (6.12) and (6.13) into Eqns. (6.4) - (6.6) gives the deterministic moment equation set to be evaluated numerically. The system parameters are chosen as $\omega_0 = 2\pi$, $\zeta = 2\%$, $\bar{\gamma} = 0.5$ and $\lambda = 0.25$. The selection of $\bar{\gamma}$ and λ corresponds to a uniformly distributed parameter range [0.07, 0.93]. The numerical scheme adopted is a fourth-order Runge-Kutta time-integration scheme with a time increment 0.02 second. Two levels of input intensity, $S_0 = 1$ and $S_0 = 4$, are chosen to vary the degree of nonlinearity.

For the case $S_0 = 1$, the evolutionary moment statistics for various methods are compared in Figs. 6.2, 6.3 and 6.4. In Fig. 6.2, all the moment statistics obtained by the proposed method agree well with that from MES. This indicates that the proposed method excellently approximates the moment response of the equivalent linearization technique in the random parameter space. MEP also provides acceptable statistics except for an oscillatory component as shown in Fig. 6.4.

From the $\bar{q}_{\dot{x}\dot{x}}$ and $\bar{q}^{+}_{\dot{x}\dot{x}}$ responses, the velocity moments are seen insignificant to variations of γ for the entire response history. In fact, the stationary $q_{\dot{x}\dot{x}}$ given by the equivalent linearization technique is the exact solution and the expression is independent of γ. Due to the deterministic nature of the stationary velocity moment, the nonstationary velocity moment is conceivably less sensitive to the parameter variation of γ. This explains the small standard deviation of velocity moment in all the proposed method, the MES method and the MCS method. In addition, the stationary velocity moment also provides a measure on the accuracy of the Monte-Carlo simulation scheme used in MCS. The validation is demonstrated through the excellent agreement of the velocity moments as shown in Fig. 6.3.

The peak $\bar{q}^{+}_{xx}$ for the given level of excitation is about 0.26. Using the square root of the peak $\bar{q}^{+}_{xx}$ and the parameter range $\gamma = [\, 0.07,\ 0.93\,]$, the degree of nonlinearity can be estimated in a statistical sense from force-displacement curves in Fig. 6.1. It shows that only a slight level of nonlinearity is developed in the system responses. For this level of nonlinearity, an excellent approximation of the displacement moment is achieved by the equivalent linearization technique as shown in Fig. 6.3.

The results for the case of $S_0 = 4$ are given in Figs. 6.5 - 6.7. The peak $\bar{q}^{+}_{xx}$ for this case reaches a value of approximated 0.8 which indicates a level of mild nonlinear responses in a statistical sense. In Fig. 6.5, the $\bar{q}^{+}_{xx}$ of the proposed method differs only slightly from that of the MES method with a small underestimation. In Fig. 6.6, the proposed method solution still qualitatively agrees with the MCS solution for this

level of nonlinearity.

The results of the MEP method become highly oscillatory and unacceptable. To understand this difference, the q_{xx} and $q_{\dot{x}\dot{x}}$ responses implied by the proposed method, MEP and MES are plotted as a function of $\gamma/\bar{\gamma}$ at a fixed time $t = 6.0$ sec. in Fig. 6.8. It is seen that the MES method shows a ripple-like moment curve as a function of γ. The MEP method seeks a local exact curvature at the mean uncertain parameter $\gamma = \bar{\gamma}$ while results in very large overall error for the given range of γ. The proposed method seeks a best quadratic curve in the sense of global approximation, in contrast to the local quadratic approximation given by the MEP method. Hence, much better results are achieved by the proposed method.

6.3.2 Uncertain Natural Frequency

In this case example, a deterministic nonlinear parameter γ and an uncertain natural frequency is considered. The dispersion on the restoring force-displacement characteristics due to the parameter variation of the natural frequency may be illustrated in Fig. 6.9. The randomness of the natural frequency is represented by

$$\omega_0 = \bar{\omega_0} + \lambda b \tag{6.14}$$

where $\bar{\omega_0}$ is the mean value of ω_0, λ is the variance and b is a random variable with zero mean and unit variance.

Following the procedures of partial differentiation with respect to the random variable b, Eqn. (6.7) becomes

$$\begin{aligned} k^{[0]} &= \bar{\omega_0}^2(1 + 3\gamma q_{xx}^{[0]}) \\ k_1^{[I]} &= 2\lambda\bar{\omega_0} + 3\gamma(2\lambda\bar{\omega_0}\lambda q_{xx}^{[0]} + \bar{\omega_0}^2 q_{xx,1}^{[I]}) \\ k_{11}^{[II]} &= 2\lambda\bar{\omega_0}(1 + 3\gamma q_{xx}^{[0]}) + 12\lambda\bar{\omega_0} q_{xx,1}^{[I]} + 3\gamma\bar{\omega_0}^2 q_{xx,11}^{[II]} \end{aligned} \tag{6.15}$$

Note that the uncertainty of the natural frequency also introduces randomness of the system damping. This gives higher-order damping components in Eqn. (6.8) as

$$\begin{aligned} c^{[0]} &= 2\zeta\bar{\omega}_0 \\ c_1^{[1]} &= 2\zeta\lambda \end{aligned} \tag{6.16}$$

The parameter values, $\bar{\omega}_0 = 2\pi$, $\zeta = 2\%$, $\gamma = 0.5$ and a 20% coefficient of variation of the natural frequency, $\lambda = 0.4\pi$, are used to study the response uncertainty. The uncertain ω_0 is assumed to be uniformly distributed. Similarly, this system is subjected to two levels of input intensity given by $S_0 = 1$ and $S_0 = 4$.

For the case $S_0 = 1$, excellent statistics prediction is again achieved by the proposed method as shown in Fig. 6.10. It is noted that not only the displacement moment but also the velocity moment exhibit severe response uncertainty. A rough calculation shows that the assumed 20% coefficient of variation in the natural frequency results in approximately a 50% coefficient of variation in the peak q_{xx} and a 25% coefficient of variation in the peak $q_{\dot{x}\dot{x}}$. The moment statistics given by the proposed method also agree well with the MCS solutions in Fig. 6.11. However, in Fig. 6.12, the MEP method already results in poor prediction for this level of excitation.

The results for the case $S_0 = 4$ are given in Figs. 6.13, 6.14 and 6.15. All the moment statistics increase as the input intensity increases. Good performance is still achieved by the proposed method, however the MEP solutions become even worse. The reason for such poor performance of MEP may be seen from Fig. 6.16, where the moment responses implied by the proposed method, MEP and MES are plotted as functions of $\omega_0/\bar{\omega}_0$ at $t = 6.0$ sec. The observations and discussions described for the case of uncertain γ are also applicable for this case.

The conclusion is drawn that the instantaneous response moment as a function defined in the random parameter space exhibits a smooth, ripple-like profile for both

types of uncertain hardening nonlinear stiffness. Hence, any locally perturbative solution scheme may not be appropriate when the the subdomain being approximated is substantially smaller than the domain the uncertain parameters are defined. This situation frequently occurs in the nonstationary response of an uncertain system subjected to a suddenly applied loading condition, especially when a hardening system or a multi-degree-of-freedom system is to be analyzed. Therefore, great caution should be excised in applying the MEP method for analyzing the nonstationary response of the systems being mentioned.

6.4 Examples of Uncertain Softening Systems

Consider a system with nonlinear softening restoring force given by

$$\ddot{x} + 2\zeta\omega_0\dot{x} + f_y\left[1 - \exp(\frac{-\omega_0^2|x|}{f_y})\right]\mathrm{sgn}(x) = \theta(t)n(t) \tag{6.17}$$

where ζ, ω_0, $\theta(t)$ and $n(t)$ are as defined previously, $\mathrm{sgn}(\cdot)$ is the signum function and f_y is the "yielding" level of the softening restoring force. Typical restoring force-displacement curves of this softening system are graphically illustrated in Fig. 6.17. The envelop function chosen is the Saragoni-Hart type [45] given by

$$\theta(t) = te^{-\alpha_s t} \quad t > 0 \tag{6.18}$$

where α_s is a decaying constant. This type of envelop function has been implemented widely to simulate the nonstationary feature of earthquake ground motion.

Applying the technique of equivalent linearization, the expression for the equivalent stiffness can be shown to be

$$k_{eq} = \omega_0^2 e^{\alpha^2}\mathrm{erfc}(\alpha) \tag{6.19}$$

where $\mathrm{erfc}(\cdot)$ is the complementary error function and the introduced parameter α is

defined as

$$\alpha \equiv \frac{\omega_0^2 \sqrt{q_{xx}}}{\sqrt{2} f_y} \tag{6.20}$$

The extreme case $f_y \to \infty$ corresponds to a linear system and the expression for the equivalent stiffness is reduced to the linear stiffness ω_0^2. The value of k_{eq} gradually decreases as the yielding level decreases. Clearly, a non-polynomial type of equivalent system parameter is present in this example problem.

Several important issues in implementing the proposed solution scheme are addressed and considered in this example problem. First, the accuracy of the evolutionary moment statistics subjected to the time-varying input intensity is to be explored. Second, the performance under the presence of non-polynomial type of equivalent system parameters is to be examined. In addition, the dimension of the uncertain parameter space is further expanded to allow both the stiffness and damping uncertainties to be presented simultaneously.

The sources of uncertainty are considered to be due to the the damping ratio ζ and the yielding parameter f_y. These parameters are assumed to be statistical independent and are represented by

$$\begin{aligned} \zeta &= \bar{\zeta} + \lambda_1 b_1 \\ f_y &= \bar{f}_y + \lambda_2 b_2 \end{aligned} \tag{6.21}$$

where b_1 and b_2 are independent random variables with zero means and unit variances.

Substituting Eqn. (6.21) into Eqn. (6.19) and performing the procedure of partial differentiation with respect to b_1 and b_2 will yield various orders of stiffness and damping components. For simplicity, introduce a constant coefficient $\beta = \lambda_2 / \bar{f}_y$ and the following set of time-dependent variables

$$\alpha_0 = \frac{\omega_0^2 \sqrt{q_{xx}^{[0]}}}{\sqrt{2} f_y}, \quad \xi_i = \frac{q_{xx,i}^{[\mathrm{I}]}}{2 q_{xx}^{[0]}}, \quad i = 1, 2, \quad \xi_{ij} = \frac{q_{xx,ij}^{[\mathrm{II}]}}{2 q_{xx}^{[0]}}, \quad i, j = 1, 2 \tag{6.22}$$

The stiffness components in Eqn. (6.7) can be shown to be given by

$$\begin{aligned} k^{[0]} &= \omega_0^2 e^{\alpha_0^2}\mathrm{erfc}(\alpha_0) \\ k_i^{[\mathrm{I}]} &= \eta(\xi_i - \beta\delta_{1i}), \quad i = 1,2 \\ k_{ij}^{[\mathrm{II}]} &= 2(\xi_i - \beta\delta_{1i})(\xi_j - \beta\delta_{1j})(\mu(1+\alpha_0^2) + \alpha_0\omega_0^2/\sqrt{\pi}) \\ &\quad +\eta(\xi_{ij} - 2\xi_i\xi_j + \beta^2\delta_{i1}\delta_{j1}), \quad i,j = 1,2 \end{aligned} \tag{6.23}$$

where η is a time-dependent variable as a function of α_0 only. The expression for η is given by

$$\eta = 2\omega_0^2(\alpha_0^2 e^{\alpha_0^2}\mathrm{erfc}(\alpha_0) - \alpha_0/\sqrt{\pi}) \tag{6.24}$$

Similarly, the nonzero damping terms in Eqn. (6.8) are given by

$$\begin{aligned} c^{[0]} &= 2\bar{\zeta}\omega_0 \\ c_i^{[\mathrm{I}]} &= 2\lambda_1\omega_0\delta_{i2}, \quad i = 1,2 \end{aligned} \tag{6.25}$$

Substituting Eqn. (6.23) into Eqn. (6.25) into Eqns. (6.4) - (6.6) gives the set of deterministic equations for numerical evaluation. The results are compared to those obtained by MES and MCS. Two levels of input intensity, $S_0 = 1$ and $S_0 = 2$, along with the parameter values $\omega_0 = 2\pi$, $\bar{\zeta} = 2\%$, $\bar{f}_y = 4\pi^2$ and $\alpha_s = \omega_0/10\pi$ are used to generate numerical results. The random parameters are all assumed to follow the Ultraspherical distribution with index $M = 2$. Two special cases will be considered: the case of only uncertain yielding force with 20% coefficient of variation represented by $\lambda_1 = 0$ and $\lambda_2 = 0.8\pi^2$, and the case of both uncertain parameters presented simultaneously given by $\lambda_1 = 0.5\%$ and $\lambda_2 = 0.8\pi^2$.

For the first level of excitation, $S_0 = 1$, the numerical results for the case with uncertain yielding force only are given in Figs. 6.18 and 6.19. It is seen that the proposed solution method again agrees well with the MES solutions. The comparison

shown in Fig. 6.19 indicates a slight underestimation on the displacement moment statistics which is concluded to be due to an error resulting from the equivalent linearization process. The velocity moment is again seen to be insensitive to the stiffness uncertainty.

Figs. 6.20 and 6.21 show the results for the case where the uncertain yielding force and uncertain damping are present simultaneously. The additional damping uncertainty slightly increases both the $\bar{q}_{xx}$ and $\bar{q}_{\dot{x}\dot{x}}$. In addition, the uncertainty in the velocity moment becomes substantial with the introduction of damping uncertainty. Using the peak value of $\bar{q}^{+}_{xx}$ and the restoring force curves shown in Fig. 6.17, a mean ductility ratio is estimated as 1.5 for this case. For this degree of softening nonlinearity, the proposed method provides good moment statistics in both the response time rate and the response magnitude.

Figs. 6.22 and 6.23 give the numerical results for the case with uncertain yielding force subjected to input intensity $S_0 = 2$. In Fig. 6.22, the solutions of the proposed method and the MES method become distinguishable but the difference is within an error level acceptable for an engineering purpose. This difference is believed to be due to the limited second-order capability of the proposed method in modeling the random equivalent stiffness. The proposed method yields higher estimations than MES for both $\bar{q}_{xx}$ and $\bar{q}^{+}_{xx}$. However, these solutions are still smaller the MCS results, which is the consequence of the conservative nature of the equivalent linearization.

The results for the case with uncertainty in both parameters are given in Figs. 6.24 and 6.25. Using the same calculation procedure mentioned previously, the mean ductility ratio reaches approximately a value of 2.8. Hence, the response is considered to be in the level of mild nonlinearity. In this case, the proposed method still yields satisfactory results.

6.5 Effect of Nonlinearity and Parameter Uncertainty

A comparison on the effect of system nonlinearity and parameter uncertainty is provided in this section. This comparison is based on the peak nonstationary moment statistics of two representative uncertain nonlinear systems. They are respectively a hardening Duffing system and the softening system introduced in the previous sections. The hardening system possesses an uncertain hardening nonlinear parameter γ, and the the softening system possesses an uncertain "yielding" level f_y. Both systems have the same values of deterministic initial linear stiffness and the same degrees of uncertain linear damping. The modulated white noise process employed previously is used as the input excitation for both systems. For a selected value of input intensity S_0, the peak moment statistics are evaluated using the proposed solution method. These peaks statistics are then plotted as a function of S_0 for the range $S_0 = [0, 3]$. Additionally, the peak moment response conditioned on the mean parameter values is also provided for comparison. These results are presented in Figs. 6.26 and 6.27, where the parameter values of the representative systems are also given.

To facilitate the discussions, a qualitative description for the response of an uncertain *linear* system is first given. For an uncertain linear system with a fixed degree of parameter uncertainty, the peak values of nonstationary $\bar{q}_{xx}$, $\bar{q}^{+}_{xx}$, $\bar{q}_{\dot{x}\dot{x}}$ and $\bar{q}^{+}_{\dot{x}\dot{x}}$ are linearly proportional to the excitation intensity S_0. This is due to a linear relationship between the response moments and the input excitation. As shown in Figs. 6.26 and 6.27, nonlinear relationships are clearly developed in the $\bar{q}_{xx}$ and $\bar{q}^{+}_{xx}$ curves for both the hardening and softening systems. For the softening system, the $\bar{q}_{xx}$ and $\bar{q}^{+}_{xx}$ curves shows a steadily increasing trend as S_0 increases. This results in a very large displacement response uncertainty for a large S_0. On the other hand, the hardening system shows much smaller $\bar{q}_{xx}$ and $\bar{q}^{+}_{xx}$ values as compared to the softening system. The $\bar{q}^{+}_{xx}$ value for the softening system at $S_0 = 3$ exceeds a value of 14, which is about 10 times larger than that of the hardening system. Hence, the type of nonlinearity

greatly affects the statistics of the displacement moment.

Furthermore, the peak unconditional $\bar{q}_{xx}$ for both systems are all greater than the conditional $\bar{q}_{xx}$. This is because of a bias in the q_{xx} response subjected to variations of nonlinear stiffness and damping coefficient. Hence, the deterministic analysis based on the mean parameter values will yield more conservative results than a statistical analysis.

Both the peak $\bar{q}_{\dot{x}\dot{x}}$ and $\bar{q}^{+}_{\dot{x}\dot{x}}$ curves as functions of S_0 are approximately linear. The difference between conditional and unconditional solutions is also less significant. The velocity moments for both systems are of the same response level, as contrast to the significant difference in the displacement moments. This shows that the peak $\bar{q}_{\dot{x}\dot{x}}$ is insensitive to the types of nonlinearity. However, the hardening system has slightly larger peak velocity statistics than the softening system. To explain this, recall that the nonlinear stiffness has no effect on the stationary velocity response. It is then clear that this difference is due to the nonstationarity of the excitation and a faster response rate of the hardening system.

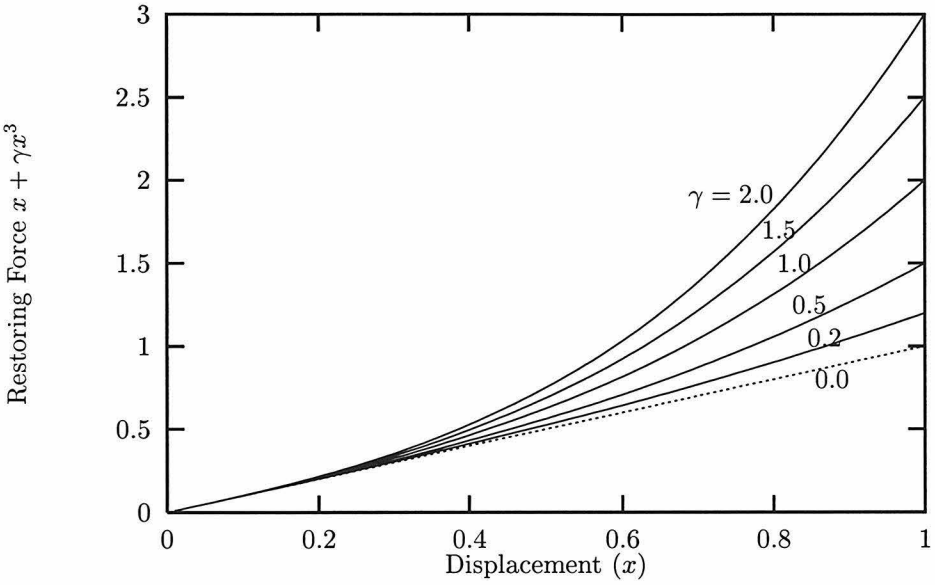

Figure 6.1: Force-displacement curves for hardening system with uncertain nonlinear parameter γ.

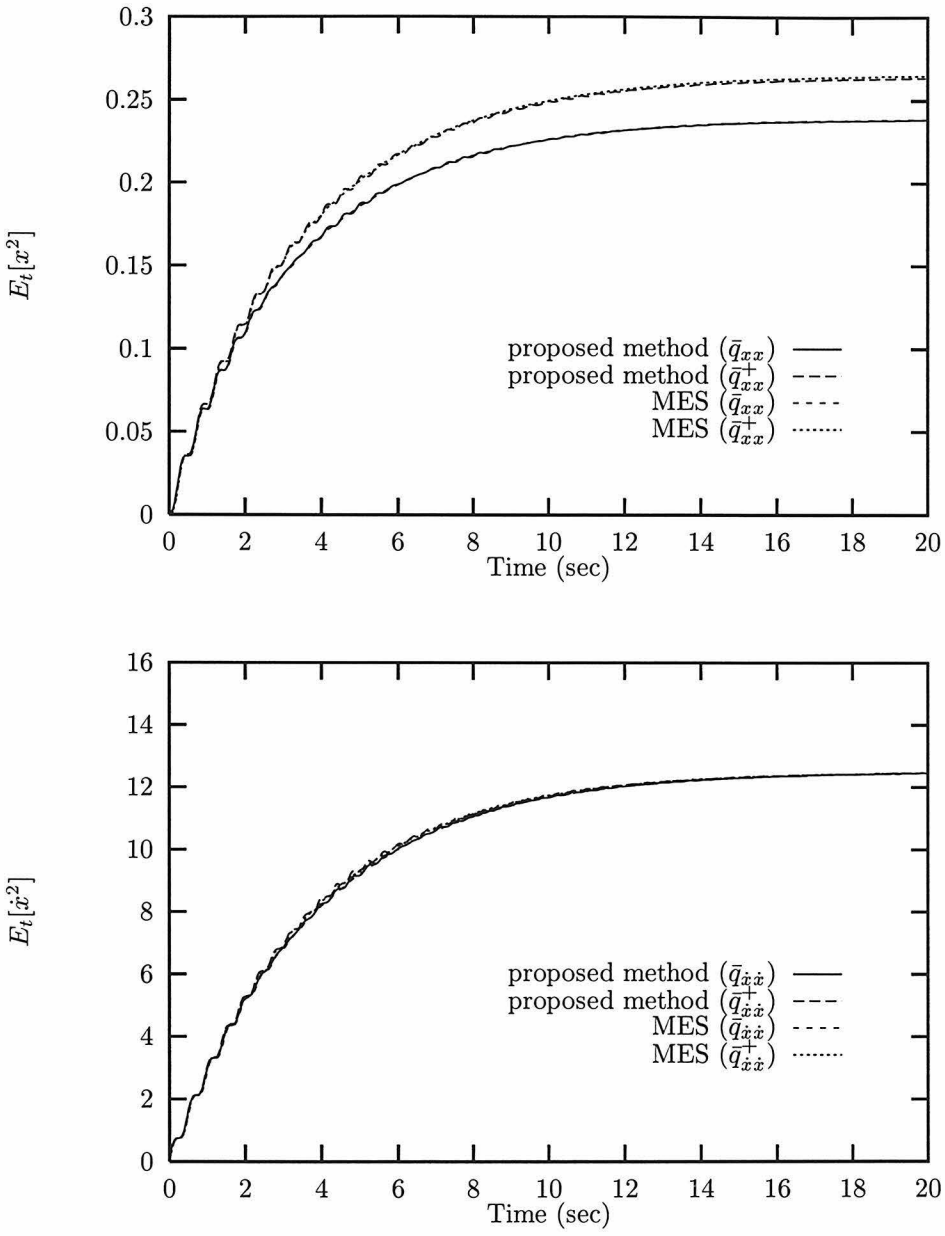

Figure 6.2: Comparison of displacement and velocity moment statistics given by the proposed method and MES (Moment Equation based Simulation) method for an uncertain hardening system, $S_0 = 1$, $\zeta = 2\%$, $\omega_0 = 2\pi$, $\bar{\gamma} = 0.5$, $\lambda = 0.25$.

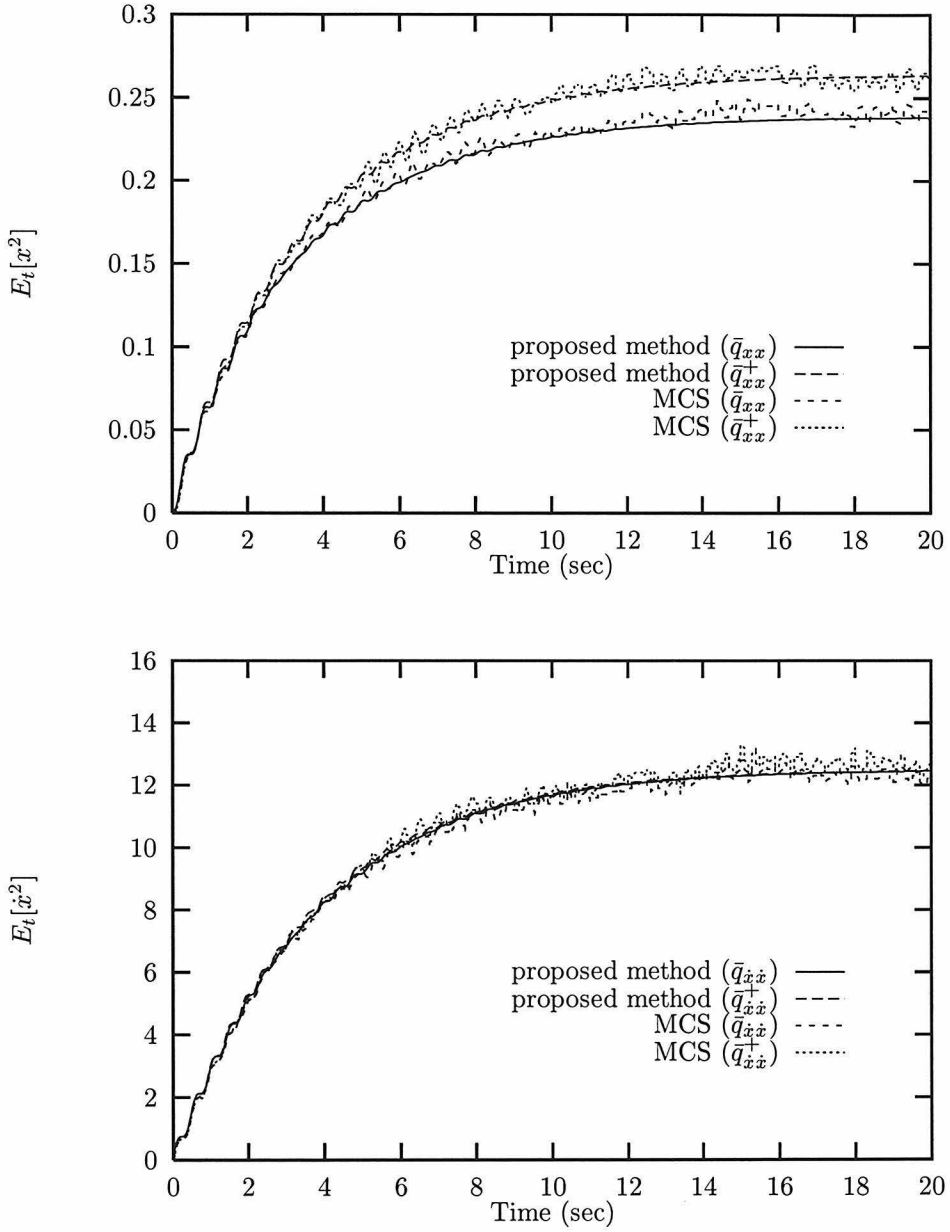

Figure 6.3: Comparison of displacement and velocity moment statistics given by the proposed method and MCS (Monte-Carlo based Simulation) method, sample size = 1000×20, for an uncertain hardening system, $S_0 = 1$, $\zeta = 2\%$, $\omega_0 = 2\pi$, $\bar{\gamma} = 0.5$, $\lambda = 0.25$.

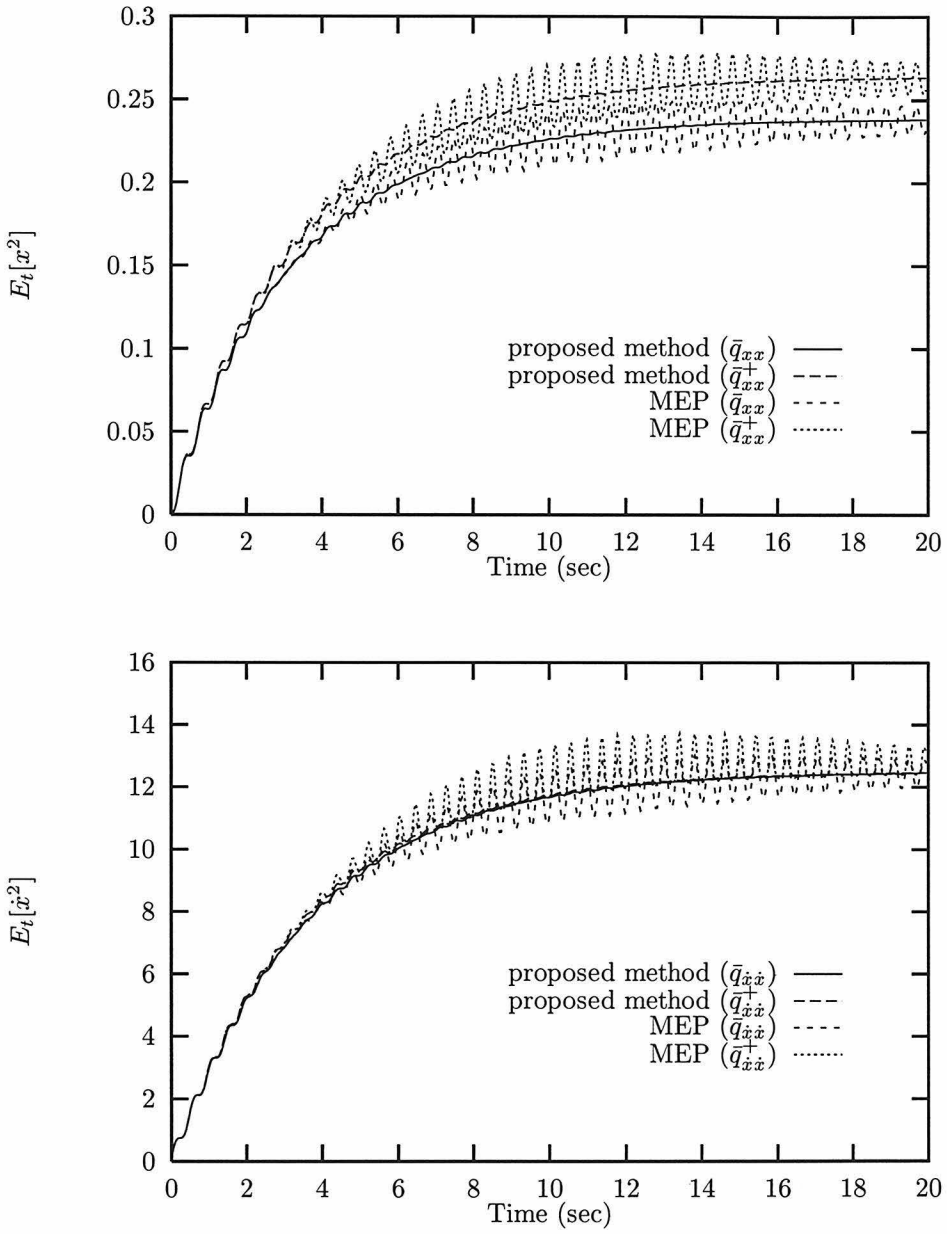

Figure 6.4: Comparison of displacement and velocity moment statistics given by the proposed method and MEP (Moment Equation based Perturbation) method for an uncertain hardening system, $S_0 = 1$, $\zeta = 2\%$, $\omega_0 = 2\pi$, $\bar{\gamma} = 0.5$, $\lambda = 0.25$.

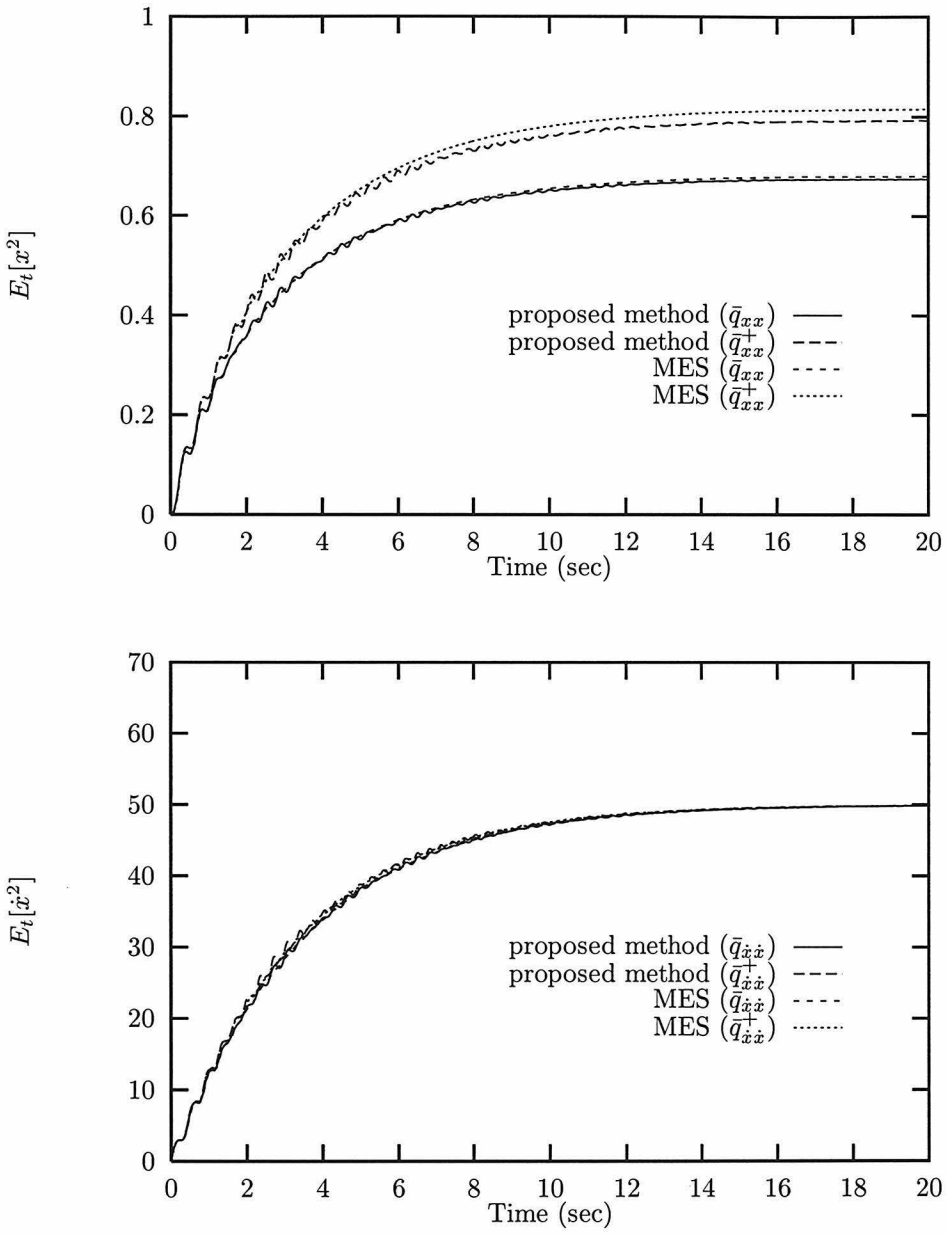

Figure 6.5: Comparison of displacement and velocity moment statistics given by the proposed method and MES method, sample size = 100, for an uncertain hardening system, $S_0 = 4$, $\zeta = 2\%$, $\omega_0 = 2\pi$, $\bar{\gamma} = 0.5$, $\lambda = 0.25$.

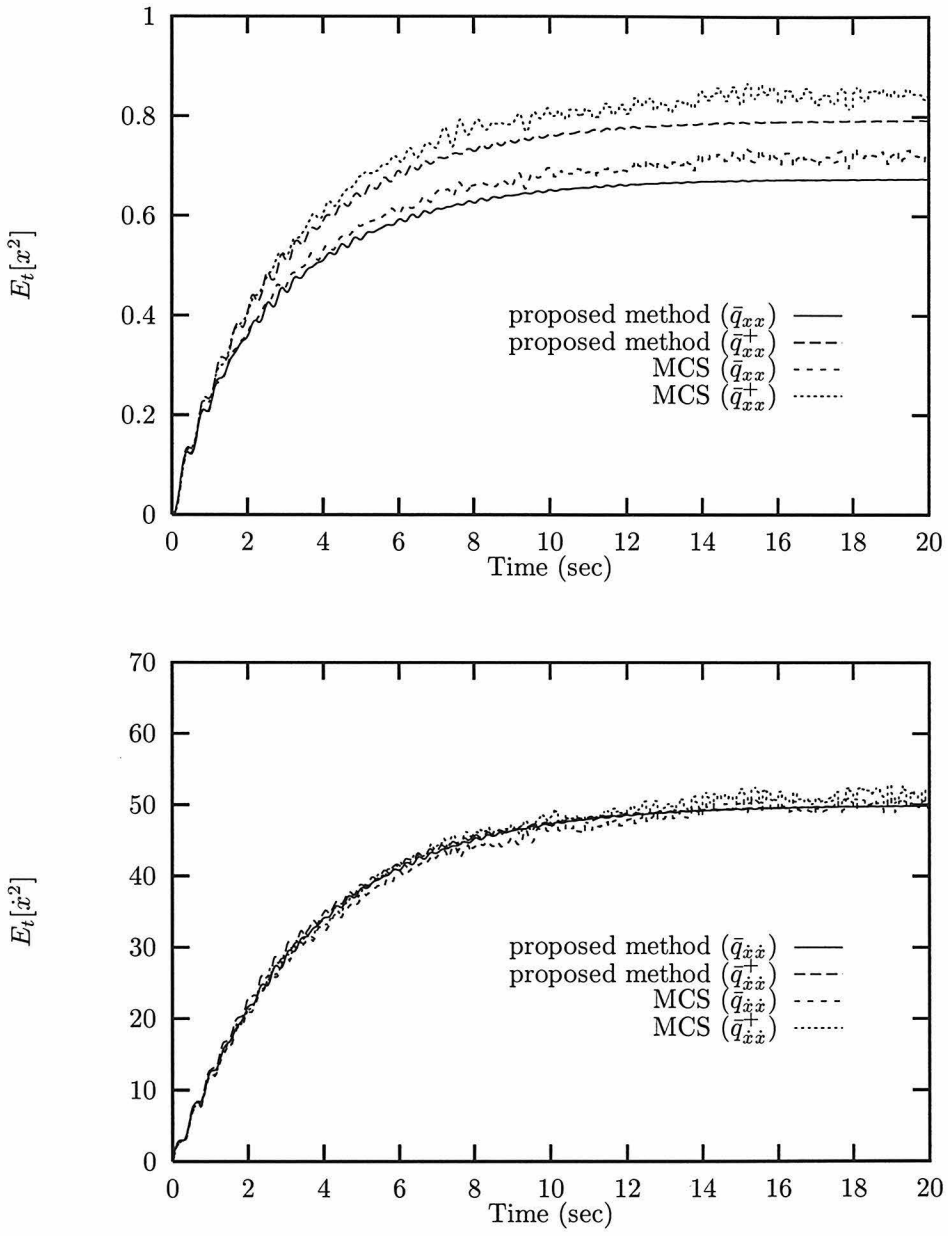

Figure 6.6: Comparison of displacement and velocity moment statistics given the proposed method and MCS method, sample size = 1000×20, for an uncertain hardening system, $S_0 = 4$, $\zeta = 2\%$, $\omega_0 = 2\pi$, $\bar{\gamma} = 0.5$, $\lambda = 0.25$.

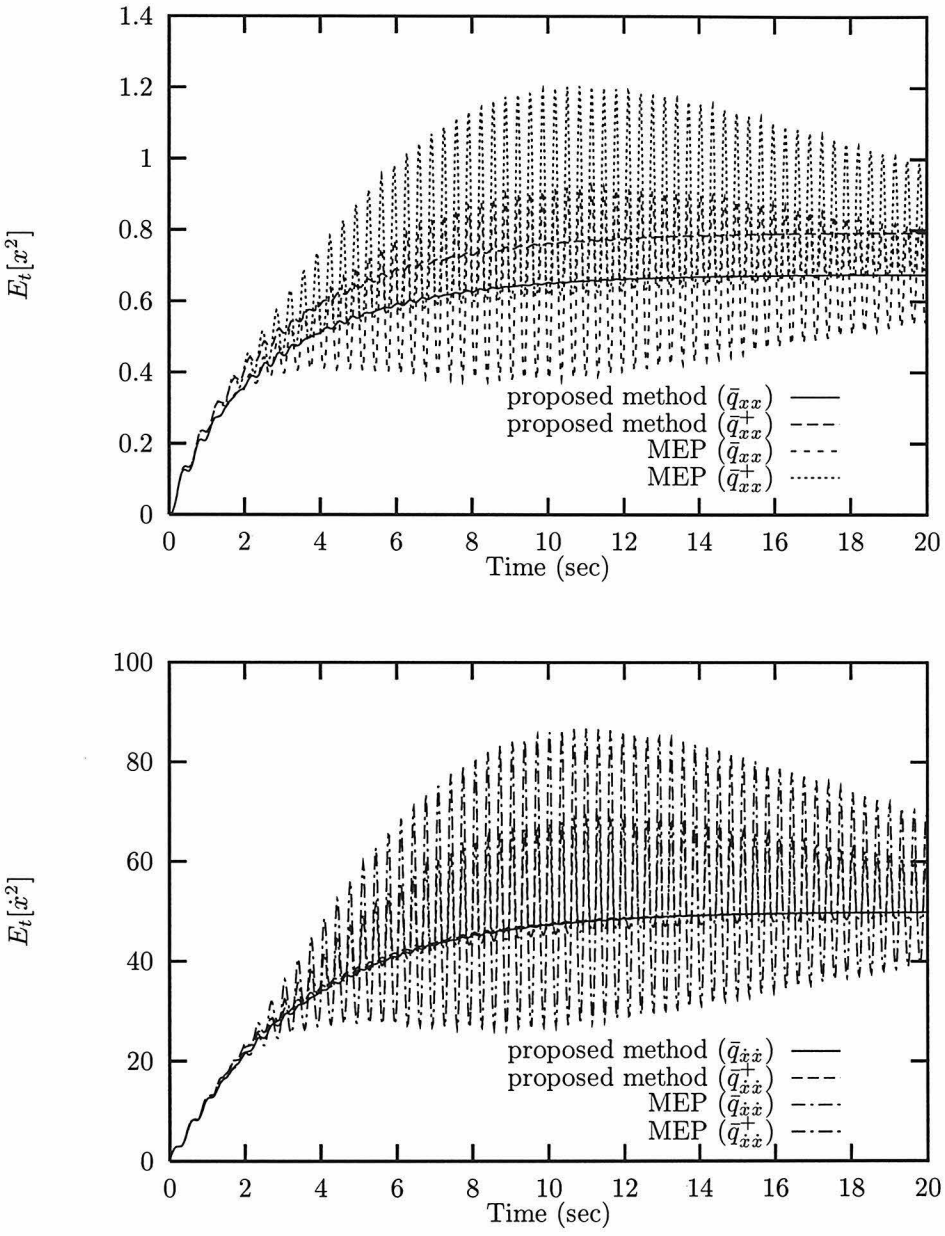

Figure 6.7: Comparison of displacement and velocity moment statistics given by the proposed method and MEP method for an uncertain hardening system, $S_0 = 4$, $\zeta = 2\%$, $\omega_0 = 2\pi$, $\bar{\gamma} = 0.5$, $\lambda = 0.25$.

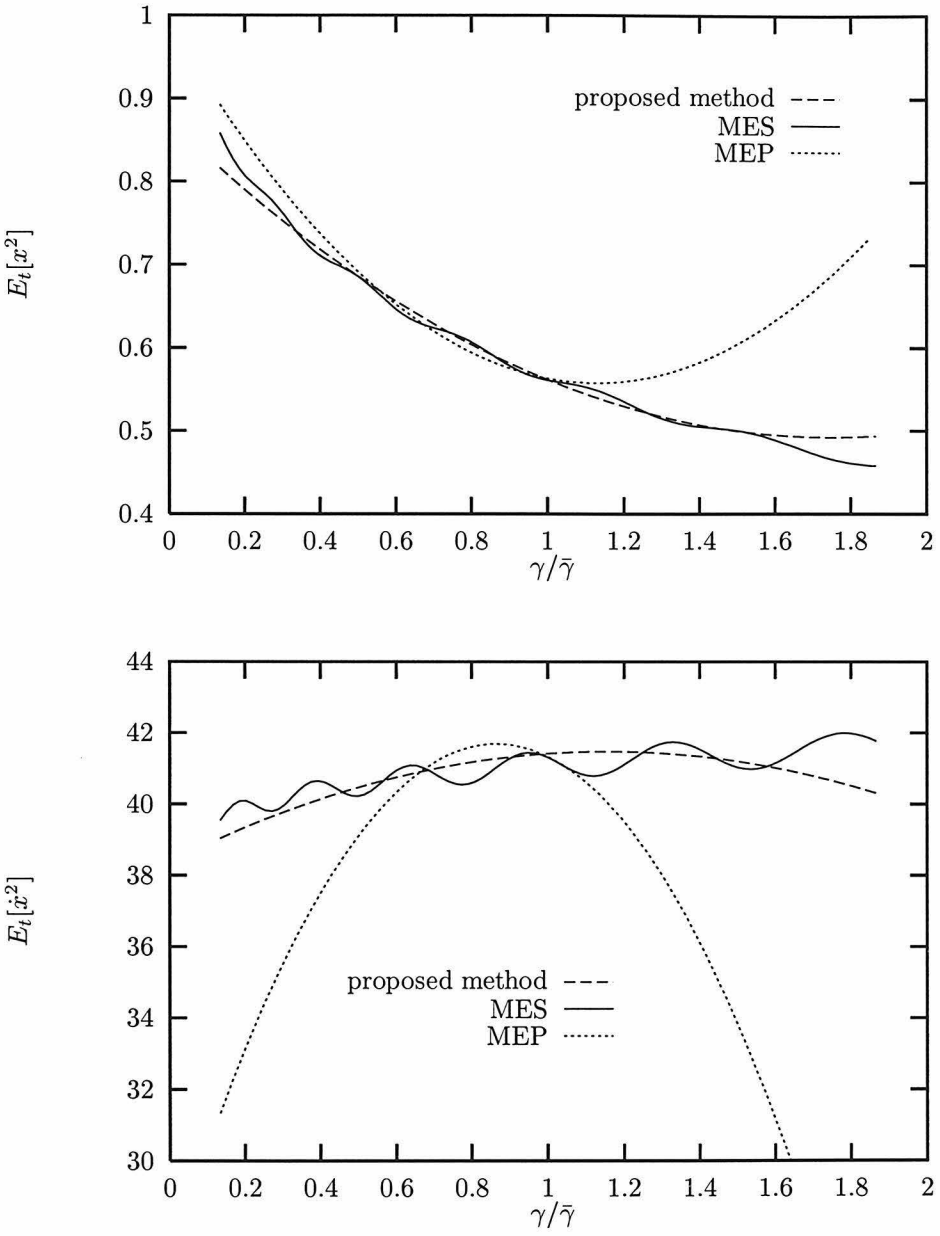

Figure 6.8: Comparison of displacement and velocity moment statistics given the proposed method and MEP method for an uncertain hardening system, $S_0 = 4$, $\zeta = 2\%$, $\omega_0 = 2\pi$, $\bar{\gamma} = 0.5$, $\lambda = 0.25$.

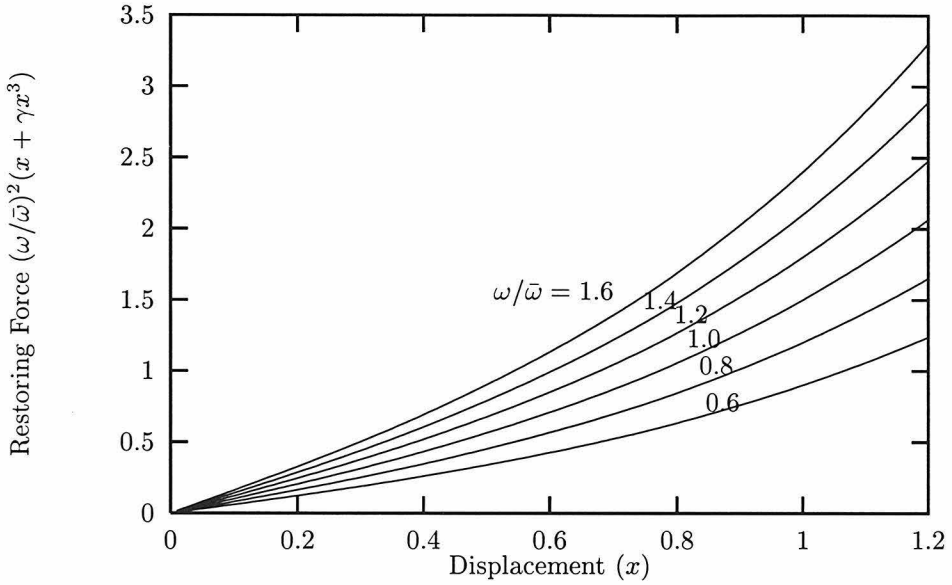

Figure 6.9: Force-displacement curves for hardening system with uncertain natural frequency, $\gamma = 0.5$.

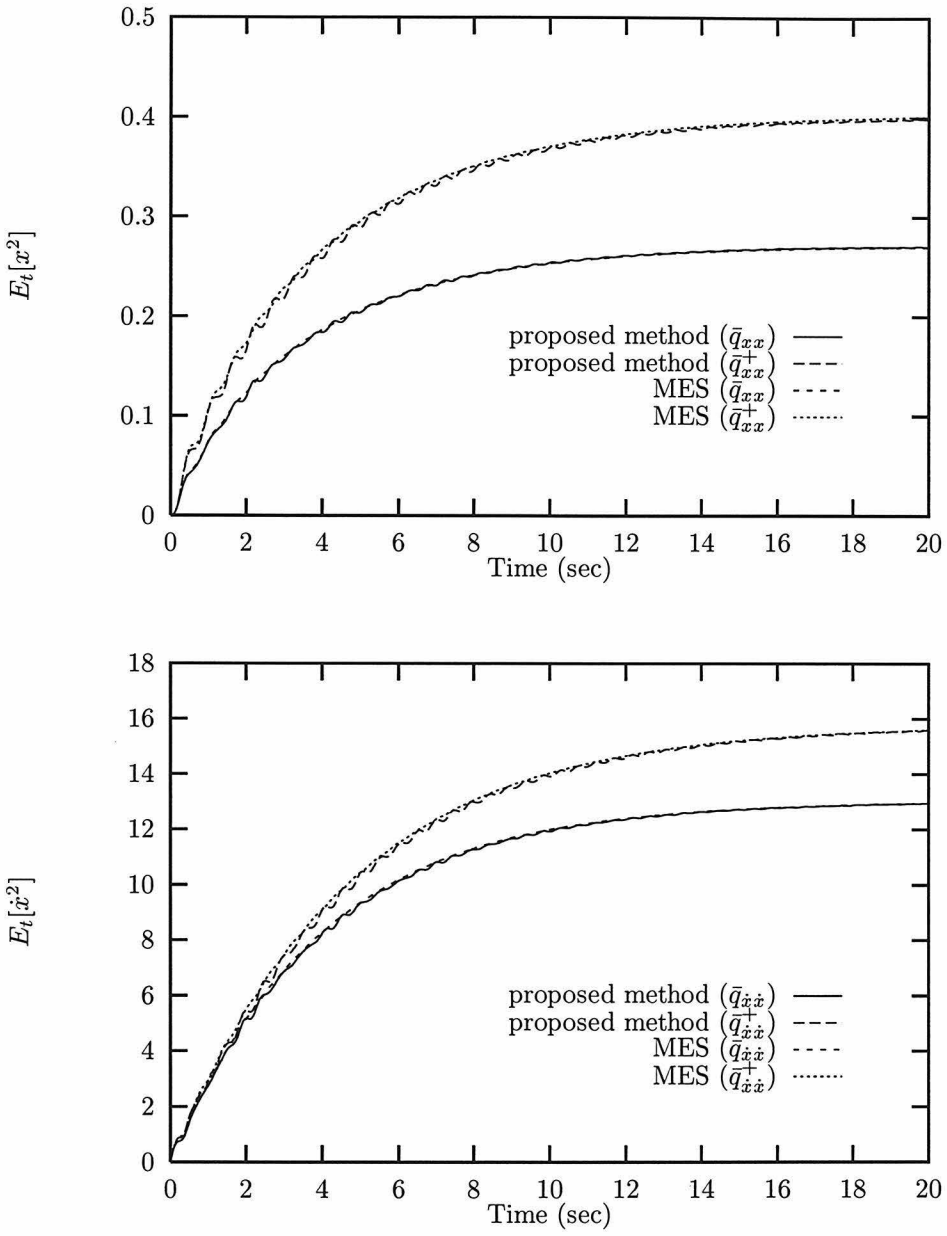

Figure 6.10: Comparison of displacement and velocity moment statistics given by the proposed method and MES method, sample size = 100, for an uncertain hardening system, $S_0 = 1$, $\zeta = 2\%$, $\bar{\omega}_0 = 2\pi$, $\gamma = 0.5$, $\lambda = 0.4\pi$.

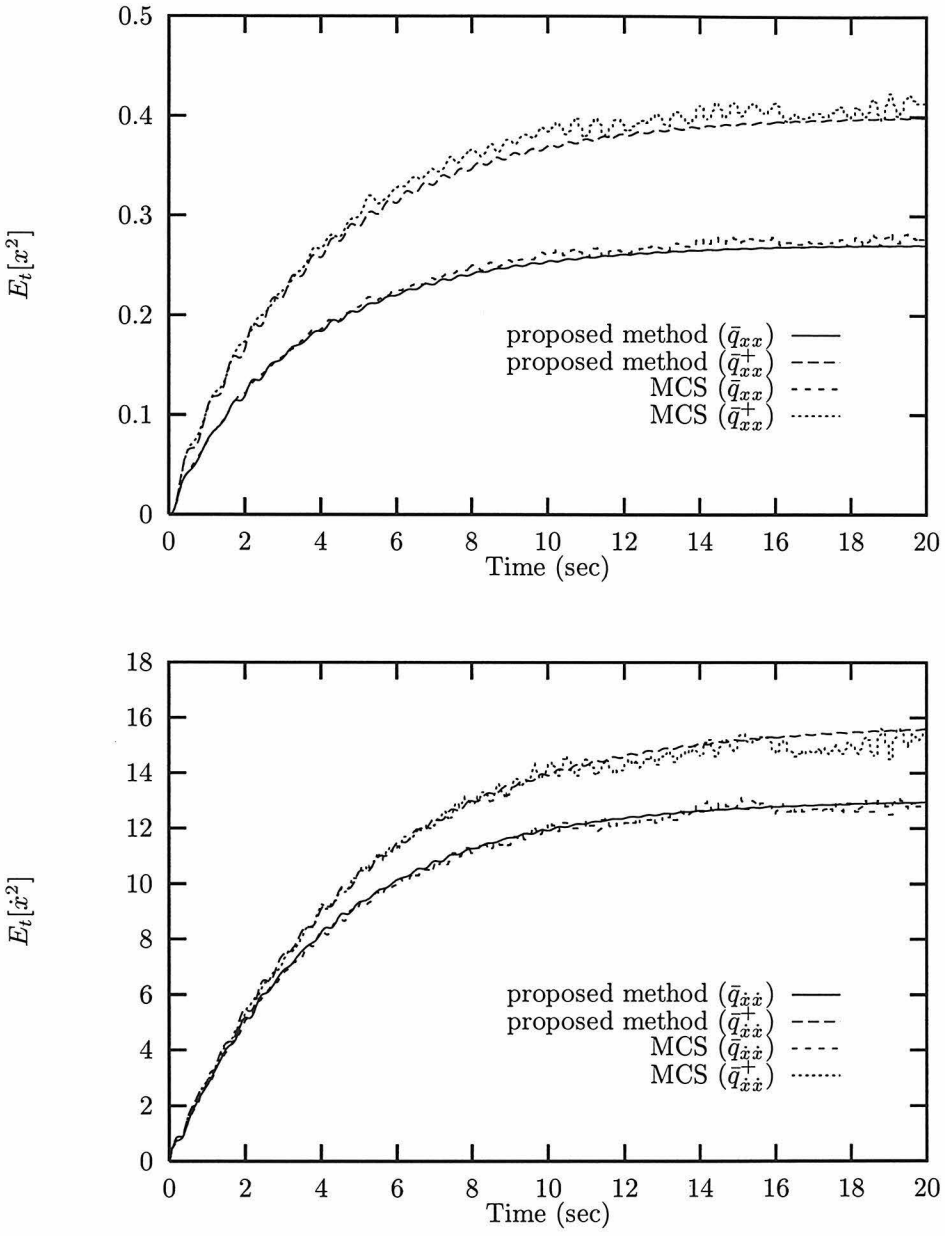

Figure 6.11: Comparison of displacement and velocity moment statistics given by the proposed method and MCS method, sample size= 1000×20, for an uncertain hardening system, $S_0 = 1$, $\zeta = 2\%$, $\bar{\omega}_0 = 2\pi$, $\gamma = 0.5$, $\lambda = 0.4\pi$.

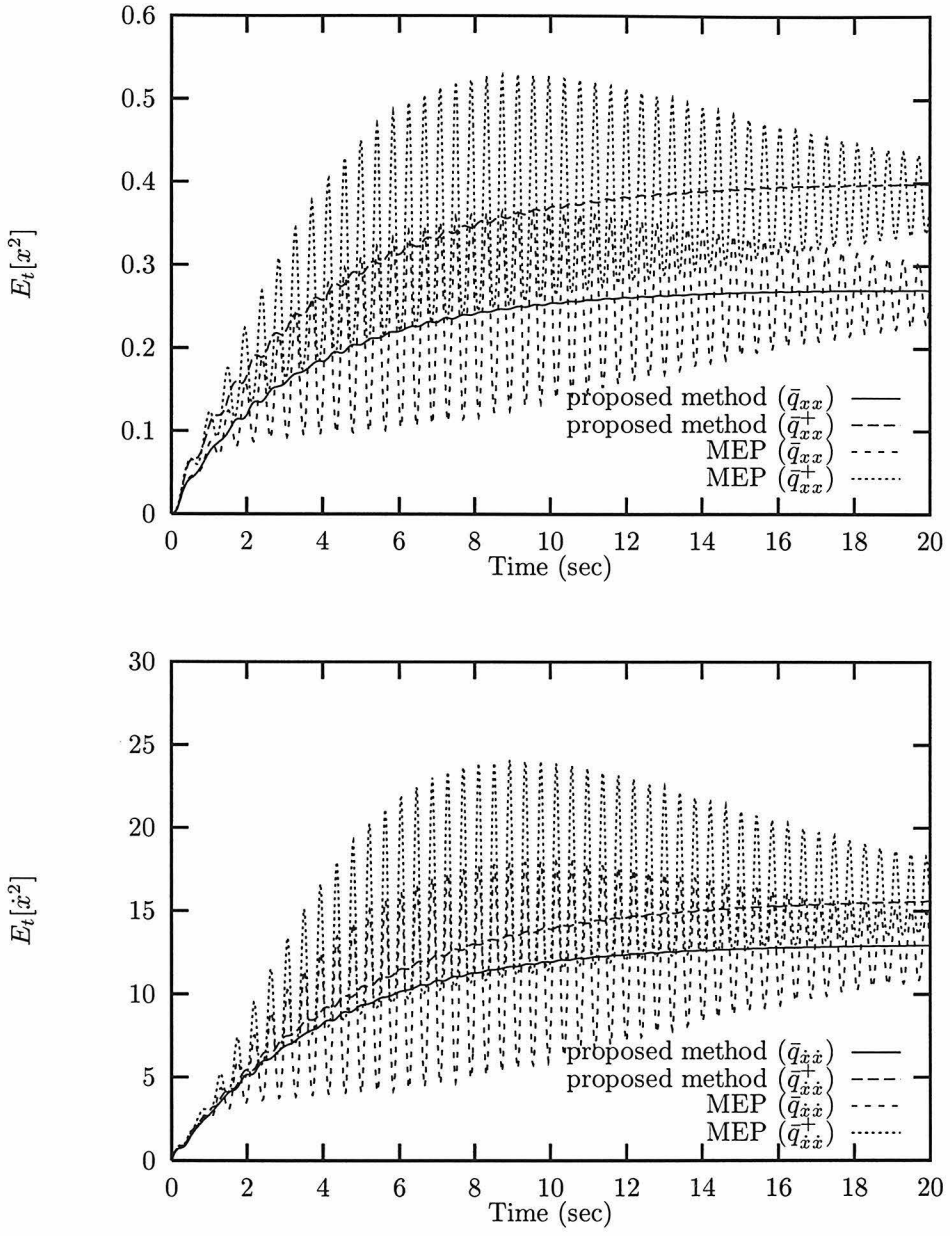

Figure 6.12: Comparison of displacement and velocity moment statistics given by the proposed method and MEP method for an uncertain hardening system, $S_0 = 1$, $\zeta = 2\%$, $\bar{\omega}_0 = 2\pi$, $\gamma = 0.5$, $\lambda = 0.4\pi$.

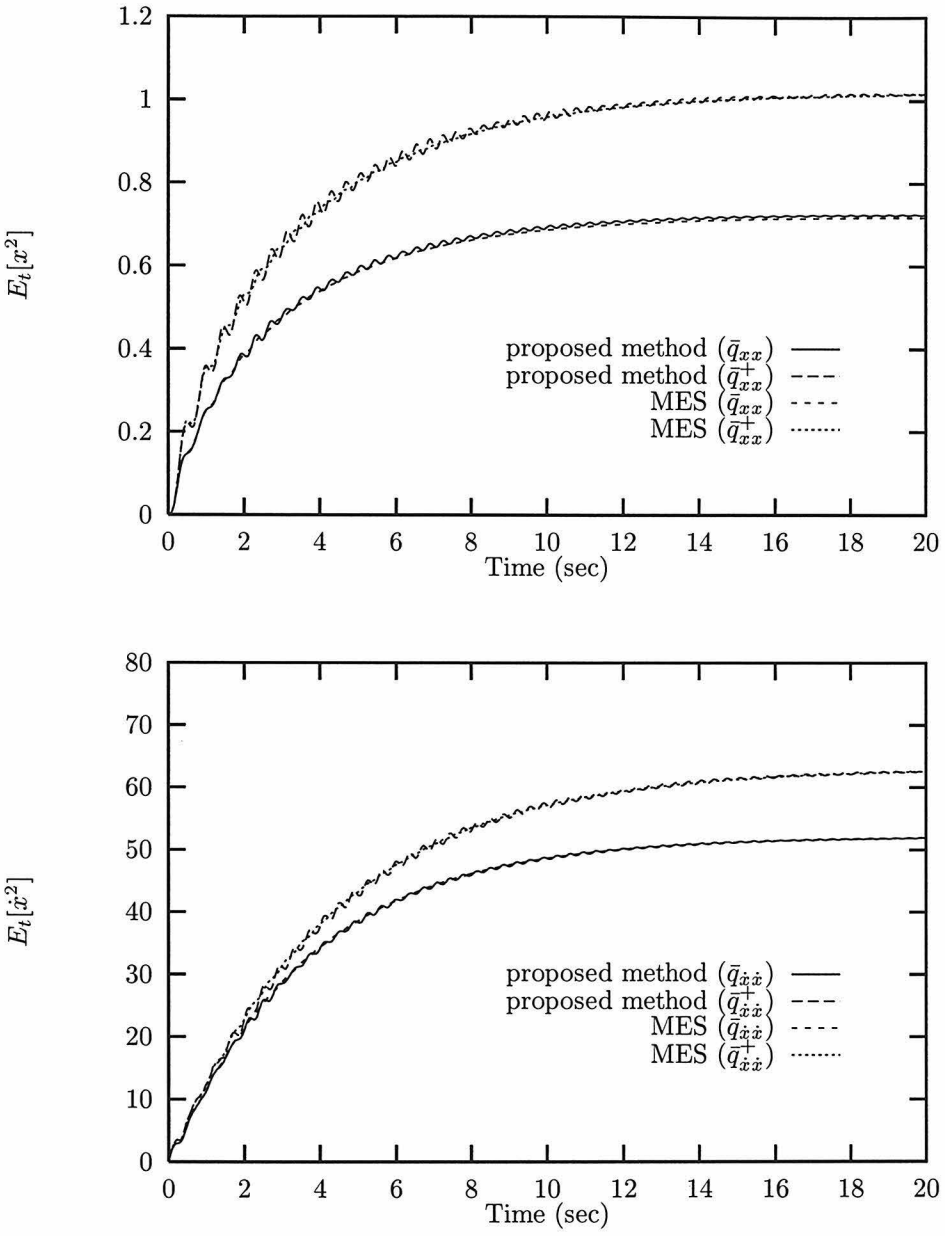

Figure 6.13: Comparison of displacement and velocity moment statistics given by the proposed method and the MES method, sample size = 100, for an uncertain hardening system, $S_0 = 4$, $\zeta = 2\%$, $\bar{\omega}_0 = 2\pi$, $\gamma = 0.5$, $\lambda = 0.4\pi$.

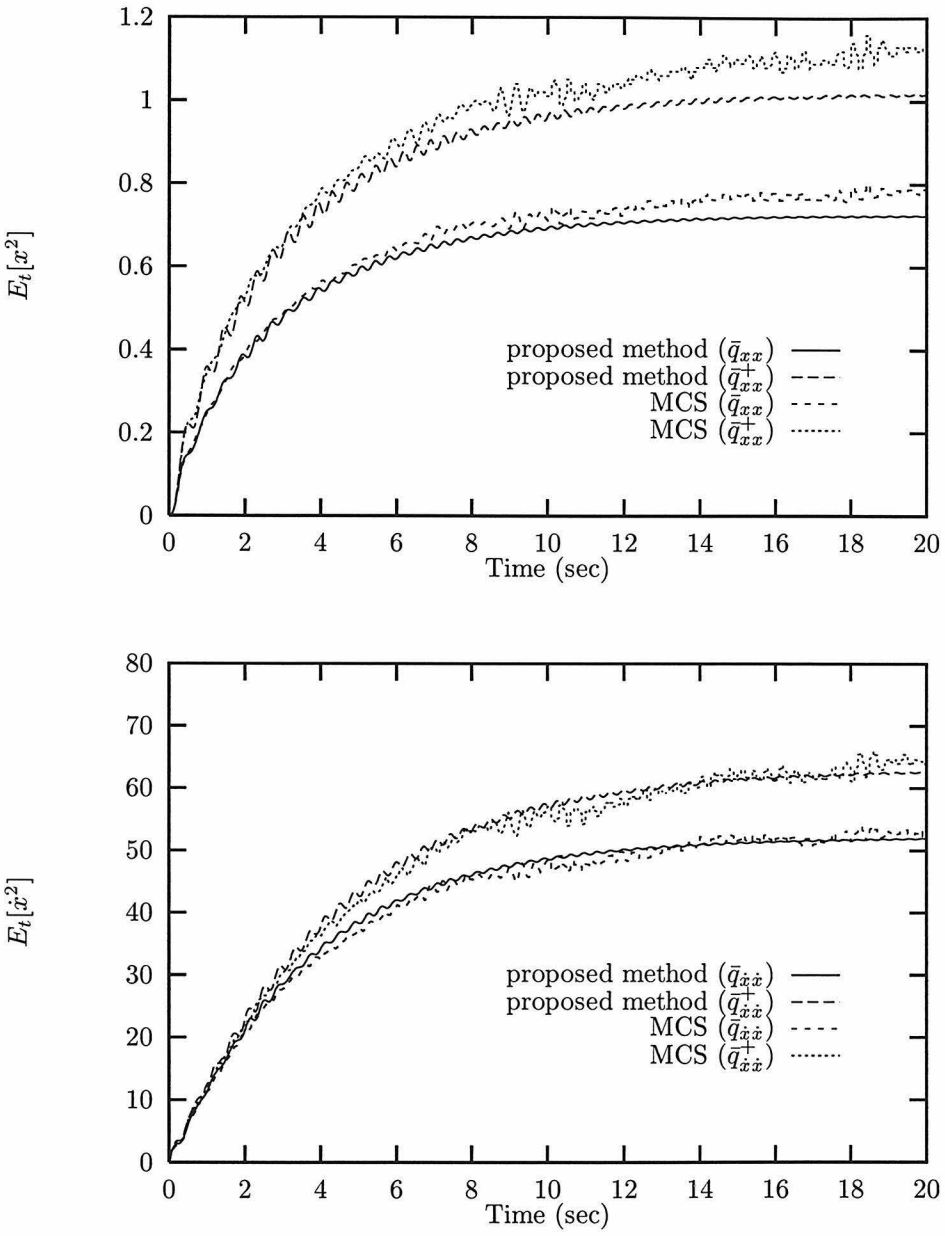

Figure 6.14: Comparison of displacement and velocity moment statistics given by the proposed method and MCS method, sample size= 1000×20, for an uncertain hardening system, $S_0 = 4$, $\zeta = 2\%$, $\bar{\omega}_0 = 2\pi$, $\gamma = 0.5$, $\lambda = 0.4\pi$.

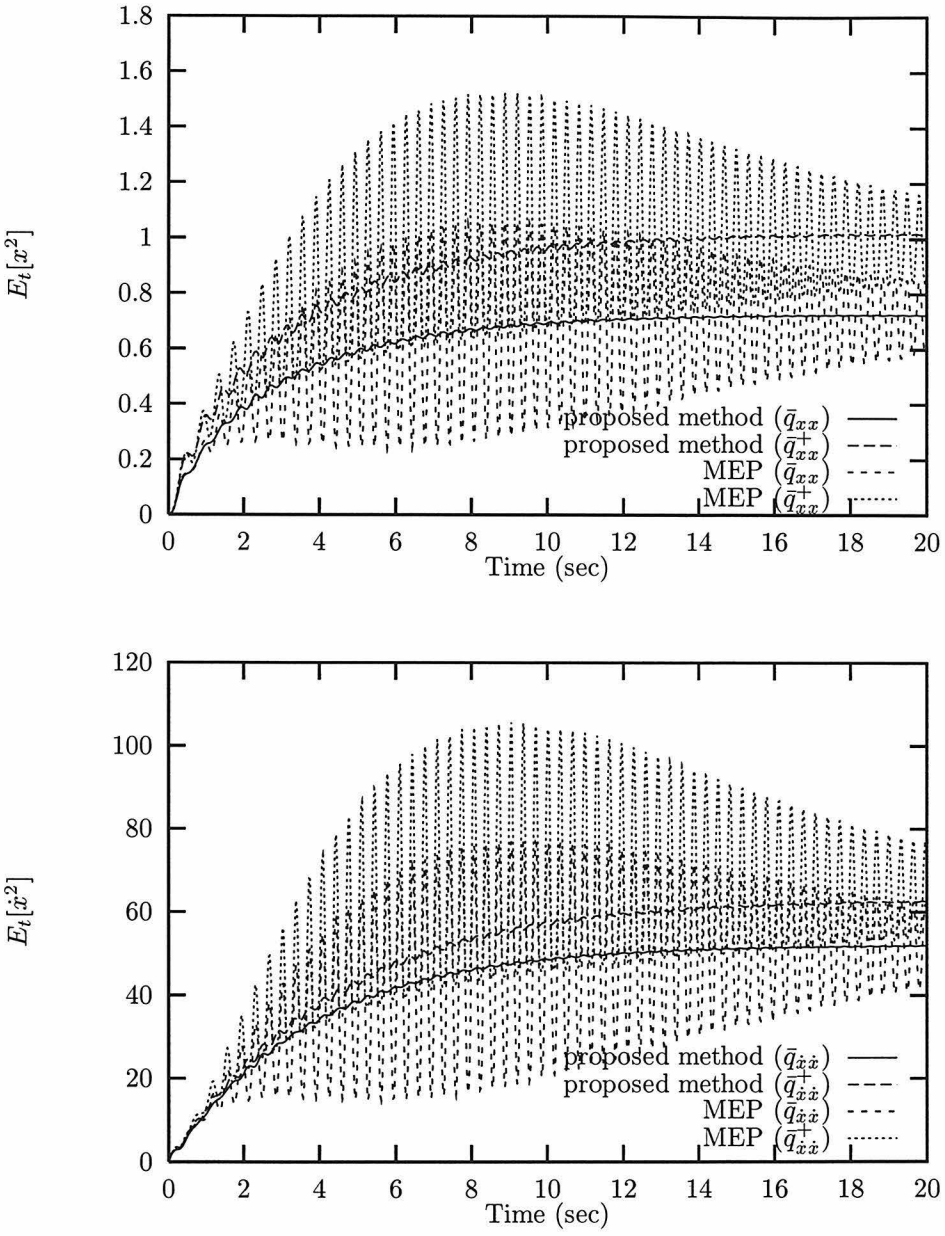

Figure 6.15: Comparison of displacement and velocity moment statistics given by the proposed method and MEP method for an uncertain hardening system, $S_0 = 4$, $\zeta = 2\%$, $\bar{\omega}_0 = 2\pi$, $\gamma = 0.5$, $\lambda = 0.4\pi$.

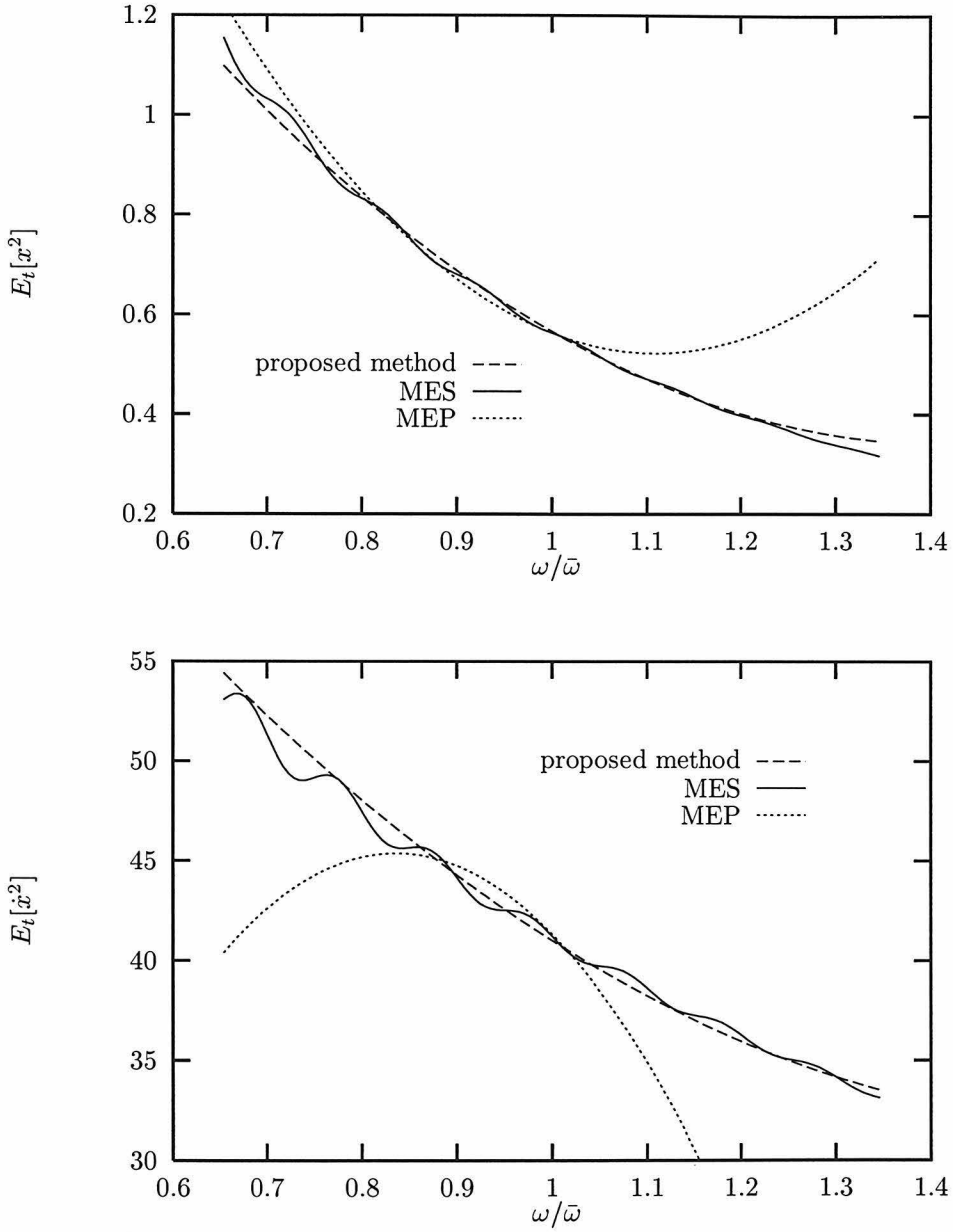

Figure 6.16: Comparison of displacement and velocity response statistics given by the proposed method and MEP method, $S_0 = 4$, $\zeta = 2\%$, $\omega_0 = 2\pi$, $\bar{\gamma} = 0.5$, $\lambda = 0.25$.

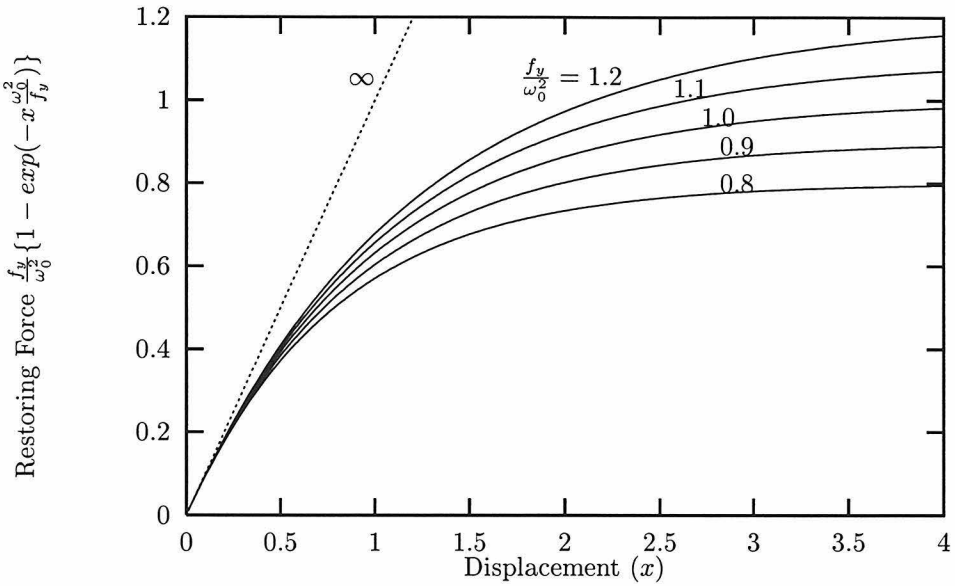

Figure 6.17: Force-displacement curves for softening system with uncertain "yielding" force.

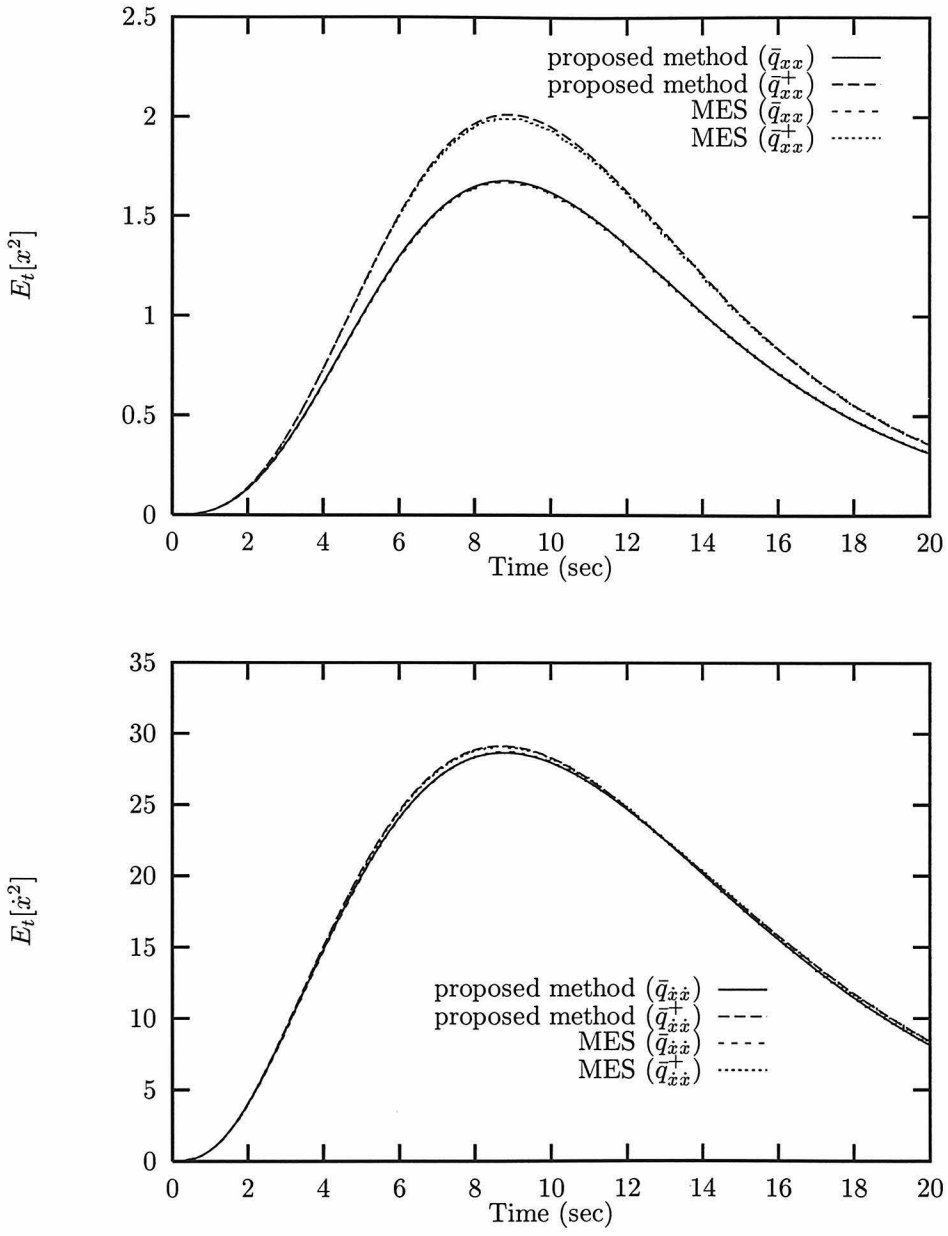

Figure 6.18: Comparison of displacement and velocity moment statistics given by the proposed method and MES method for a softening system with uncertain "yielding" force, $\omega_0 = 2\pi$, $\bar{\zeta} = 2\%$, $\bar{f}_y = 4\pi^2$, $\lambda_1 = 0$, $\lambda_2 = 0.8\pi^2$, $S_0 = 1$.

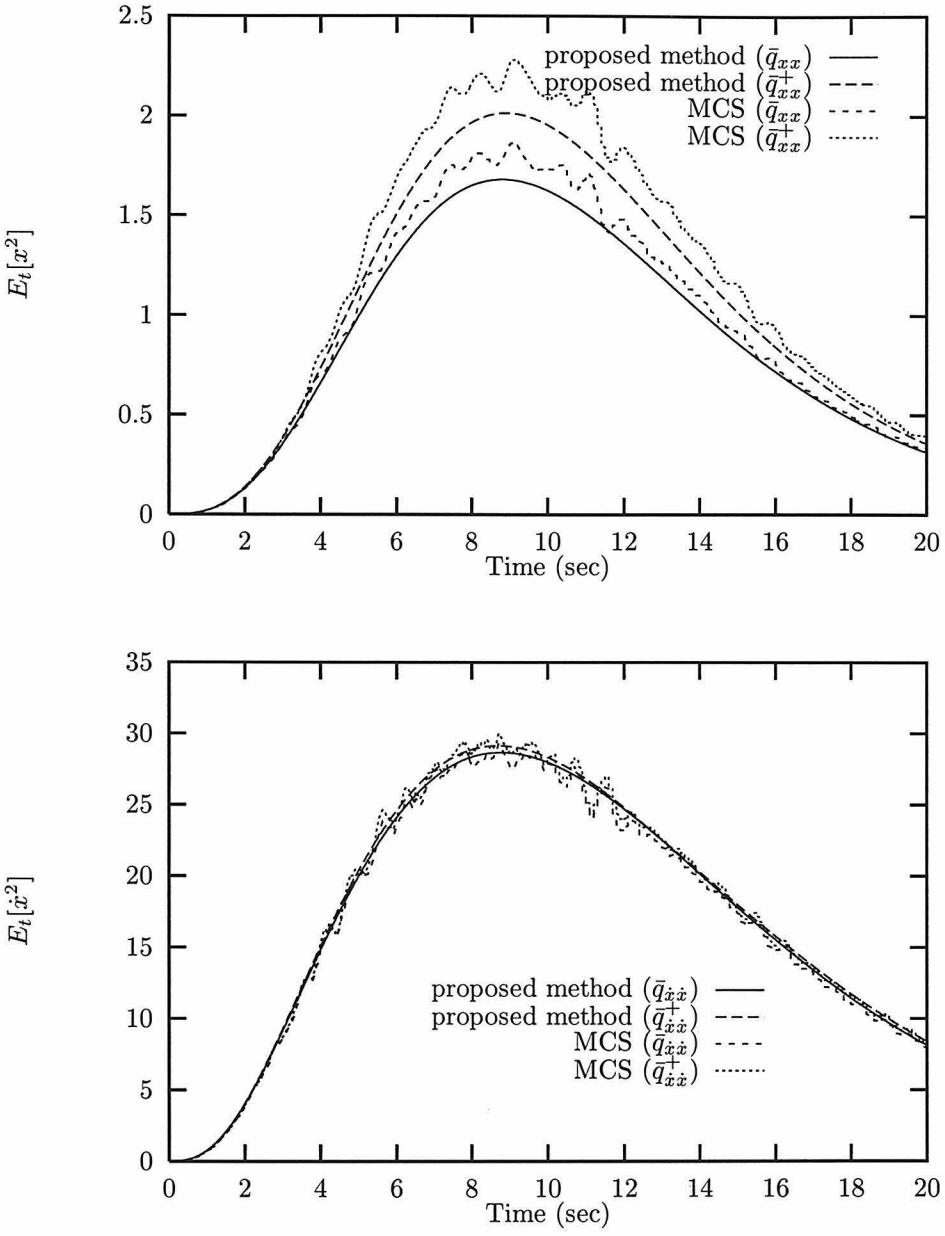

Figure 6.19: Comparison of displacement and velocity moment statistics given by the proposed method and MCS method, sample size= 500×20, for a softening system with uncertain "yielding" force , $\omega_0 = 2\pi$, $\bar{\zeta} = 2\%$, $\bar{f}_y = 4\pi^2$, $\lambda_1 = 0$, $\lambda_2 = 0.8\pi^2$, $S_0 = 1$.

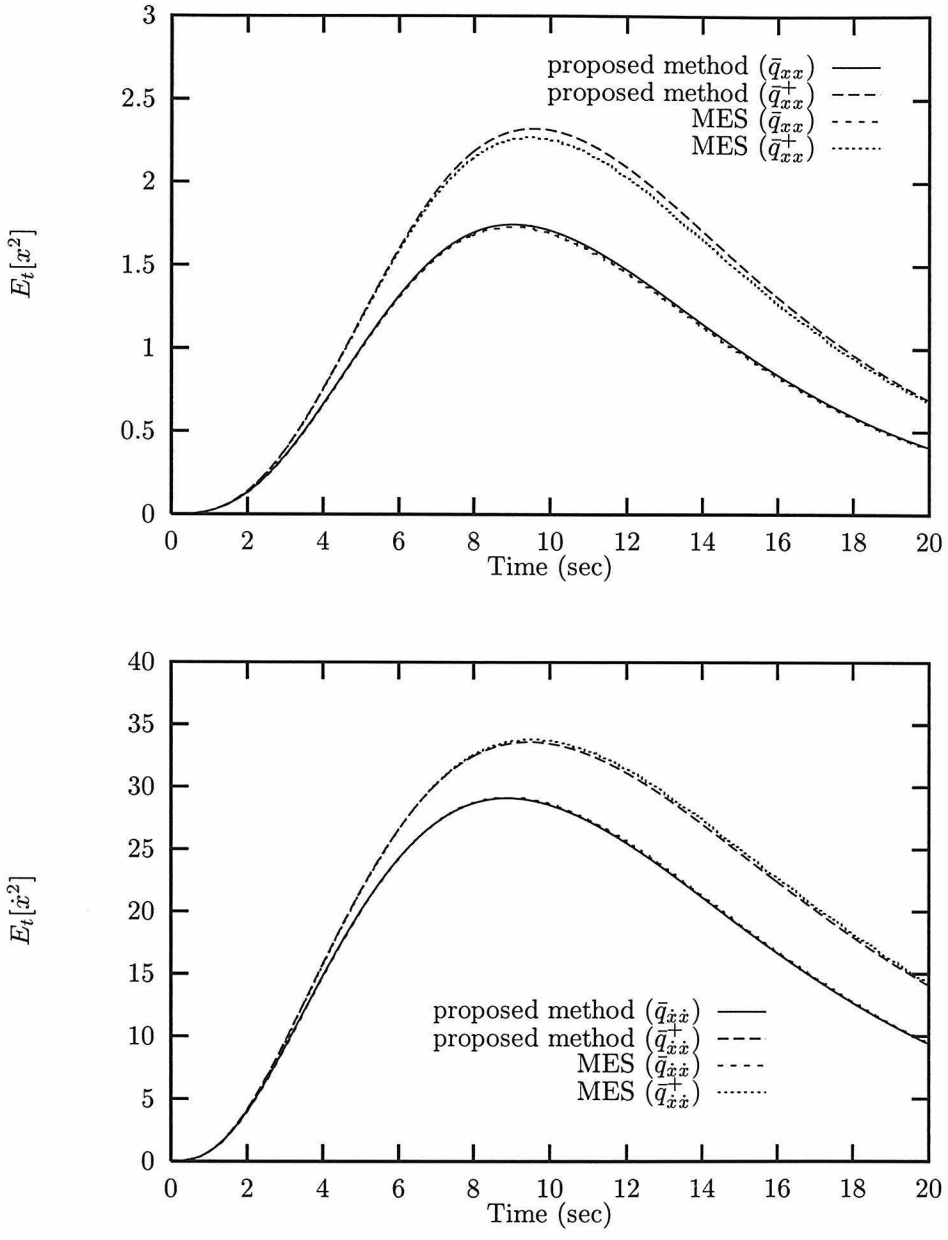

Figure 6.20: Comparison of displacement and velocity moment statistics given by the proposed method and MES method for a softening system with uncertain "yielding" force and damping, $\omega_0 = 2\pi$, $\bar{\zeta} = 2\%$, $\bar{f}_y = 4\pi^2$, $\lambda_1 = 0.5\%$, $\lambda_2 = 0.8\pi^2$, $S_0 = 1$.

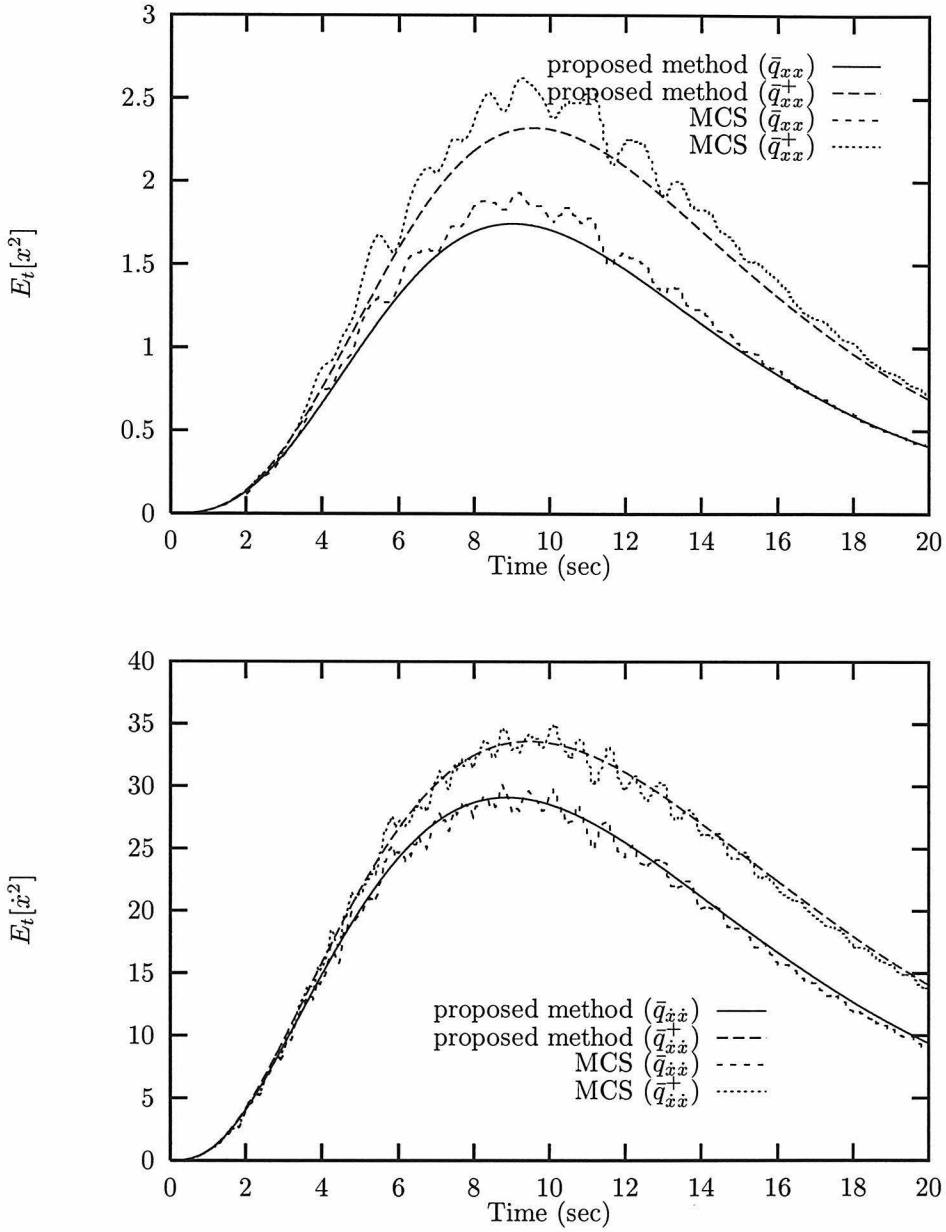

Figure 6.21: Comparison of displacement and velocity moment statistics given by the proposed method and MCS method, sample size = 500×10×10, for a softening system with uncertain "yielding" force and uncertain damping, $\omega_0 = 2\pi$, $\bar{\zeta} = 2\%$, $\bar{f}_y = 4\pi^2$, $\lambda_1 = 0.5\%$, $\lambda_2 = 0.8\pi^2$, $S_0 = 1$.

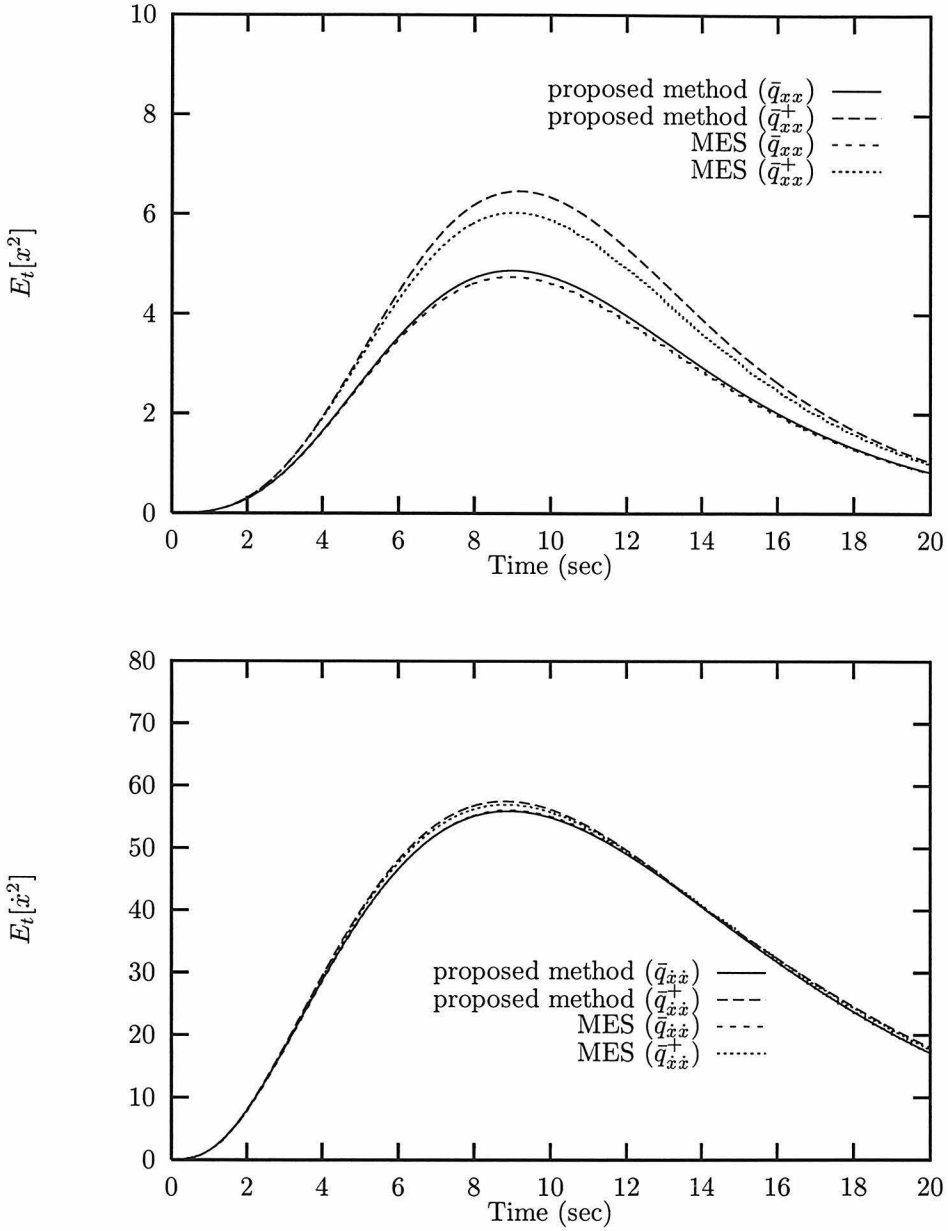

Figure 6.22: Comparison of displacement and velocity moment statistics given by the proposed method and MES method for a softening system with uncertain "yielding" force, $\omega_0 = 2\pi$, $\bar{\zeta} = 2\%$, $\bar{f}_y = 4\pi^2$, $\lambda_1 = 0$, $\lambda_2 = 0.8\pi^2$, $S_0 = 2$.

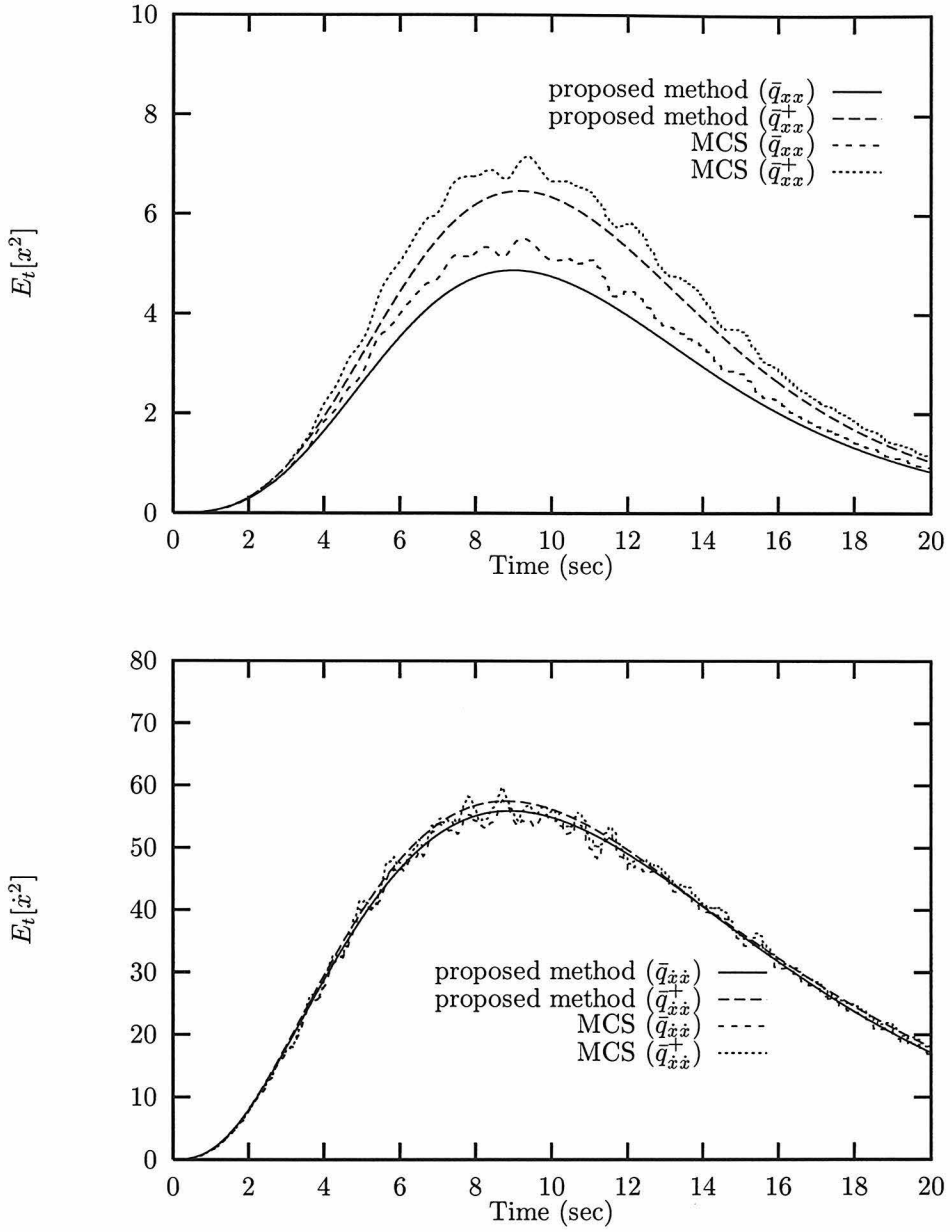

Figure 6.23: Comparison of displacement and velocity moment statistics given by the proposed method and MCS method, sample size = 500×20, for a softening system with uncertain "yielding" force , $\omega_0 = 2\pi$, $\bar{\zeta} = 2\%$, $\bar{f}_y = 4\pi^2$, $\lambda_1 = 0$, $\lambda_2 = 0.8\pi^2$, $S_0 = 2$.

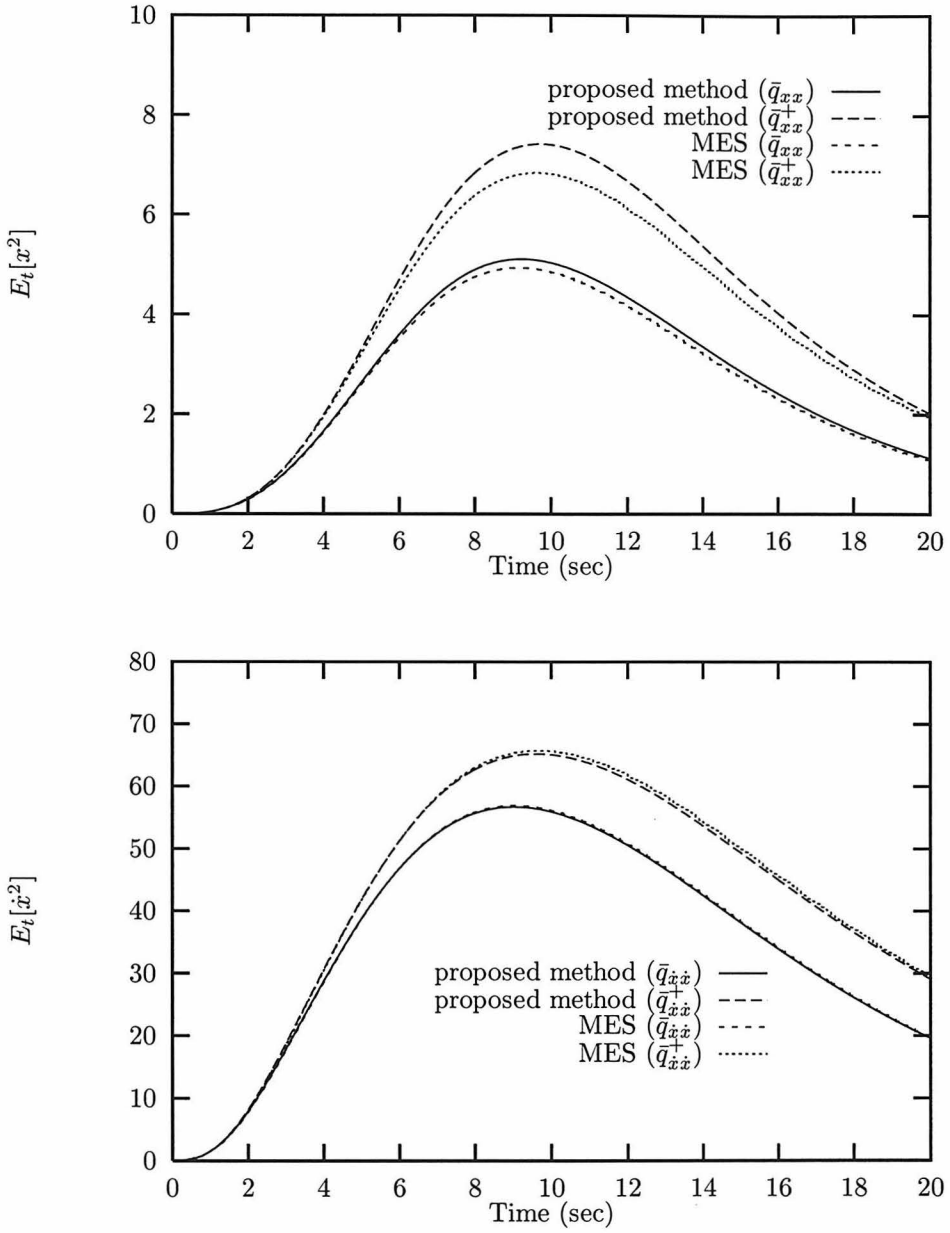

Figure 6.24: Comparison of displacement and velocity moment statistics given by the proposed method and MES method, sample size = 20×20, for a softening system with uncertain "yielding" force and damping, $\omega_0 = 2\pi$, $\bar{\zeta} = 2\%$, $\bar{f}_y = 4\pi^2$, $\lambda_1 = 0.5\%$, $\lambda_2 = 0.8\pi^2$, $S_0 = 2$.

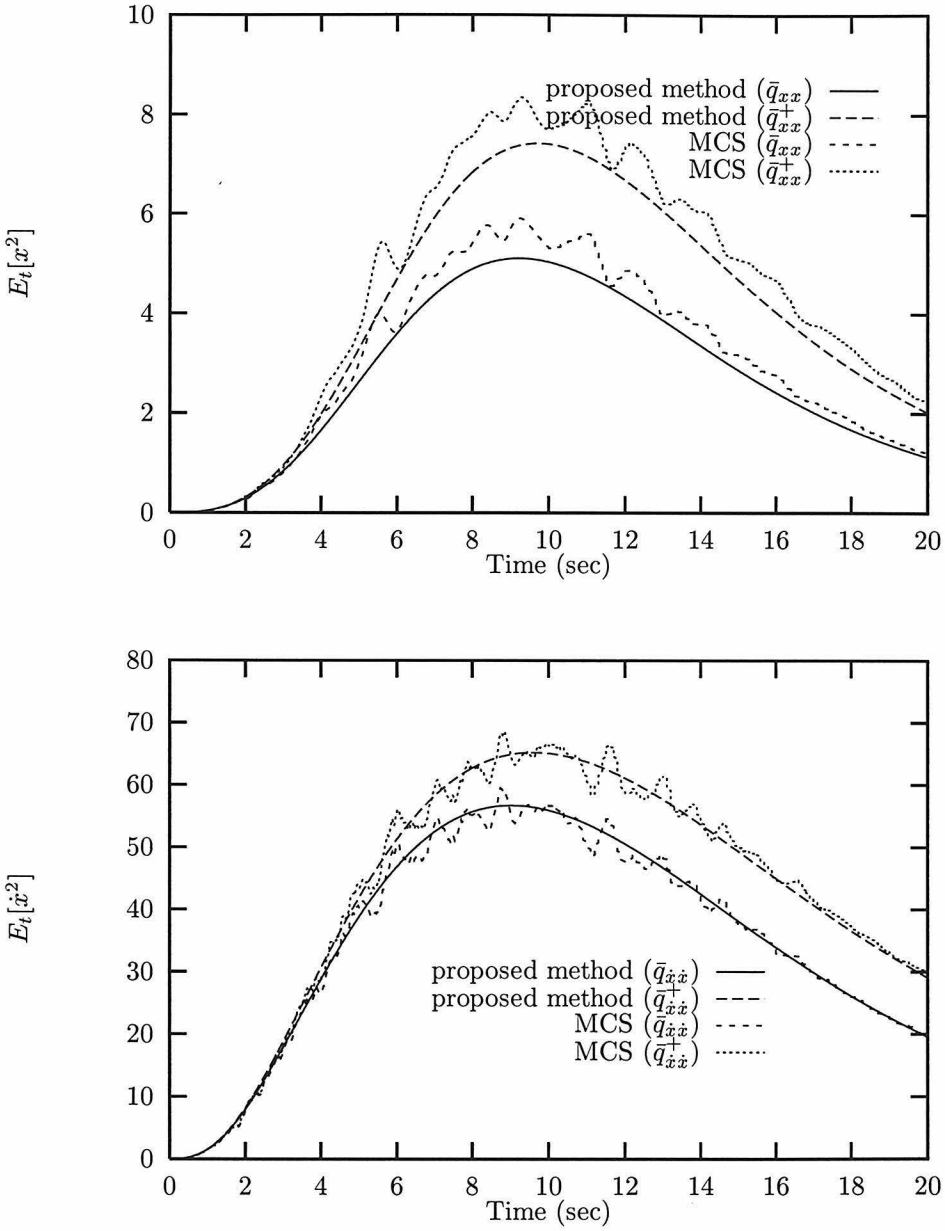

Figure 6.25: Comparison of displacement and velocity moment statistics given by the proposed method and MCS method, sample size = 500×10×10, for a softening system with uncertain "yielding" force and uncertain damping, $\omega_0 = 2\pi$, $\bar{\zeta} = 2\%$, $\bar{f}_y = 4\pi^2$, $\lambda_1 = 0.5\%$, $\lambda_2 = 0.8\pi^2$, $S_0 = 2$.

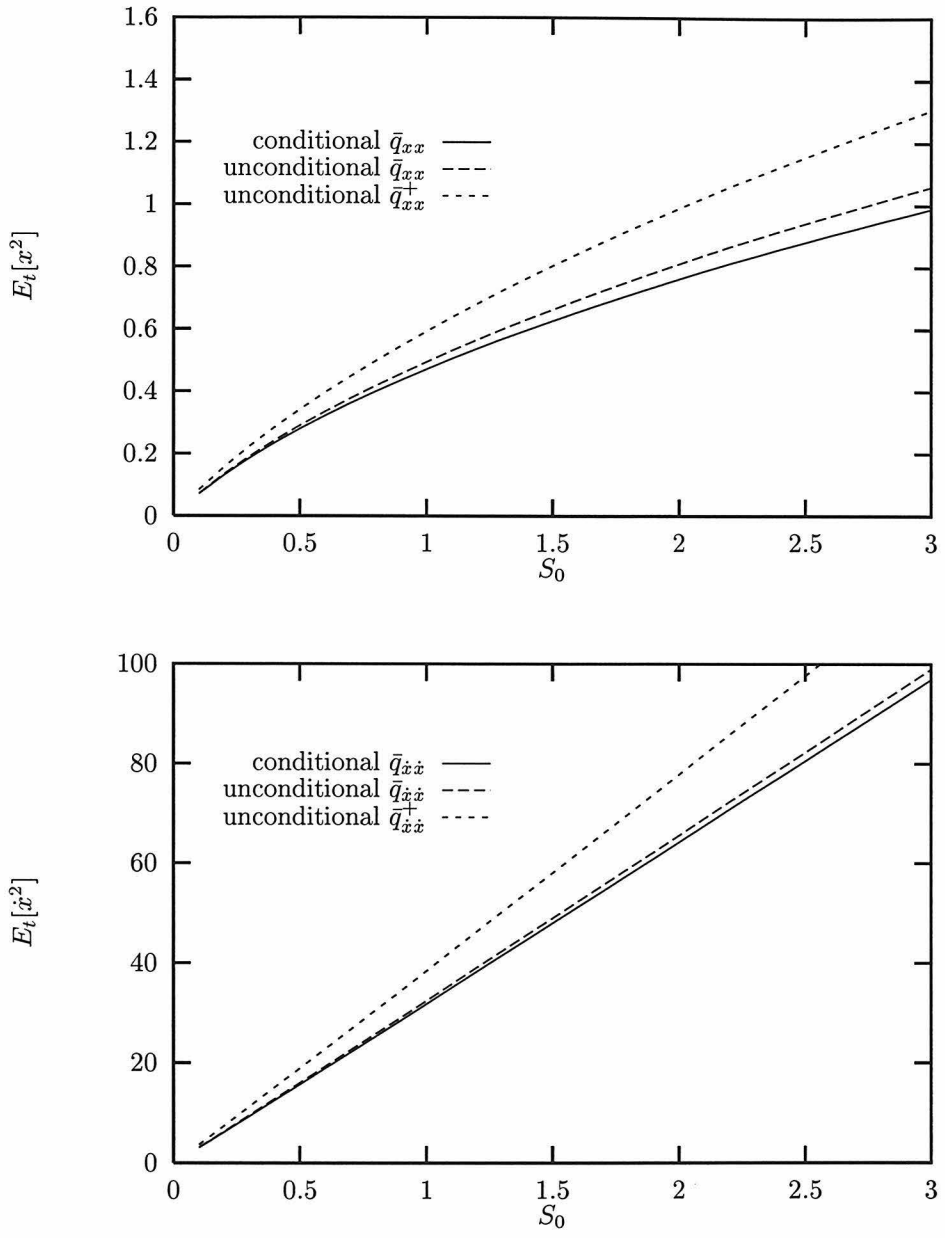

Figure 6.26: Comparison of peak moment statistics for uncertain hardening system, $\omega_0 = 2\pi$, $\zeta = 2\%$ with 25% coefficient of variation, $\bar{\gamma} = 0.5$, $\lambda = 0.25$, Ultraspherical distribution with index M=2.

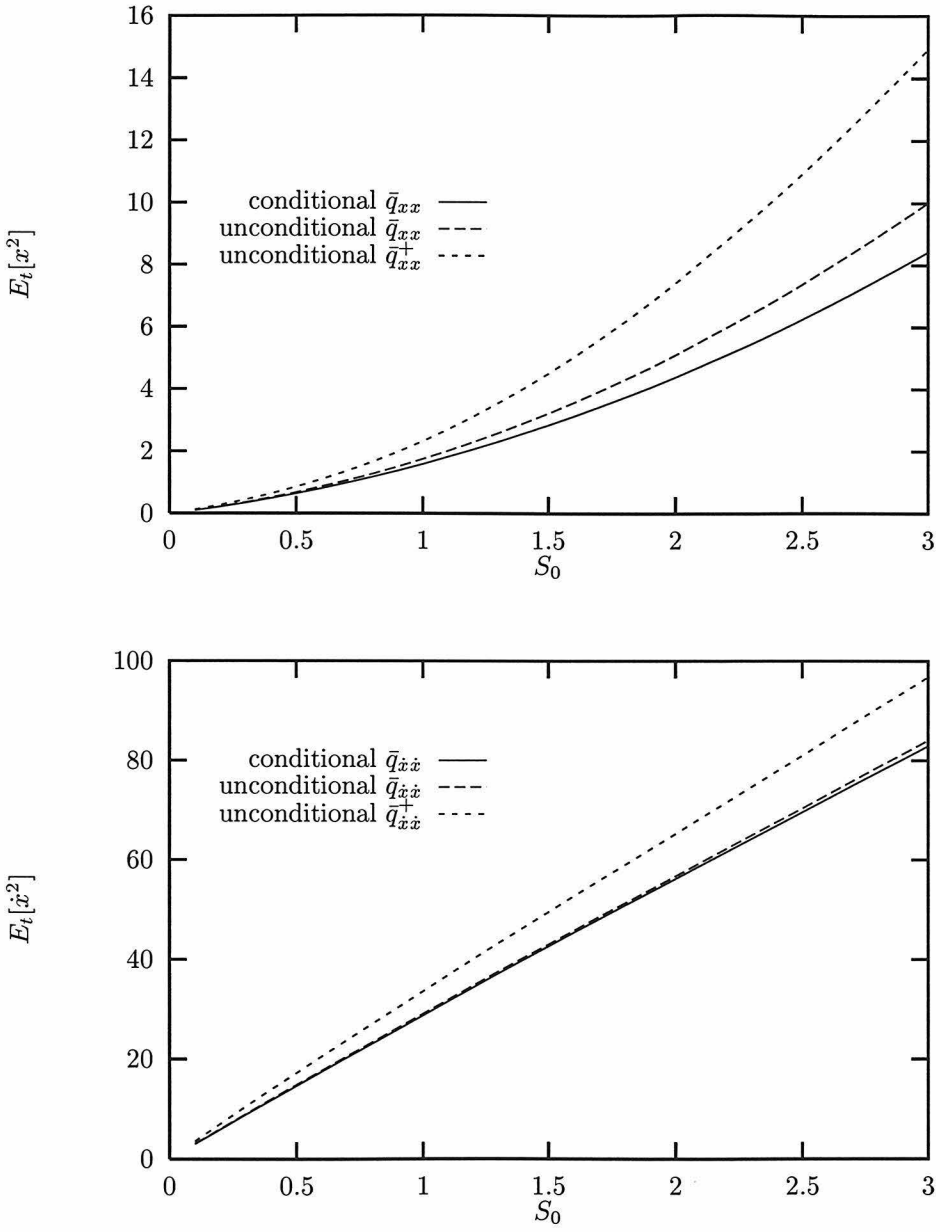

Figure 6.27: Comparison of peak moment statistics for uncertain softening system, $\omega_0 = 2\pi$, $\bar{\zeta} = 2\%$, $\lambda_1 = 0.5\%$, $\bar{f}_y = 4\pi^2$, $\lambda_2 = 0.8\pi^2$, Ultraspherical distribution with index M=2.

Chapter 7

Summary and Conclusions

A solution approach is introduced in this thesis for obtaining response moments of nonlinear dynamical systems with uncertain parameters. The uncertain parameters are idealized as time-independent random variables with an assumed statistical distribution. A set of orthogonal polynomials associated with this distribution is employed as a solution basis. The method of weighted residuals is used to derive a deterministic nonlinear ordinary differential equation set which can be evaluated numerically using a step-by-step time-integration scheme.

The main features of this solution approach are:

1. The approximation of random response variables is based on the global response profile defined over the random parameter space. Such a solution approach can better handle cases where a severe response variation in the vicinity of the mean parameter values is present. Very often, the above mentioned phenomenon is observed in the transient response of uncertain dynamical systems. Therefore, this solution approach generally yields more accurate and reliable transient moment solutions than the perturbation method.

2. Various types of distribution functions for the uncertain parameters may be incorporated into the analyses. This statistical information is also used in defining the minimization criterion for obtaining the polynomial approximation. Hence, the introduced solution approach can better characterize the dependence of the response moments on the probability distribution of uncertain parameters.

This approach is considered to be more appropriate than other non-statistical approaches, such as repeated response simulations using numerical integration methods.

The introduced solution approach is more suitable to problems with polynomial nonlinearity due to an inherent difficulty in evaluating the resulting probability integrals. However, for problems where a lower-order solution scheme is appropriate, approximations to the probability integrals can be adopted and this limitation can be removed.

This solution approach is employed in the subsequent formulations for nonlinear discrete and continuous systems with parameter uncertainty subjected to deterministic dynamic loadings, as well as uncertain nonlinear systems subjected to random excitation. A synopsis of these formulations and applications is given below.

In Chapter 2, a method is proposed for analyzing nonlinear discrete dynamical systems subjected to deterministic external excitation. Applications to nonlinear single-degree-of-freedom systems with uncertain nonlinear stiffness, and uncertain damping are given. For validation and comparison purposes, a perturbation method and a simulation technique are also employed. Numerical results show that the response dependence to the parameters can be highly nonlinear at large times. This nonlinear dependence is strongly related to the amount of damping, the nonlinearity of the system, the response history and the range of uncertain parameters. For the cases examined, the proposed method gives much better solutions than the perturbation method for both a second-order and a third-order solution scheme. This comparison reveals the difference in performance when different solution approaches are considered.

Chapter 3 is an extension to the above formulation to nonlinear continuous systems with uncertain parameter fields. Following theoretical descriptions for a random field and a general finite representation, a discrete Karhunen-Loève decomposition is employed to derive a set of basis random variables. Then, a generalized spatial

discretization is used to obtain a variational formulation for the continuous random systems. The resulting discrete systems with random parameters can be readily solved using the method developed in Chapter 2.

As an application of solution method developed in Chapter 3, a nonlinear analysis of an uncertain continuous shear-beam model subjected to a near-field earthquake excitation is given in Chapter 4. The finite element method of spatial discretization is employed for the discretization of random shear rigidity, and the spatial representation of response variables as well. Consideration is given to both hardening and softening nonlinear stress-strain characteristics. This study shows that the type of nonlinearity highly affects the peak statistics of the local shear strain for the earthquake excitation considered. The softening type of stress-strain characteristics results in much larger response statistics and response uncertainty. The peak statistics are seen insensitive to the spatial fluctuation of the shear rigidity when the correlation distance is large relative to the total length of the beam. Hence, a totally correlated shear rigidity can be used to approximate a finite correlated shear rigidity for analyzing the peak response statistics.

A general solution framework for uncertain nonlinear systems subjected to external white noise excitation is presented in Chapter 5. This solution framework is based on an extended formulation of the standard equivalent linearization where the parameter randomness and the response nonstationarity are considered simultaneously. The instantaneous equivalent random stiffness and damping matrices are respectively approximated as quadratic random functions via a second-order Taylor series expansion. The resulting random Liapunov equation with explicit random coefficients is then converted to a deterministic Liapunov equation. By numerically solving the deterministic equation, the statistics of the response moments can be evaluated.

Applications of the solution framework to nonlinear single-degree-of-freedom systems are presented in Chapter 6. In numerical examples, extensive studies are given

for a hardening Duffing oscillator subjected to a suddenly applied white noise excitation. The nonstationary moment response shows a ripple-like profile over the random space when either an uncertain natural frequency or an uncertain hardening parameter is assumed. For the levels of excitation intensity considered, the proposed solution framework again results in much better statistics than the second-order perturbation method. A softening system with uncertain damping and uncertain yielding level is also examined. Good performance is also achieved, by which the proposed solution approach combined with the equivalent linearization technique is concluded as a suitable means of analyzing uncertain nonlinear random vibration problems.

In the examples presented, the velocity moment is insensitive to variations of nonlinear stiffness, of either a hardening or a softening type. On the other hand, the type of nonlinearity and the degree of nonlinearity play a significant role in the response uncertainty of the displacement moment. Such an observation is particularly evident from the analysis presented in the last section of Chapter 6.

The treatment of problems with time-independent uncertain parameters may also be extended to problems with time-dependent uncertain parametric excitation. The application domain is directed toward linear or nonlinear systems subjected to nonstationary, non-white stochastic parametric excitation. Such a generalization is considered as the suggested future research to the current study. A problem description and a potential solution approach are briefly described in the following paragraph.

Traditional studies of parametric excitation primarily focus on stability issues. Nevertheless, it can be of great engineering interest to evaluate the stable evolutionary moment response for systems under such as combined external and parametric stochastic excitation. Unfortunately, research studies and development of solution techniques for such a problem are extremely limited. The posed problem may be characterized as an ordinary differential equation with a temporally correlated parametric excitation which, to some extent, resembles the partial differential equation with a

spatially correlated parameter field as considered in Chapter 3. Due to such a similarity, the proposed solution scheme may also be used to solve response moments of the posed problems. To achieve this, the nonstationary parametric excitation can be decomposed into a set of independent random variables with deterministic time-varying excitation functions. The resulting governing equation with random coefficients may then be solved using the solution method given in the Chapter 2.

Bibliography

[1] R. Singh and C. Lee. Frequency response of linear systems with parameter uncertainties. *Journal of Sound and Vibration*, 168(1):71–92, 1993.

[2] C. G. Bucher and C. E. Brenner. Stochastic response of uncertain systems. *Archive of Applied Mechanics*, 62:507–516, 1992.

[3] T. Belytschko W. K. Liu and A. Mani. Probabilistic finite elements for nonlinear structural dynamics. *Computer Methods in Applied Mechanics and Engineering*, 56:61–81, 1986.

[4] T. Belytschko W. K. Liu and A. Mani. Random field finite element. *International Journal for Numerical Methods in Engineering*, 23:1831–1845, 1986.

[5] T. Belytschko W. K. Liu and A. Mani. Transient probabilistic system. *Computer Methods in Applied Mechanics and Engineering*, 67:27–54, 1988.

[6] P-C Chen and W. W. Soyoka. Impulse response of a dynamic system with statistical properties. *Journal of Sound and Vibration*, 31:309–314, 1973.

[7] L. S. Katafygiotis and J. L. Beck. A very efficient moment calculation method for uncertain linear dynamic systems. *Probabilistic Engineering Mechanics*, 10:117–128, 1995.

[8] J. L. Beck and L. S. Katafygiotis. Treating model uncertainties in structural dynamics. In *Proceedings of Ninth World Conference on Earthquake Engineering*, volume V, Tokyo-Kyoto, Japan, August 1988.

[9] C. Papadimitriou, L. S. Katafygiotis, and J. L. Beck. Approximate analysis of response variability of uncertain linear systems. *Probabilistic Engineering Mechanics*, 10:251–264, 1995.

[10] M. Shinozuka. Monte-Carlo solution of structural dynamics. *Computers and Structures*, 2:855–874, 1972.

[11] P. D. Spanos and B. A. Zeldin. Galerkin sampling method for stochastic mechanics. *Journal of Engineering Mechanics*, 120(5):1091–1106, 1994.

[12] Z. Hou. *Nonstationary Response of Structures and its Application to Earthquake Engineering.* Ph.D. thesis, California Institute of Technology, 1990.

[13] T. K. Caughey and F. Ma. The exact steady-state solution of a class of dynamic systems to stochastic excitation. *International Journal of Nonlinear Mechanics*, 17:137–142, 1982.

[14] T. K. Caughey and F. Ma. The steady-state response of a class of dynamical systems to stochastic excitation. *Journal of Applied Mechanics*, 49:629–632, 1982.

[15] Y. Yong and Y. K. Lin. Exact stationary-response solution for second order nonlinear systems under parametric and external white-noise excitations. *Journal of Applied Mechanics*, 54:415–418, 1987.

[16] T. K. Caughey. Nonlinear theory of random vibration. *Advanced Applied Mechanics*, 11:209–253, 1971.

[17] W. D. Iwan. A generalization of the concept of equivalent linearization. *International Journal of Nonlinear Mechanics*, 8:279–287, 1973.

[18] W. D. Iwan. On defining equivalent systems for certain ordinary non-linear differential equations. *International Journal of Nonlinear Mechanics*, 4:325–334, 1969.

[19] W. D. Iwan and I-M. Yang. Application of statistical linearization techniques to nonlinear multidegree-of-freedom systems. *Journal of Applied Mechanics*, 39:545–550, 1972.

[20] P-T. D. Spanos. *Linearization Techniques for Nonlinear Dynamical Systems.* Ph.D. thesis, California Institute of Technology, 1976.

[21] T. S. Atalik and S. Utku. Stochastic linearization of multi-degree-of-freedom nonlinear systems. *Earthquake Engineering and Structural Dynamics*, 4:411–420, 1976.

[22] W. D. Iwan and Jr. A. B. Mason. Equivalent linearization for systems subjected to non-stationary random excitation. *International Journal of Nonlinear Mechanics*, 15:71–82, 1980.

[23] Y. K. Wen. Equivalent linearization for hysteretic systems under random excitation. *Journal of Applied Mechanics*, 47:150–154, 1980.

[24] K. Asano and W. D. Iwan. An alternative approach to the random response of bilinear hysteretic systems. *Earthquake Engineering and Structural Dynamics*, 12:229–236, 1984.

[25] R. H. Cherng and Y. K. Wen. Reliability of uncertain nonlinear trusses under random excitation (I). *Journal of Engineering Mechanics*, 120:733–757, 1994.

[26] C. C. Chang and T. Y. Yang. Random vibration of flexible, uncertain beam element. *Journal of Engineering Mechanics*, 117:2329–2350, 1991.

[27] J. M. Klosner, S. F. Haber, and P. Voltz. Response of nonlinear systems with parameter uncertainties. *International Journal of Nonlinear Mechanics*, 27:547–563, 1992.

[28] H. Benaroya and M. Rehak. Finite element methods in probabilistic structural analysis: A selective review. *Applied Mechanics Reviews*, 41(5):201–213, 1988.

[29] H. Jensen and W. D. Iwan. Response variability in structural dynamics. *Earthquake Engineering and Structural Dynamics*, 20:949–959, 1991.

[30] M. Abramowitz and I. A. Stegun. *Handbook of Mathematical Functions.* Dover Publications, New York, 1964.

[31] R. Ghanem and P. D. Spanos. *Stochastic Finite Element: A Spectral Approach.* Springer Verlag, 1991.

[32] R. Ghanem and P. D. Spanos. Polynomial chaos in stochastic finite element. *Journal of Applied Mechanics, ASME*, 57(1):197–202, March 1990.

[33] R. Ghanem and P. D. Spanos. Stochastic finite element expansion for random media. *Journal of Engineering Mechanics, ASCE*, 115(5):1035–1053, May 1989.

[34] R. Ghanem and P. D. Spanos. A stochastic Galerkin expansion for nonlinear random vibration analysis. *Probabilistic Engineering Mechanics*, 8:255–264, 1993.

[35] S. Dham and R. Ghanem. Finite element analysis of multiphase flow in porous media with the polynomial chaos expansion. In *Second International Conference on Computational Stochastic Mechanics*, Athens, Greece, June 1994.

[36] Y. Shigeno R. Ghanem, H. Seya and T. Shiomi. Stochastic finite element analysis for the transport of trichloroethylene. In *International Conference on Computational Methods in Water Resources*, Heidelberg, Germany, July 1994.

[37] P. C. Jennings. Periodic response of a general yielding structure. *Journal of the Engineering Mechanics, Proceedings of the ASCE*, 90(EM2), April 1964.

[38] A. W. Naylor and G. R. Sell. *Linear Operator Theory in Engineering and Science.* Springer Verlag, 1982.

[39] O. C. Zienkiewicz and R. L. Taylor. *The Finite Element Method, Vol 2.* McGraw-Hill, 1989.

[40] T. H. Heaton, J. F. Hall, D. J. Wald, and M. W. Halling. Response of high-rise and base-isolated buildings to a hypothetical m_w 7.0 blind thrust earthquake. *Science*, 267:206–211, January 1995.

[41] J. F. Hall, T. H. Heaton, M. W. Halling, and D. J. Wald. Near-source ground motion and its effects on flexible buildings. *Earthquake Spectra*, 2(4):569–605, November 1995.

[42] W. D. Iwan. Near-field consideration in specification of seismic design motions for structures. In *Proceedings of the Tenth European Conference on Earthquake Engineering*, Vienna, Austria, 1994.

[43] International Conference of Building Officials (ICBO). Uniform building code. Whittier, California, 1994.

[44] W. D. Iwan and X. Chen. Important near-field ground motion data from the Landers earthquake. In *Proceedings of the Tenth European Conference on Earthquake Engineering*, Vienna, Austria, 1994.

[45] G. R. Saragoni and G. C. Hart. Simulation of artificial earthquakes. *Earthquake Engineering and Structural Dynamics*, 2:249–269, 1974.